



# **CENTER FOR INFRASTRUCTURE ENGINEERING STUDIES**

## **SHEAR PERFORMANCE OF REINFORCED CONCRETE BEAMS STRENGTHENED WITH ADVANCED COMPOSITES**

by

**Ahmed Mahmoud Khalifa**

University of Missouri-Rolla

**CIES  
99-14**

### Disclaimer

The contents of this report reflect the views of the author(s), who are responsible for the facts and the accuracy of information presented herein. This document is disseminated under the sponsorship of the Center for Infrastructure Engineering Studies (CIES), University of Missouri -Rolla, in the interest of information exchange. CIES assumes no liability for the contents or use thereof.

The mission of CIES is to provide leadership in research and education for solving society's problems affecting the nation's infrastructure systems. CIES is the primary conduit for communication among those on the UMR campus interested in infrastructure studies and provides coordination for collaborative efforts. CIES activities include interdisciplinary research and development with projects tailored to address needs of federal agencies, state agencies, and private industry as well as technology transfer and continuing/distance education to the engineering community and industry.

Center for Infrastructure Engineering Studies (CIES)  
University of Missouri-Rolla  
223 Engineering Research Lab  
1870 Miner Circle  
Rolla, MO 65409-0710  
Tel: (573) 341-6223; fax -6215  
E-mail: [cies@umr.edu](mailto:cies@umr.edu)  
[www.cies.umr.edu](http://www.cies.umr.edu)



**ALEXANDRIA UNIVERSITY  
FACULTY OF ENGINEERING**

**SHEAR PERFORMANCE OF REINFORCED CONCRETE  
BEAMS STRENGTHENED WITH ADVANCED COMPOSITES**

A Thesis Submitted to the Structural Engineering Department  
for the Degree of Doctor of Philosophy  
In Civil Engineering

**By**

**Ahmed Mahmoud Khalifa**

Registered: March, 1996  
Submitted: , 1999

## ABSTRACT

Shear collapse of reinforced concrete (RC) members is catastrophic and occurs suddenly with no advance warning of distress. In several occasions existing RC beams have been found to be deficient in shear and in need of strengthening. Conventional shear strengthening methods such as external post tensioning, member enlargement along with internal transverse steel, and bonded steel plates are very costly, requiring extensive equipment, time, and significant labor. Conversely, the relatively new alternative strengthening technique using advanced composite materials, known as fiber reinforced polymer (FRP), offers significant advantages such as flexibility in design, ease of installation, reduced construction time, and improved durability.

The overall objective of this study was to investigate the shear performance and failure modes of RC beams strengthened with externally bonded carbon FRP (CFRP) sheets. The specific goals were to address the factors affecting the shear strength, and to propose a design approach for computing the shear capacity of the strengthened beams. In order to achieve these objectives, an extensive experimental program consisting of testing twenty-seven, full-scale RC beams was carried out. The variables investigated in this experimental study included steel stirrups, shear span-to-depth ratio, and CFRP amount and configurations. As part of the research program, the experimental study examined the effectiveness of CFRP reinforcement in enhancing the shear capacity of RC beams in negative and positive moment regions, and rectangular and T cross-section beams. Furthermore, an innovative proprietary end anchor system to allow a better exploitation of the strengthening system was described and tested.

The experimental results indicated that the contribution of externally bonded CFRP to the shear capacity is significant and depends on the variable investigated. In this thesis, the proposed design approach for computing the shear capacity of the strengthened beams is presented. The design model addresses the CFRP contribution similar to the conventional shear reinforcement, according to the design format of ACI and two other design codes (Egyptian code and Eurocode). Compared with the current test results and all available published in literature up to date, the design approach gives satisfactory and conservative results.

## ACKNOWLEDGMENTS

I would like to thank the members of my advisory committee: Drs. Mostafa Swelem, Hossam Ghanem, Abdel Aziz Ibrahim, and Abdeljelil Belarbi, for their guidance and assistance during the course of my Ph.D work.

I wish words could express my gratitude and full appreciation to my overseas advisor Dr. Antonio Nanni, Professor of Civil Engineering at the university of Missouri-Rolla, for his technical guidance, valuable suggestions, and encouragement throughout the experimental and analytical study and in preparing this thesis. It has been an honor to work under the tutelage of Dr. Nanni, whose expertise and discernment were key in the completion of this research. Special thanks also expressed to my overseas advisor Dr. Belarbi for his helpful comments and advice.

This research work was sponsored by the Egyptian Cultural and Educational Bureau, Washington, D.C. and the University Transportation Center on Advanced Materials and Non-Destructive Testing (NDT) Technologies based at the University of Missouri-Rolla, USA. The financial assistance is gratefully acknowledged.

Many thanks go to my friend Dr. Tarek Ibrahim for his helpful and suggestions. His friendship was precious, especially during the period we spent together in the United States. I would like also to thank my colleagues and friends: Tarek Alkhrdaji, William Gold, Gustavo Tumialan, Brian Miller, and Dr. Hong Yong Park who provided their help during my stay at UMR. I would like also to express my appreciation to my brother Adel for his advice, support, and encouragement.

This acknowledgement would not be complete without expressing my sincere gratitude to my wife Mrs. Hanan Khalifa and my sons Mokhtar, Adel and Motaz. Their love, patience, encouragement, and understanding are the source of my motivation and inspiration throughout my work. Finally, I would like to dedicate my work and this thesis to my parents.

## TABLE OF CONTENT

	page
ADVISORY COMMITTEE .....	iii
EXAM COMMITTEE .....	iv
ABSTRACT .....	v
ACKNOWLEDGMENTS .....	vi
LIST OF ILLUSTRATIONS .....	xi
LIST OF TABLES .....	xvi
NOTATION .....	xvii
ACRONYMS AND ABBREVIATIONS .....	xx
<b>CHAPTER 1</b>	
<b>INTRODUCTION</b>	
1-1 General .....	1
1-2 Objectives and Scope of Investigation .....	2
1-3 Summary of Contents .....	3
<b>CHAPTER 2</b>	
<b>LITERATURE REVIEW</b>	
2-1 General .....	5
2-2 Definition of FRP .....	5
2-3 Application of FRP in Structural Engineering .....	6
2-4 Shear Strengthening of RC Beams Using FRP .....	8
2-5 Shear Strengthening Options .....	12
2-5-1 General .....	12
2-5-2 Bonded surface Configuration .....	12
2-5-3 End Anchor .....	13
2-5-4 Shear reinforcement spacing .....	14
2-5-5 Fiber Orientation .....	14
2-5-6 Bi-axial Reinforcement .....	15

**CHAPTER 3****EXPERIMENTAL PROGRAM**

	page
3-1 General .....	16
3-2 Simply Supported Beams with Rectangular Cross-Section .....	16
3-2-1 General .....	16
3-2-2 Test Specimens .....	17
3-2-3 Materials .....	17
3-2-3-1 Concrete .....	17
3-2-3-2 Steel Reinforcement .....	18
3-2-3-3 Composite strengthening system .....	19
3-2-3-4 Summary of the Material Properties .....	21
3-2-4 Strengthening Schemes .....	22
3-2-5 Test Setup and Instrumentation .....	23
3-2-6 Test Procedure .....	25
3-3 Continuous Beam with Rectangular Cross-Section .....	25
3-3-1 General .....	25
3-3-2 Test Specimen and Materials .....	25
3-3-3 Strengthening Schemes .....	27
3-3-4 Test Setup and Instrumentation .....	29
3-4 Simply Supported Beams with T-Cross-Section .....	30
3-4-1 General .....	30
3-4-2 Test Specimen and Materials .....	31
3-4-3 Strengthening Schemes .....	32
3-4-3-1 U-wrap with End Anchor .....	33
3-4-4 Test Setup and Instrumentation .....	36
3-5 Summary of the Test Specimens .....	36

**CHAPTER 4****EXPERIMENTAL RESULTS**

4-1 General .....	38
4-2 Test Results of Series A .....	38

	page
4-2-1 Subgroup A-SW3 .....	38
4-2-2 Subgroup A-SW4 .....	42
4-2-3 Subgroup A-SO3 .....	43
4-2-4 Subgroup A-SO4 .....	49
4-2-5 Summary and Results Evaluation of Series A .....	50
4-3 Test Results of Series B .....	53
4-3-1 Group B-CW .....	53
4-3-2 Group B-CO .....	55
4-3-3 Group B-CF .....	57
4-3-4 Summary and Results Evaluation of Series B .....	60
4-4 Test Results of Series C .....	61
4-4-1 Test Results and Discussions .....	61
4-4-2 Summary and Results Evaluation of Series C .....	68

## **CHAPTER 5**

### **DESIGN APPROACH**

5-1 General .....	70
5-2 Factors Affecting the Shear Contribution of FRP .....	70
5-3 Shear Design of RC Strengthened Beams in ACI Code Format .....	71
5-3-1 ACI Code Provision for Shear .....	71
5-3-2 Shear Capacity of a CFRP Strengthened Section .....	73
5-3-2-1 Contribution of CFRP reinforcement ( $v_f$ ) to the Shear Capacity .....	73
5-3-2-2 Design Considerations .....	87
5-3-3 Summary of the proposed Design procedure .....	89
5-3-4 Model Prediction .....	90
5-3-5 Design example .....	93
5-4 Shear Design of RC Strengthened Beams in Egyptian Code Format .....	94
5-4-1 Background and Basic Remarks .....	94
5-4-2 Shear Capacity of a CFRP Strengthened Section .....	95
5-5 Shear Design of RC Strengthened Beams in Eurocode Format .....	97
5-5-1 Background and Basic Remarks .....	97

	page
5-5-2 Shear Capacity of a CFRP Strengthened Section .....	98
<b>CHAPTER 6</b>	
<b>SUMMARY, CONCLUSIONS, AND RECOMMENDATIONS</b>	
6-1 Summary .....	99
6-2 Conclusions .....	100
6-3 Recommendations for Future Work .....	101
<b>APPENDIX (A)</b>	
<b>PHOTOS OF THE TESTED BEAMS</b> .....	103
<b>APPENDIX (B)</b>	
<b>LOAD VS. DEFLECTION CURVES</b> .....	111
<b>APPENDIX (C)</b>	
<b>LOAD VS. STRAIN CURVES</b> .....	126
<b>APPENDIX (D)</b>	
<b>DESIGN EXAMPLE</b> .....	139
REFERENCES .....	149
VITA .....	155
ARABIC SUMMARY .....	156

## LIST OF ILLUSTRATIONS

Figure	page
<b>Chapter 2</b>	
2-1. Comparison among CFRP, AFRP, and GFRP sheets and reinforcing steel in terms of stress-strain relationship.....	6
2-2. Comparison between the correct experimental results and Equations 2-2 a&b.....	11
2-3. Various schemes for wrapping transverse FRP reinforcement. (a) FRP bonded to the two beam sides. (b) FRP “U” wrap. (c) FRP wrapped entirely around the beam.....	13
2-4. End anchor options. (a) U-wrap without end anchor. (b) U-wrap with end anchor.....	13
2-5. Shear reinforcement distributions. (a) Continuous. (b) Strips .....	14
2-6. Fibers orientation. (a) 90 <sup>0</sup> wrap. (b) 45 <sup>0</sup> .....	14
2-7. Bi-axial FRP sheet reinforcement orientation. (a) 9 <sup>0</sup> /0 <sup>0</sup> . (b)± 45 <sup>0</sup> .....	15
<b>Chapter 3</b>	
3-1. Configuration and reinforcement details for beam specimens of Series A... ..	18
3-2. Components of the strengthening system .....	20
3-3. Schematic representation of CFRP strengthening schemes .....	22
3-4. Schematic representation of test set-up for Series A .....	23
3-5. Test set-up of Specimen A-SO4-2 .....	24
3-6. Configuration and reinforcement details for beam specimens of Series B .....	26
3-7. Strengthening schemes and test set-up for beam specimens of Series B .....	28
3-8. Test set-up of Specimen B-CO2 .....	30
3-9. Configuration and reinforcement details for beam specimens of Series C .....	31
3-10. Casting of beam specimens of Series C .....	32
3-11. Strengthening schemes and test set-up for beam specimens of Series C .....	33
3-12. Details of the U-anchor obtained by slicing a beam .....	34
3-13. End anchor details for Specimen C-BT6 .....	35

Figure	Page
<b>Chapter 4</b>	
4-1. Crack pattern at ultimate failure of Specimen A-SW3-1 .....	39
4-2. Splitting failure of Specimen A-SW3-2 .....	40
4-3. Experimental load-deflection relationship of Specimens A-SW3-1 and A-SW3-2 ...	40
4-4. Applied load versus strain in the stirrups for Specimens A-SW3-1 and A-SW3-2 ...	41
4-5. Experimental load-deflection relationship of Specimens A-SW4-1 and A-SW4-2 ...	43
4-6. Crack pattern at ultimate failure of Specimen A-SO3-1 .....	44
4-7. Ultimate failure of Specimen A-SO3-2 .....	45
4-8. Experimental load-deflection relationship for Subgroup A-SO3 specimens .....	45
4-9. Ultimate failure of Specimen A-SO3-3 .....	46
4-10. Ultimate failure of Specimen A-SO3-4 .....	47
4-11. Applied load versus measured vertical CFRP strain for Specimen A-SO3-4 .....	47
4-12. Final failure of Specimen A-SO3-5 .....	48
4-13. Experimental load-deflection relationship for Subgroup A-SO4 specimens .....	50
4-14. Splitting failure of Specimen B-CW2 .....	54
4-15. Experimental shear force-deflection relationship for Group B-CW specimens .....	54
4-16. Applied shear force versus strain in the stirrups for Specimens B-CW1 and B-CW2	55
4-17. Experimental shear force-deflection relationship for Group B-CO specimens .....	56
4-18. Applied shear force versus measured vertical CFRP strain for Specimen B-CO3 ...	57
4-19. Ultimate failure of Specimen B-CF1 .....	58
4-20. Experimental shear force-deflection relationship for Group B-CF specimens .....	59
4-21. Ultimate failure of Specimen B-CF4 .....	59
4-22. Ultimate failure of Specimen C-BT1 .....	62
4-23. Ultimate failure of Specimen C-BT2 .....	62
4-24. Experimental load-deflection relationship for Series C specimens .....	63
4-25. Ultimate failure of Specimen C-BT3 .....	64
4-26. Ultimate failure of Specimen C-BT4 .....	65
4-27. Applied load versus measured vertical CFRP strain for Specimen C-BT4 .....	65
4-28. Ultimate failure of Specimen C-BT5 .....	66
4-29. Applied load versus vertical CFRP strain for Specimens C-BT2 and C-BT6 .....	67

Figure	page
4-30. Ultimate failure of Specimen C-BT6 .....	68

## Chapter 5

5-1. Definition of area of FRP in shear reinforcement (a) Vertical FRP strips. (b) Inclined strips .....	74
5-2. Strength reduction coefficient in terms of $\rho_f E_f$ for FRP fracture.....	80
5-3. Layout of the bond test specimen of Miller.....	82
5-4. Effective width of FRP reinforcement .....	84
5-5. Comparison of calculated and experimental results based on bond model .....	86
5-6. Effect of strength reduction factor .....	88
5-7. Comparison of experimental results with calculated values based on proposed design procedure .....	91
5-8. Comparison of experimental results with calculated values of shear strengthening for The strengthened beams .....	93

## Appendix A

A-1. Ultimate failure of Specimen A-SW4-1 (control specimen) .....	104
A-2. Splitting failure of Specimen A-SW4-2 (CFRP 90 <sup>0</sup> /0 <sup>0</sup> ) .....	104
A-3. Ultimate failure of Specimen A-SO4-1 (control specimen) .....	105
A-4. Debonding failure of Specimen A-SO4-2 (U-wrap strips) .....	105
A-5. Splitting failure of Specimen A-SO4-3 (continuous U-wrap) .....	106
A-6. Ultimate failure of Specimen B-CW1 (control specimen) .....	107
A-7. Ultimate failure of Specimen B-CW2 (CFRP 90 <sup>0</sup> /0 <sup>0</sup> ) .....	107
A-8. Ultimate failure of Specimen B-CO1 (control specimen) .....	108
A-9. Debonding failure of Specimen B-CO2 (U-wrap strips) .....	108
A-10. Ultimate failure of Specimen B-CO3 (continuous U-wrap) .....	109
A-11. Ultimate failure of Specimen B-CF2 (continuous U-wrap) .....	110
A-12. Ultimate failure of Specimen B-CF3 (CFRP 90 <sup>0</sup> /0 <sup>0</sup> ) .....	110

Figure		page
<b>Appendix B</b>		
B-1.	Applied load versus mid-span deflection for Specimen A-SW3-1 .....	112
B-2.	Applied load versus mid-span deflection for Specimen A-SW3-2 .....	112
B-3.	Applied load versus mid-span deflection for Specimen A-SW4-1 .....	113
B-4.	Applied load versus mid-span deflection for Specimen A-SW4-2 .....	113
B-5.	Applied load versus mid-span deflection for Specimen A-SO3-1 .....	114
B-6.	Applied load versus mid-span deflection for Specimen A-SO3-2 .....	114
B-7.	Applied load versus mid-span deflection for Specimen A-SO3-3 .....	115
B-8.	Applied load versus mid-span deflection for Specimen A-SO3-4 .....	115
B-9.	Applied load versus mid-span deflection for Specimen A-SO3-5 .....	116
B-10.	Applied load versus mid-span deflection for Specimen A-SO4-1 .....	116
B-11.	Applied load versus mid-span deflection for Specimen A-SO4-2 .....	117
B-12.	Applied load versus mid-span deflection for Specimen A-SO4-3 .....	117
B-13.	Applied shear force versus mid-span deflection for Specimen B-CW1 .....	118
B-14.	Applied shear force versus mid-span deflection for Specimen B-CW2 .....	118
B-15.	Applied shear force versus mid-span deflection for Specimen B-CO1 .....	118
B-16.	Applied shear force versus mid-span deflection for Specimen B-CO2 .....	119
B-17.	Applied shear force versus mid-span deflection for Specimen B-CO3 .....	120
B-18.	Applied shear force versus mid-span deflection for Specimen B-CF1 .....	120
B-19.	Applied shear force versus mid-span deflection for Specimen B-CF2 .....	121
B-20.	Applied shear force versus mid-span deflection for Specimen B-CF3 .....	121
B-21.	Applied shear force versus mid-span deflection for Specimen B-CF4 .....	122
B-22.	Applied load versus mid-span deflection for Specimen C-BT1 .....	123
B-23.	Applied load versus mid-span deflection for Specimen C-BT2 .....	123
B-24.	Applied load versus mid-span deflection for Specimen C-BT3 .....	124
B-25.	Applied load versus mid-span deflection for Specimen C-BT4 .....	124
B-26.	Applied load versus mid-span deflection for Specimen C-BT6 .....	125

Figure page

## Appendix C

C-1.	Applied load versus strain in stirrups for Specimen A-SW3-1 .....	127
C-2.	Applied load versus strain in stirrups for Specimen A-SW3-2 .....	128
C-3.	Applied load versus CFRP vertical strain for Specimen A-SW3-2 .....	128
C-4.	Applied load versus strain in stirrups for Specimen A-SW4-1 .....	129
C-5.	Applied load versus strain in stirrups for Specimen A-SW4-2 .....	130
C-6.	Applied load versus CFRP vertical strain for Specimen A-SW4-2 .....	130
C-7.	Applied load versus CFRP vertical strain for Specimen A-SO3-2 .....	131
C-8.	Applied load versus CFRP vertical strain for Specimen A-SO3-3 .....	131
C-9.	Applied load versus CFRP vertical strain for Specimen A-SO3-4 .....	132
C-10.	Applied load versus CFRP vertical strain for Specimen A-SO3-5.....	132
C-11.	Applied load versus CFRP vertical strain for Specimen A-SO4-2.....	133
C-12.	Applied load versus CFRP vertical strain for Specimen A-SO4-3.....	133
C-13.	Applied shear force versus strain in stirrups for Specimen B-CW1 .....	134
C-14.	Applied shear force versus strain in stirrups for Specimen B-CW2 .....	135
C-15.	Applied shear force versus CFRP vertical strain for Specimen B-CW2 .....	135
C-16.	Applied shear force versus CFRP vertical strain for Specimen B-CO2 .....	136
C-17.	Applied shear force versus CFRP vertical strain for Specimen B-CO3 .....	136
C-18.	Applied load versus CFRP vertical strain for Specimen C-BT2.....	137
C-19.	Applied load versus CFRP vertical strain for Specimen C-BT3.....	137
C-20.	Applied load versus CFRP vertical strain for Specimen C-BT4.....	138
C-21.	Applied load versus CFRP vertical strain for Specimen C-BT6.....	138

## Appendix D

D-1.	T-beam cross-section .....	140
D-2.	Factored shear envelope .....	141
D-3.	Shear diagram-showing demand versus existing capacity .....	142
D-4.	Final design and shear diagram .....	145
D-5.	Final design of the alternative solution .....	148

## LIST OF TABLES

Table	page
3-1 Resin properties in tension .....	19
3-2 Materials properties for Series A specimens .....	21
3-3 Materials properties for Series B specimens .....	27
3-4 Materials properties for Series C specimens .....	31
3-5 Summary of the test specimens .....	37
4-1 Summary of the test results of Series A .....	52
4-2 Summary of the test results of Series B .....	61
4-3 Summary of the test results of Series C .....	69
5-1 Experimental data on shear strengthening using CFRP .....	77
5-2 Comparison between Experimental Results and Calculated Values .....	92

## NOTATIONS

a	shear span
$A_f$	area of CFRP shear reinforcement = $2 t_f w_f$
$A_{sw}$	area of steel shear reinforcement within a distance s (Eurocode format)
$A_v$	area of steel shear reinforcement within a distance s (Egyptian code format)
b	width of the beam cross section (Egyptian code format)
$b_w$	width of the web of beam cross section (ACI format)
d	depth from the top of the section to the tension steel reinforcement centroid
$d_f$	effective depth of the CFRP shear reinforcement (usually equal to d for rectangular sections and $d-t_s$ for T-sections)
$E_f$	elastic modulus of FRP (GPa)
$f'_c$	nominal concrete compressive strength in MPa (ACI format)
$f_{cd}$	design value of concrete cylinder compressive strength (Eurocode format)
$f_{ck}$	characteristic compressive cylinder strength of concrete at 28 days in MPa (Eurocode format)
$f_{ctk}$	characteristic axial tensile strength of concrete (Eurocode format)
$f_{cu}$	characteristic cube strength of concrete in $\text{kg/cm}^2$ (Egyptian code format)
$f_{fe}$	effective tensile stress in the FRP sheet in the direction of the principal fibers (stress level in the FRP at ultimate)
$f_{fu}$	ultimate tensile strength of the FRP sheet in the direction of the principal fibers
$f_y$	yield strength of steel reinforcement
$f_{ywk}$	yield strength of steel reinforcement (Eurocode format)
$L_e$	effective bond length (mm)
$M_u$	factored bending moment at section
$P_{max}$	ultimate load carried by CFRP sheet
$q_{cu}$	nominal shear strength provided by concrete in $\text{kg/cm}^2$ (Egyptian code format)
$q_{fu}$	nominal shear strength provided by externally bonded CFRP reinforcement (Egyptian code format)

$q_{su}$	nominal shear strength provided by shear reinforcement (Egyptian code format)
$q_{sub}$	nominal shear strength provided by bent-up bars or inclined stirrups (Egyptian code format)
$q_{sus}$	nominal shear strength provided by vertical stirrups (Egyptian code format)
$q_u$	nominal ultimate shear strength (Egyptian code format)
$Q_u$	ultimate shear force
$R$	reduction coefficient (ratio of effective average stress or strain in the FRP sheet to its ultimate strength or elongation)
$s$	spacing of steel stirrups
$s_f$	spacing of FRP strips
$t_f$	thickness of the FRP sheet on one side of the beam (mm)
$t_s$	slab thickness
$V_c$	nominal shear strength provided by concrete
$V_f$	nominal shear strength provided by FRP shear reinforcement (ACI format)
$V_n$	nominal shear strength (ACI format)
$V_s$	nominal shear strength provided by steel shear reinforcement (ACI format)
$V_u$	factored shear force at section (ACI format)
$V_{fd}$	design shear contribution of CFRP to the shear capacity (Eurocode format)
$V_{Rd1}$	design shear capacity of concrete (Eurocode format)
$V_{Rd2}$	maximum design shear force that can be carried without web failure (Eurocode format)
$V_{wd}$	design contribution of steel shear reinforcement (Eurocode format)
$w_f$	width of FRP strip
$w_{fe}$	effective width of FRP sheet (mm)
$\alpha$	angle between inclined stirrups and longitudinal axis of member
$\beta$	angle between the principal fiber orientation and the longitudinal axis of the beam
$\varepsilon_{fe}$	effective strain of FRP
$\varepsilon_{fu}$	ultimate tensile elongation of the fiber material in the FRP composite
$\phi$	strength reduction factor (ACI format)
$\gamma_c$	strength reduction coefficient for concrete (Egyptian code format) or partial safety

	factor for concrete (Eurocode format) , $\gamma_c = 1.5$
$\gamma_f$	strength reduction coefficient or partial safety factor for CFRP materials ( $\gamma_f = 1.4$ in Egyptian code format and 1.3 in Eurocode format)
$\gamma_s$	strength reduction coefficient for steel (Egyptian code format) or partial safety factor for concrete (Eurocode format) , $\gamma_s = 1.15$
$\rho_f$	FRP fraction area = $(2t_f / b_w) (w_f / s_f)$
$\rho_l$	ratio of longitudinal reinforcement (Eurocode format)
$\rho_w$	ratio of longitudinal reinforcement (ACI format)
$\tau_{Rd}$	basic design shear strength of concrete (Eurocode format)
$\tau_{bu}$	average bond strength (GPa)

## ACRONYMS AND ABBREVIATIONS

ACI	American Concrete Institution
AFRP	Aramid fiber reinforced polymer
ASCE	American Society of Civil Engineers
ASTM	American Society for testing and Materials
CFRP	Carbon fiber reinforced polymer
FRP	Fiber reinforced polymer
GFRP	Glass fiber reinforced polymer
RC	Reinforced concrete
UMR	The University of Missouri-Rolla

# CHAPTER 1

## INTRODUCTION

### 1-1 GENERAL

The aging infrastructure worldwide has prompted many researchers and organizations to seek alternative materials and techniques to revive the deteriorating and deficient structures. Advanced composite materials, known as fiber reinforced polymer (FRP) composites, have received significant attention as one of the most promising materials for use as external reinforcement in repair and strengthening of reinforced concrete (RC) structures.

FRP is a composite material generally consisting of high strength carbon, aramid, or glass fibers in a polymeric matrix (e.g., thermosetting resin) where the fibers are the main load-carrying element. Among many options, this reinforcement may be in the form of preformed laminates or flexible sheets. The laminates are stiff plates or shells that come pre-cured and are installed by bonding them to the concrete surface with a thermosetting resin. The sheets are either dry or pre-impregnated with resin (known as pre-preg) and cured after installation onto the concrete surface. This installation technique is known as wet lay-up.

FRP materials offer the engineer an outstanding combination of physical and mechanical properties, such as high tensile strength, lightweight, high stiffness, high fatigue strength, and excellent durability. The lightweight and formability of FRP reinforcement make FRP systems easy to install. Since these systems are non-corrosive, non-magnetic, and generally resistant to chemicals, they are an excellent option for external reinforcement. The properties of FRP composites and their versatility have resulted in significant saving in construction costs and reduction in shut down time of facilities as compared to the conventional strengthening methods (e.g., section enlargement, external post-tensioning, and bonded steel plates).

Strengthening with externally bonded FRP sheets has been shown to be applicable to many types of RC structural elements. FRP sheets may be adhered to the tension side of structural members (e.g., slabs or beams) to provide additional flexural strength.<sup>1</sup> They may be adhered to web sides of joists and beams or wrapped around columns to provide additional shear strength.<sup>2-18</sup> They may be wrapped around columns to increase concrete confinement and thus strength and ductility of columns.<sup>19</sup> Among many other applications, FRP sheets may be used to strengthen concrete and masonry walls to better resist lateral loads<sup>20,21</sup> as well as circular structures (e.g., tanks and pipelines) to resist internal pressure and reduce corrosion.<sup>22</sup> As of today, several millions of square meters of surface bonded FRP sheets have been used in many strengthening projects worldwide.<sup>23</sup>

In recent years, several studies have been conducted to investigate the flexural strengthening of RC members with FRP, however, few studies have specifically addressed shear strengthening. Shear failure of RC members is catastrophic and occurs with no advance warning of distress. In order to take full advantage of the ductility of an RC member, it is desirable to ensure that flexure rather than shear governs ultimate strength. In several occasions, existing RC beams have been found to be deficient in shear and in need of strengthening. Deficiencies occur due to many factors such as insufficient shear reinforcement resulting from design errors or use of outdated codes, reduction in steel area due to corrosion, increase in demand of service load, and construction defects. The research studies on shear strengthening using externally bonded FRP reinforcement, started by Berset<sup>2</sup> in 1992, have been limited and the design algorithms for computing the shear contribution of FRP sheets are to a certain degree controversial and not yet clear.

## **1-2 OBJECTIVES AND SCOPE OF INVESTIGATION**

The overall objective of this research program was to investigate the shear performance and modes of failure of RC beams after strengthening with externally bonded carbon FRP (CFRP) sheets. More specific objectives were to:

- 1- Examine the effectiveness of CFRP reinforcement in enhancing the shear capacity of RC beams in negative and positive moment regions, and rectangular and T cross-section beams.

- 2- Eliminate the problems associated with traditional FRP end anchor.
- 3- Address the factors that influence shear capacity of strengthened beams such as: steel stirrups, shear span-to-depth ratio, CFRP amount and distribution, bonded surface, fiber orientation, and end anchor.
- 4- Propose a design approach for computing the shear capacity of the strengthened beams.

In order to fulfill these objectives, an extensive experimental program was performed at the Engineering Research Laboratory of the University of Missouri-Rolla (UMR). This program included the test of twenty-seven, full-scale, RC beams which were designed to fail in shear and strengthened with different CFRP configurations. The beams were grouped into three main series. The first series focused on shear strengthening of rectangular simply supported beams, the second series addressed the shear strengthening of continuous beams, and the last series investigated the strengthening of simply supported T-beams. Furthermore, in order to enhance the effectiveness of CFRP reinforcement, a novel end anchor system was developed and examined in this study. Finally, a design approach for computing the shear capacity of the strengthened beams in ACI, Egyptian code, and Eurocode design format was proposed.

### **1-3 SUMMARY OF CONTENTS**

Chapter 2 of this dissertation contains a brief review of FRP materials and their applications in the structural engineering field. Research programs conducted to investigate the shear performance as well as to evaluate the shear capacity of the strengthened beams are surveyed. In addition, shear strengthening options of RC beams with FRP composites are presented.

Chapter 3 deals with the description of the experimental program. The constituent materials, the beam specimens, and FRP installation procedure are presented. A brief description of test set up and procedure is given.

Chapter 4 contains the test results and discussion. The observed crack patterns and modes of failure are reported. In addition, comparisons among test results to address factors affecting shear strength.

Chapter 5 deals with the design approach for computing the shear capacity of the strengthened beams.

At the end, Chapter 6 provides the summary of this research program, and conclusions emerged from it. Recommendations for future research are also presented.

Four appendices are attached to this dissertation containing photos of the tested beams, plots of load-deflection relationships, plots of load-strain relationships, and a design example. At the end of this document, an abstract in Arabic is presented.

## CHAPTER 2

### LITERATURE REVIEW

#### 2-1 GENERAL

In the last decade, the use of FRP composites to reinforce concrete members has emerged as one of the most promising technologies in materials/structural engineering. There is a wide range of applications of FRP reinforcement that covers new construction as well as rehabilitation of the existing structures. This section provides brief information on FRP materials and their applications in structural engineering field. The section focuses on shear strengthening of RC beams with externally bonded FRP composites. The research programs conducted to investigate the shear performance and to evaluate the shear capacity of the strengthened beams are reviewed. In addition, shear strengthening options of RC beams with FRP composites are presented.

#### 2-2 DEFINITION OF FRP

FRP composites consist of high strength fibers embedded in a polymer resin. The fibers are the main load-carrying element and have a wide range of strengths and stiffnesses with a linear stress-strain relationship up to failure. Fiber types typically used in the fabrication of FRP composites for construction are carbon, glass, and aramid. All these fibers are available commercially as continuous filaments.

The polymer resin surrounds and encapsulates the fibers to bind them together, protect them from damage, maintain their alignment, and allow distribution of load among them. Polymers are available as two categories; thermosetting polymers (e.g. epoxy and polyester) and thermoplastic polymers (e.g. nylon). The chemical compositions and mechanical properties of the various types of fibers and polymers are currently given in many textbooks.<sup>24,25</sup>

FRP composites have become more popular and accepted by designers, contractors, and owners due to combinations of their unique characteristics. FRP composites have significantly

higher strength-to-weight ratio than metals and other construction materials. In addition, these materials are non-corrosive, non-magnetic, and generally resistant to chemicals. A comparison among carbon FRP, aramid FRP (AFRP), and glass FRP (GFRP) sheets<sup>25</sup> (based on fiber area only), and reinforcing steel in terms of stress strain relationship is illustrated in **Figure (2-1)**.

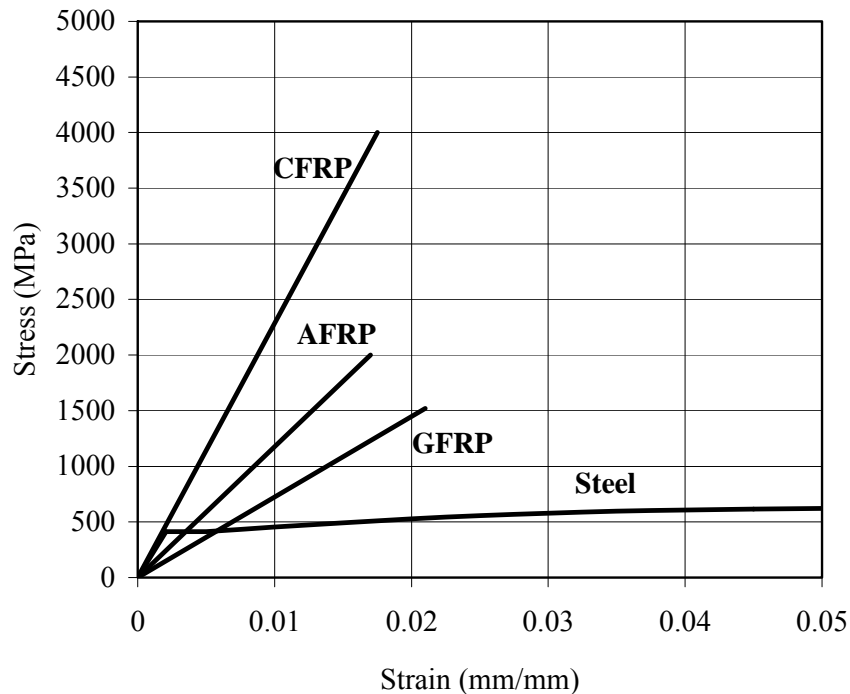


**Figure 2-1.** Comparison among CFRP, AFRP, and GFRP sheets and reinforcing steel in terms of stress-strain relationship

### 2-3 APPLICATIONS OF FRP IN STRUCTURAL ENGINEERING

To resolve corrosion problems in reinforcing steel and to increase the efficiency of repair work for the deteriorating RC infrastructure, professionals have turned to alternative materials such as FRP composites. The interest in the use of composites is attributable to declining manufacturing costs combined with ease and speed of installation.

FRP composites can be produced by different manufacturing methods in many shapes and forms; the most popular ones for concrete reinforcement are bars, prestressing tendons, pre-

cured laminates/shells, and fiber sheets. FRP bars and tendons are currently produced with sizes and deformation patterns similar of those of steel bars, strands and solid wires. They are commonly used for internal concrete reinforcement. FRP pre-cured laminates/shells and sheets are commonly used as external reinforcement for repair and strengthening purposes.

The initial developments of FRP-strengthening technique took place in 1987, in Switzerland, under the leadership of Meier.<sup>26</sup> It was there that the first on-site repair by externally bonded FRP took place in 1991. Since then, strengthening by externally bonded FRP composites has been studied worldwide. The sudden increase in the use of FRP composites was attained after the 1995 Hyogoken Nanbu Earthquake In Japan. By 1997, more than 1,500 concrete structures worldwide had been reinforced with externally bonded FRP composites<sup>27</sup>

Strengthening with externally bonded FRP reinforcement has been shown to be applicable to many types of RC structures.<sup>28</sup> Currently, this method has been implemented to strengthen such structural elements as columns, beams, slabs, walls, chimneys, tunnels, and silos. The uses of external FRP reinforcement may be generally classified as flexural strengthening, improving the confinement and ductility of compression members, and shear strengthening. Although several studies have been conducted to investigate the flexural strengthening of RC members with externally bonded FRP reinforcement, studies on shear strengthening have been limited.

## **2-4 SHEAR STRENGTHENING OF RC BEAMS USING FRP**

This section presents some of the published research studies regarding the shear strengthening of RC members with externally bonded FRP reinforcement.

As stated previously, the first research focusing on shear strengthening of RC beams with composite materials was performed by Berset<sup>2</sup> in 1992 by testing RC beams with externally bonded glass FRP (GFRP) laminates. Berset proposed a simple analytical model to compute the contribution of the external reinforcement to the shear capacity similarly to stirrups contribution and based on a maximum allowable strain, which is determined from experiments.

Uji<sup>3</sup> carried out the tests of eight simply supported RC beams strengthened for shear with CFRP sheets using two different wrapping schemes; total wrap or two sides of the beam. He concluded that the application of CFRP substantially improves the shear capacity of RC members. He also found that the strains in the stirrups and the CFRP are different even at the same location. This is because a stirrup stretches evenly over its length, while only a limited area of CFRP stretches at the crack. Thus, the strain in CFRP is greater than in stirrups at the crack location. In his study, the maximum shear force carried by CFRP was assumed to be the product of the bond area assumed as the triangle above the middle point of the diagonal crack and the bond stress of 1.27 MPa, which was determined based on his test results.

Chajes et al.<sup>5</sup> tested T-beams to study the effectiveness of externally bonded composites for shear capacity. Woven composites fabrics made of aramid, E-glass, and carbon fibers were used in their study. For beams with external reinforcement, the average increase in ultimate strength of 83 to 125 percent was achieved. In their study, the FRP contribution to shear capacity was modeled similar to stirrups contribution. It was assumed that an average FRP strain of 0.005 mm/mm, determined from the tests, governed the design. However, the specimens used in this study were very small and only one wrapping scheme was used (i.e. U-wrap) which limited more general conclusions.

Umezu et al.<sup>8</sup> carried out an extensive experimental program in order to determine the effects of aramid and carbon FRP sheets on the shear capacity of simply supported RC beams. They used total wrap as strengthening scheme for all of their test beams. The application of FRP sheets was found to enhance shear capacity and deformation characteristics. In their analysis, they stated that the contribution of AFRP to shear capacity could be evaluated by the truss theory, based on an average stress of AFRP equal to the tensile strength of the sheet multiplied by a reduction coefficient, determined from the test results, equal to 0.4.

Araki et al.<sup>9</sup> tested RC beams strengthened with various types and amount of totally wrapped FRP sheets under anti-symmetrical moment condition. The conclusion drawn was that the shear capacity of RC members increased in proportion to the amount of FRP sheets. The contribution of FRP to the shear capacity was evaluated similar to calculation of stirrups

contribution. A reduction factor to the tensile strength of the sheets was proposed. In their study the values of 0.6 and 0.45 were adopted for CFRP and AFRP sheets, respectively.

Malek and Saadatmanesh<sup>15</sup> presented a method for calculating the inclination angle of the shear cracks as well as the ultimate shear capacity of RC beams strengthened for shear with bonded FRP plates. The compression field theory was used in their analysis. The model included simplified assumptions such as no stress concentration effect and complete composite action between the FRP plate and the beam. It was, however, shown that shear failure of the strengthened beams was controlled by either FRP fracture at a stress level below its ultimate due to stress concentration or by debonding of FRP from the concrete surface.

A design model for computing the shear capacity of RC beams strengthened with FRP composites was presented by Triantafillou<sup>16</sup> in 1998. In his model, the external FRP shear reinforcement was treated similar to the internal reinforcement. It was assumed that at the ultimate shear limit state the FRP develops an effective strain,  $\varepsilon_{fe}$ , which is less than the ultimate tensile strain,  $\varepsilon_{fu}$ , of FRP. The expression for computing the FRP contribution to the shear capacity of an RC beam,  $V_f$ , was written as follows:

$$V_f = \frac{0.9}{\gamma_f} \rho_f E_f \varepsilon_{fe} b_w d (1 + \cot\beta) \sin\beta \quad (2-1)$$

where  $\gamma_f$  is the partial safety factor for FRP in uniaxial tension (taken 1.15 for CFRP),  $\rho_f$  is the FRP area fraction (equal to  $(2t_f/b_w)(w_f/s_f)$ ),  $t_f$  is the FRP reinforcement thickness and  $w_f$  is the width of FRP strip,  $s_f$  is the spacing of strips,  $b_w$  is the beam width,  $E_f$  is the elastic modulus of FRP,  $d$  is the effective depth of the beam, and  $\beta$  is angle between principal fiber orientation and longitudinal axis of the beam.

The application of Equation (2-1) requires the quantification of the effective strain,  $\varepsilon_{fe}$ . Triantafillou observed the effective strain to be a function of the axial rigidity of the FRP sheet expressed by  $\rho_f E_f$ . The effective strain was, therefore, determined by finding  $V_f$  experimentally for several rigidities of FRP sheet. Based on the experimental results, the effective strain was back calculated and plotted versus the axial rigidity. A relationship between effective strain and

axial rigidity was derived experimentally through curve fitting of about 38 test results found in the literature and he proposed the following equation:

$$\varepsilon_{fe} = 0.0119 - 0.0205 (\rho_f E_f) + 0.0104 (\rho_f E_f)^2 \quad \text{for } 0 \leq \rho_f E_f \leq 1 \text{ GPa} \quad (2-2a)$$

$$\varepsilon_{fe} = 0.00245 - 0.00065 (\rho_f E_f) \quad \text{for } \rho_f E_f > 1 \text{ GPa} \quad (2-2b)$$

The modeling approach of Triantafillou had the following shortcomings:

1. Equation (2-2b) was based on fitting some wrong data considering the value of  $\rho_f E_f$  equals to 2.76 instead of 0.25 for two of the test specimens. A comparison between the correct experimental results and Equations 2-2 a&b is shown in Figure 2-2. As shown in this graph, there is no data of  $\rho_f E_f = 2.76$ .
2. The data used to produce Equations (2-2a and b), 38 test results, included three types of FRP (CFRP, AFRP, and GFRP), whereas the fracture capacity of each type could be different.
3. The wrapping schemes (totally wrapped, U-wrap, and FRP on two beam sides), that have a significant affect on FRP contribution and mode of failure were not considered as design variables.
4. The concrete strength, which is expected to affect the bond behavior, was not considered.
5. One equation was used to describe both modes of failure (FRP fracture and debonding).
6. The partial safety factor for CFRP material (Eurocode design format) was suggested to be equal to the partial safety factor for steel,  $\gamma_f = 1.15$ . A more conservative partial safety factor should be considered for the relatively new material.
7. In equation (2-1), the depth of concrete section,  $d$ , should be modified to be the effective depth of FRP reinforcement,  $d_f$ .
8. The control of shear crack was not addressed or considered.
9. No limit on the maximum amount of additional shear strength provided by FRP to preclude the web crushing was addressed.
10. The maximum spacing of FRP strips was not addressed.

In spite of the above shortcomings, Triantafillou's model was the first systematic attempt to characterize the contribution of externally bonded FRP to the shear capacity. In addition,

most of the shortcomings may be due to the relative lack of suitable experimental results available at that time.

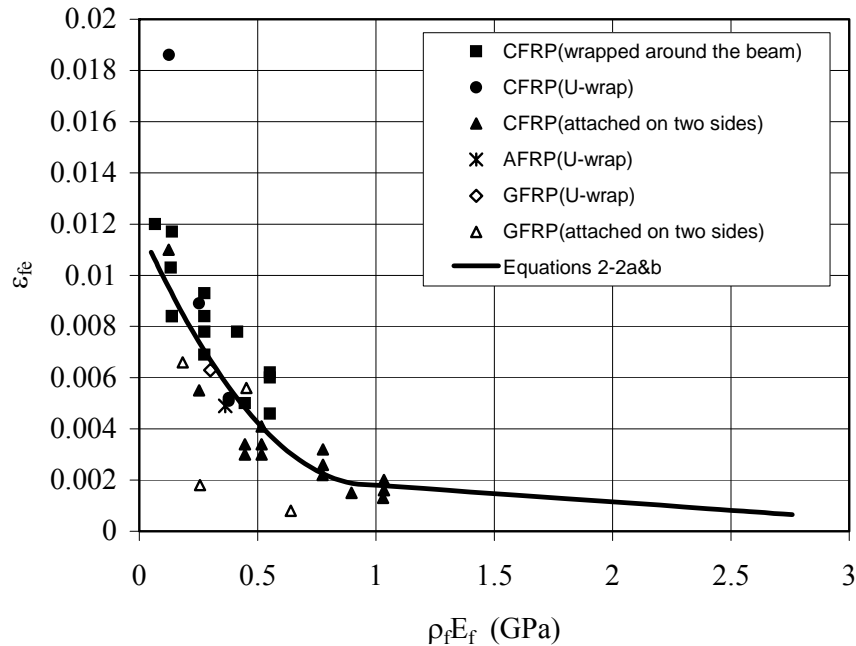


**Figure 2-2.** Comparison between the correct experimental results and Equations 2-2 a&b

From the review of the literature, most of the experimental studies focused on the capability of the externally bonded FRP composites to enhance the shear capacity of RC beams, and the investigation of the possible failure modes. However, the factors that influence shear strength of the strengthened beams were not systematically addressed. Most of the studies dealt with simply supported rectangular beams and the effectiveness of the strengthening system to increase the shear capacity in negative moment regions and T cross-section beams not clearly investigated. In addition, some of the available tests were conducted on specimens with unpractical dimensions,<sup>5,16</sup> which might have affected the failure mode.

From an analytical standpoint, it is clear from the above review that although some studies on shear strengthening of RC beams exist, the design of such members is far from being straightforward and contradictory. Moreover, the relatively good agreement between models and experimental results is attributed to the fact that, the same set of data have been used for both calibration and comparison.<sup>2,3,5,8,9</sup>

Based on the present level of knowledge and the above review, it can be concluded that more experimental and analytical work is needed to investigate the performance and the factors affecting the shear capacity of strengthened beams and to propose a better and more rational design approach for those members.

## **2-5 SHEAR STRENGTHENING OPTIONS**

### **2-5-1 General**

In shear strengthening situations of RC beam, externally bonded FRP reinforcement is used to wrap the beam cross section with the fibers in the transverse direction in order to reinforce diagonal tension cracks in much the same way as steel stirrups. From this general approach, several configurations of FRP shear reinforcement have been devised and investigated.<sup>29</sup> The goal of this section is to describe several alternatives that are available to the designer.

### **2-5-2 Bonded Surface Configurations**

In shear strengthening situations of RC beams, three options of FRP bonded surface configurations, as shown in Figure (2-3), have been investigated.<sup>2,6,10</sup> The first option is to apply the FRP reinforcement on both sides of the beam. The effectiveness of this configuration is limited due to possible debonding failure of the FRP reinforcement.<sup>29</sup> The second option is to wrap the sides and bottom of the beam, U-wrap. The U-wrap is practical and is relatively effective in increasing the shear capacity of the beams.<sup>10</sup> However, when the shear cracks develop at approximately 45 degree, the FRP reinforcement (U-wrap) may have minimal bonded length near the compression flange of a T-section, usually leading to a premature failure due to debonding. This situation is even more critical in negative moment regions as cracks develop from the topside of the member. It has been found that total wrap or U-wrap with end anchor are the alternative solution for U-wrap if debonding is to be avoided.<sup>9,17</sup> However, total wrap is not practical from a constructability standpoint. The presence of monolithic slabs often prevents wrapping the sheet around the top of the section. One option might be to drill holes through the slab and wrap strips of FRP around the section. However this method is rather complicated. On

the other hand, It has been shown that the anchorage of the ends of U-wrap is practical and effective.<sup>7,17</sup>

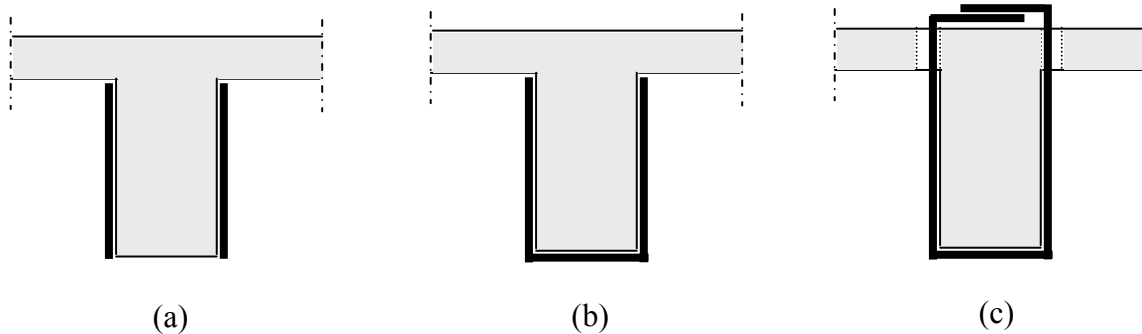


**Figure 2-3.** Various schemes for wrapping transverse FRP reinforcement. (a) FRP bonded to the two beam sides. (b) FRP “U” wrap. (c) FRP wrapped entirely around the beam.

### 2-5-3 End Anchor

It has been shown that the anchorage of the ends of the sheets with steel plates and bolts is effective and can increase the shear capacity of RC members (Fig. 2- 4). In the case of U-wraps, it was observed that anchoring increased the shear capacity by about 20% above that of specimens with no end anchorage.<sup>7</sup> By using this technique and testing specimens under a cyclic load, Sato et al.<sup>17</sup> showed that the seismic retrofitting of RC beams using FRP sheets becomes practical and efficient. Mechanical anchors made of steel, although effective in the laboratory, are not very practical for field application due to drawbacks such as stress concentration and, in the case of bolting, discontinuity of the FRP at drilling locations. In the case of carbon FRP, the likelihood of galvanic corrosion due to steel-carbon fiber contact is also a concern.

In order to eliminate the problems associated with traditional anchors, an innovative anchoring system was proposed<sup>30</sup> using FRP materials only. The system has been called U-anchor and discussed later in Chapters 3 and 4.

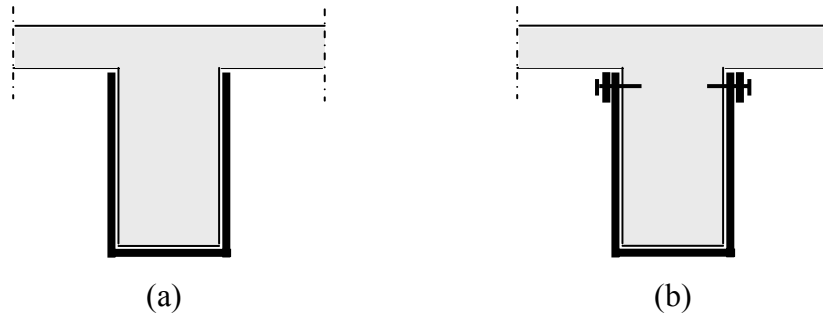


**Figure 2-4.** End anchor options. (a) U-wrap without end anchor. (b) U-wrap with end anchor.

#### 2-5-4 Shear reinforcement spacing

The transverse FRP reinforcement may be in the form of a continuous wrap or as spaced strips as illustrated in [Figure 2-5](#). The use of strips may be effective in optimizing the amount of material used.

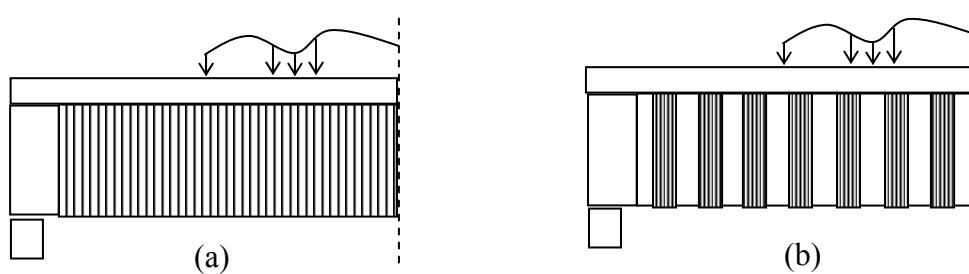


**Figure 2-5.** Shear reinforcement distributions. (a) Continuous. (b) Strips.

#### 2-5-5 Fiber Orientation

Because FRP is an anisotropic material with high strength in the direction of the fibers, the fibers may be oriented in such a way to best reinforce diagonal tension cracks. This is achieved by the use of inclined strips ([Fig. 2-6](#)). However, vertical plies are easier to install just as in the case of vertical and inclined stirrups.

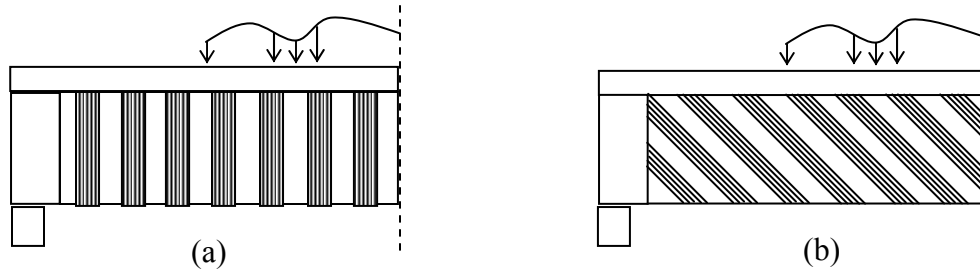


**Figure 2-6.** Fiber orientations. (a)  $90^{\circ}$  wrap. (b)  $45^{\circ}$  wrap.

### 2-5-6 Bi-axial Reinforcement

It has been found that the use of bi-axial FRP reinforcement may enhance the overall performance of the strengthening system.<sup>31</sup> Bi-axial FRP reinforcement is achieved by applying two unidirectional FRP plies in perpendicular directions (Fig. 2-7).

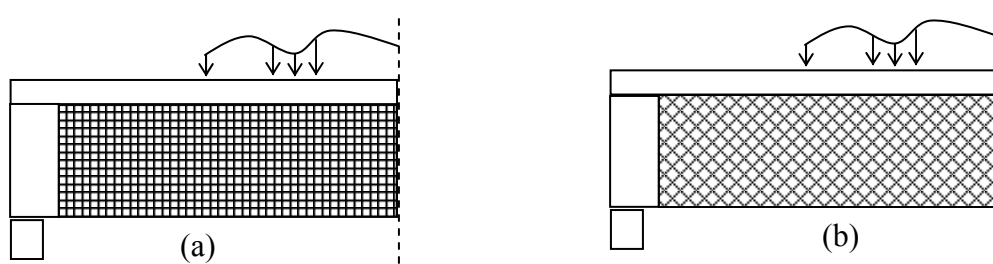


**Figure 2-7.** Bi-axial FRP sheet reinforcement orientations. (a)  $90^{\circ}/0^{\circ}$ . (b)  $\pm 45^{\circ}$

## CHAPTER 3

### EXPERIMENTAL PROGRAM

#### 3-1 GENERAL

The experimental program consisted of testing twenty-seven, full-scale, RC beams. The beams were grouped into three main series designated A, B, and C. The first series of tests, Series A, focused on shear strengthening of simply supported beams with rectangular cross-section.<sup>32,33</sup> The second series, Series B, addressed the shear strengthening of continuous beams.<sup>34</sup> The last series of tests, Series C, investigated the strengthening of simply supported beams with T-shaped cross-section.<sup>35</sup>

The variables investigated in this research study included steel stirrups (i.e., beams with and without steel stirrups), shear span-to depth ratio (i.e., a/d ratio 3 versus 4), CFRP amount and distribution (i.e., continuous wrap versus strips), bonded surface (i.e., lateral sides versus U-wrap), fiber orientation (i.e.,  $90^0/0^0$  fiber combination versus  $90^0$  direction), and end anchor (i.e., U-wrap with and without end anchor).

#### 3-2 SIMPLY SUPPORTED BEAMS WITH RECTANGULAR CROSS-SECTION

##### 3-2-1 General

In this series, twelve full-scale rectangular beam specimens designed to fail in shear were strengthened with different CFRP schemes. These members were tested as simply supported beams using a four-point loading configuration. The variable investigated in this test series included steel stirrups, shear span-to-depth ratios (a/d ratios), and CFRP amount and distribution.

### 3-2-2 Test Specimens

The beam specimens of Series A had a total span of 3050 mm and a rectangular cross section of 150 mm wide and 305 mm deep. The specimens were grouped into two main groups designated as A-SW for specimens with stirrups and A-SO for specimens without stirrups in the shear span of interest. The details and dimensions of the specimens of those two groups are illustrated in [Figure \(3-1\)](#).

Group A-SW consisted of four specimens. In this group, four 32-mm bars were used as longitudinal reinforcement with two at top and two at bottom face of the cross section. The specimens were reinforced with 10-mm steel stirrups throughout their entire span. The stirrups spacing in the shear span of interest, right half, was selected to allow failure in that span ([Fig. 3-1 \(a\)](#)).

Group A-SO consisted of eight specimens, which had the same cross section dimensions and longitudinal steel reinforcement as for Group A-SW. No stirrups were provided in the test half span as illustrated in [Figure \(3-1\(b\)\)](#).

Each main Groups (i.e., Groups A-SW and A-SO) was subdivided into two subgroups according to shear span-to-depth ratio, namely:  $a/d = 3$  and 4, and resulting in the following four Subgroups: A-SW3, A-SW4, A-SO3, and A-SO4.

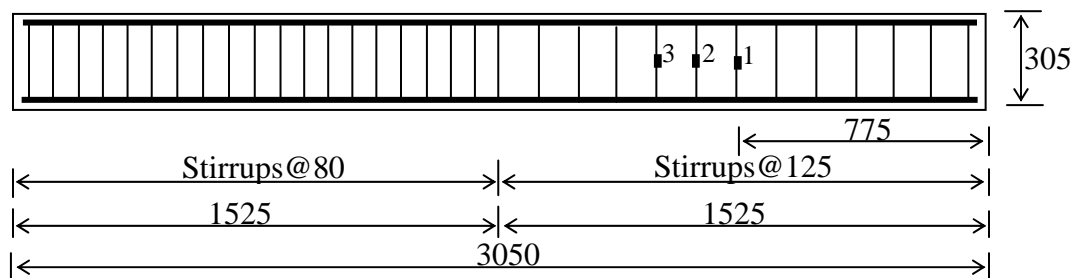
### 3-2-3 Materials

#### 3-2-3-1 Concrete

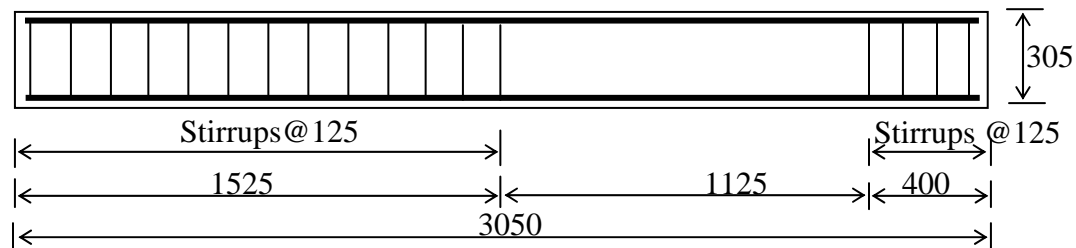
Each of the specimen of the main groups (i.e., Groups A-SW and A-SO) was made from the same batch of a ready-mix normal weight concrete using conventional fabrication and curing techniques. Twelve 150×300 mm concrete cylinders were cast along with each group and cured under the same conditions as the specimens. The cylinders were tested just after the completion of the specimen test. The average concrete strength was determined to be 19.3 MPa and 27.5 MPa for specimens of Groups A-SW and A-SO, respectively.

### 3-2-3-2 Steel Reinforcement

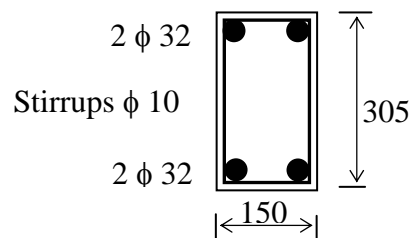
The longitudinal steel reinforcing bars were deformed, hot-rolled, high-yield strength, with 32-mm diameter. The stirrups were made from deformed steel bars with 10-mm diameter. Three coupons of steel bars were tested under uniaxial tension in accordance with ASTM specifications. For 32-mm bars, the average yield stress was 460 MPa, the average ultimate tensile strength was 730 MPa, and the average modulus of elasticity was 200 GPa. In the case of 10-mm bars, the values were 350 MPa for the average yield stress, 530 MPa for the average ultimate tensile strength, and 200 GPa for the average modulus of elasticity.



(a) Group A-SW



(b) Group A-SO



(c) Specimens cross-section for Groups A-SW and A-SO

Dimensions in mm

■ Strain gauge location on stirrups

**Figure 3-1.** Configuration and reinforcement details for beam specimens of Series A

### 3-2-3-3 Composite Strengthening System

The composite strengthening system used in this research study was provided by Master Builder Technologies, Inc. The system is comprised of four basic components namely: primer, putty, saturant, and fiber sheets. The combination of these four components forms a high-strength FRP laminate.

**Resins:** The fiber sheets were bonded to the concrete surface using three epoxy-based resins. The resins used were primer, putty and saturant. The properties of the resins in tension are listed in **Table (3-1)**. The values listed were obtained from the manufacturer.<sup>29</sup>

**Table 3-1** Resin properties in tension

Material	Stress at yield (MPa)	Stress at rupture (MPa)	Strain at yield	Strain at rupture	Elastic modulus (MPa)	Poisson's ratio
Primer	14.50	17.20	0.040	0.040	715.0	0.48
Putty	13.10	14.50	0.020	0.070	1790.0	0.48
Saturant	53.80	54.50	0.025	0.035	3035.0	0.40

**Carbon Fiber Sheets:** The carbon fibers used in this program were in the form of dry unidirectional flexible sheets. The sheets had a paper backing and were supplied in a roll of 500-mm width. The carbon fibers were manufactured<sup>29</sup> by pyrolyzing polyacrylonitrile (PAN) based precursor fibers at temperatures of approximately 1500 °C. The result of the pyrolyzation process was a highly aligned carbon fiber chain. The carbon fiber filaments were assembled into untwisted tows that were then used to create a continuous unidirectional sheet.

According to the manufacturer's information, the tensile strength of CFRP sheet is 3790 MPa, the modulus of elasticity is 228 GPa, and the design thickness is 0.165 mm (fiber only). These values were determined by tensile testing of CFRP specimens.<sup>29</sup> Note that, the tensile strength and the elastic modulus of the resin is neglected in computing the strength of the system. Therefore, stresses are calculated using the net area of the fiber only.

**Installation Procedure:** CFRP sheets were attached to the concrete surface by manual lay-up. The components of the strengthening system are illustrated in **Figure (3-2)**.

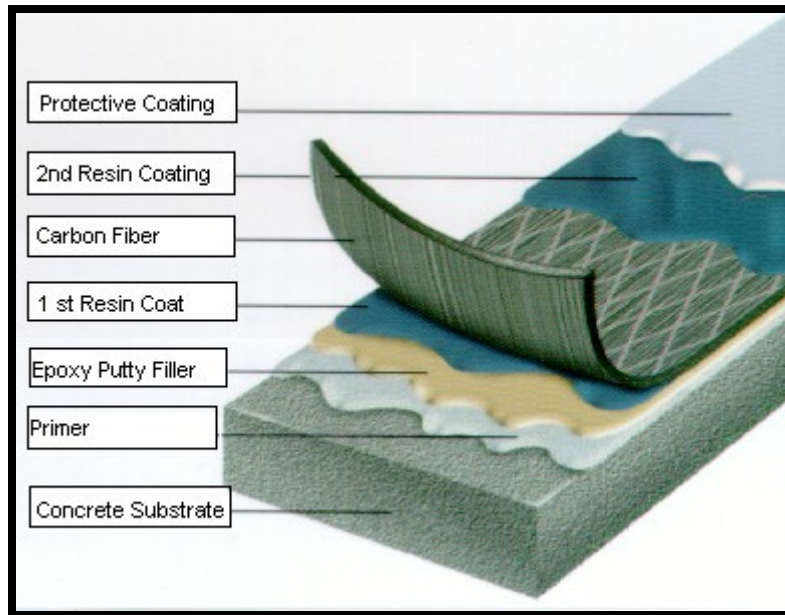


**Figure 3-2** Components of the strengthening system

The procedure employed to apply the CFRP sheets was that recommended by the manufacturer, which may be summarized as follows:

- Prior to installing the FRP sheets, the edges of the beams were rounded (radius of approximately 15mm) at the positions of wrapping. The concrete surface was prepared using water blasting (it is allowed to use either sand blasting, water basting or any other mechanical abrasion techniques) to open the pore structure. The beams were allowed to dry prior to FRP application. In field applications, cracks, spalls and corroding reinforcing steel should be addressed prior to installing the FRP system. All cracks greater than 0.25mm in width should be epoxy injected. Corroding reinforcing steel should be cleaned (or replaced). The surface of concrete should be free of loose materials.
- The prepared concrete surface was coated with a layer of epoxy-based primer using a short nap roller. The function of the primer is to penetrate the concrete pores to provide an improved adhesive bond for the saturating resin.

- After the primer had become tack-free, a thin layer of putty, a thick epoxy-based paste, was applied using a trowel. The functions of the putty are to level the surface and to patch the small holes.
- A first coat of saturant resin was then applied using a medium nap roller after the putty had become tack free. The functions of the saturant resin are to impregnate the dry fibers, to maintain the fibers in their intended orientation, to distribute stress to the fibers, and to protect the fibers from abrasion and environmental effects.
- The fiber sheets were measured and pre-cut prior to installing on the surface. Each sheet was then placed on the concrete surface and gently pressed into the saturant. Prior to removing the backing paper, a trowel was used to remove any air bubbles. After the backing paper was removed, a ribbed roller was rolled in the fiber direction to facilitate impregnation by separating the fibers.
- The sheet was then coated with a second layer of saturant resin and the excessive resin was removed.

#### 3-2-3-4 Summary of the Material Properties

The summary of the mechanical properties of the materials used for manufacturing the test specimens of Series A (i.e., concrete, steel, and CFRP sheets) is listed in [Table \(3-2\)](#).

**Table 3-2** Materials properties for Series A specimens

Material	Specifications	Compressive strength (MPa)	Yield point (MPa)	Ultimate tensile strength (MPa)	Modulus of elasticity (GPa)
Concrete	Group A-SW	19.3	-----	-----	20
	Group A-SO	27.5	-----	-----	25
Steel reinforcing	$\phi = 32$ mm	-----	460	730	200
	$\phi = 10$ mm	-----	350	530	200
CFRP sheet*	$t_f = 0.165$ mm	-----	-----	3,790	228

\* fiber only

### 3-2-4 Strengthening Schemes

One specimen from each subgroup (A-SW3-1, A-SW4-1, A-SO3-1, and A-SO4-1) was kept without strengthening as a control specimen, whereas eight beam specimens were strengthened with externally bonded CFRP sheets following three different schemes as illustrated in [Figure \(3-3\)](#).

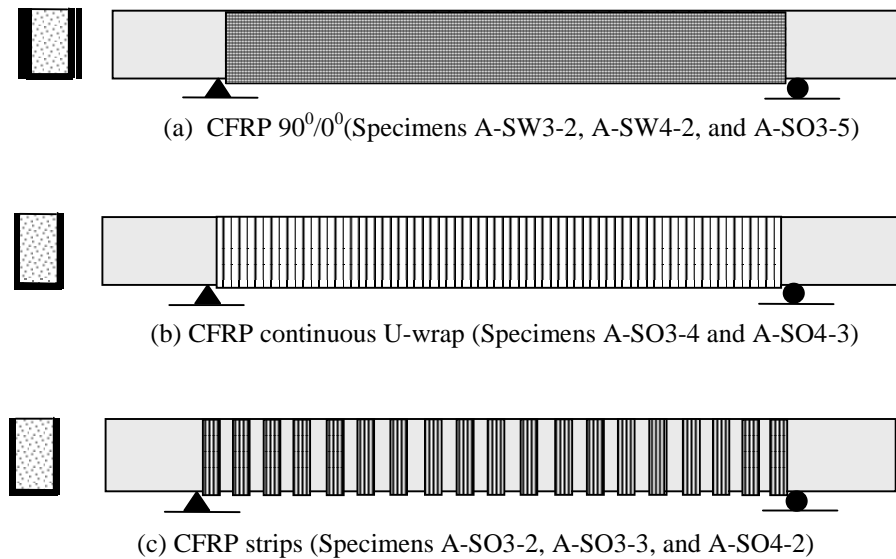


**Figure 3-3.** Schematic representation of CFRP strengthening schemes

In Subgroup A-SW3, Specimen A-SW3-2 was strengthened with two CFRP plies having perpendicular fiber directions ( $90^{\circ}/0^{\circ}$ ) as shown in [Figure \(3-3\(a\)\)](#). The first ply was attached in the form of continuous U-wrap with the fiber direction oriented perpendicular to the longitudinal axis of the specimen ( $90^{\circ}$ ). The second ply was bonded on the two sides of the specimen with the fiber direction parallel to the beam axis ( $0^{\circ}$ ). This ply (i.e.,  $0^{\circ}$  ply) was added to investigate the impact of horizontal restraint on shear strength. The CFRP sheets were applied to the specimens following the manufacturer's recommendations as discussed earlier. In Subgroup A-SW4, Specimen A-SW4-2 was strengthened with two CFRP plies having perpendicular fiber direction ( $90^{\circ}/0^{\circ}$ ) as for Specimen A-SW3-2.

Four specimens were strengthened in Subgroup A-SO3. Specimen A-SO3-2 was strengthened with one-ply CFRP strips in the form of U-wrap with  $90^0$  fiber orientation as shown in Figure (3-3(c)). The strip width was 50 mm with center-to-center spacing of 125 mm. Specimen A-SO3-3 was strengthened in a manner similar to that of Specimen A-SO3-2 but with strip width equal to 75 mm. Specimen A-SO3-4 was strengthened with one-ply continuous U-wrap ( $90^0$ ). Specimen A-SO3-5 was strengthened with two CFRP plies ( $90^0/0^0$ ) similar to Specimens A-SW3-2 and A-SW4-2. In Subgroup A-SO4, two beam specimens were strengthened. Specimen A-SO4-2 was strengthened with one-ply CFRP strips in the form of U-wrap similar to Specimen A-SO3-2. Specimen A-SO4-3 was strengthened with one-ply continuous U-wrap ( $90^0$ ) similar to A-SO3-4.

### 3-2-5 Test Setup and Instrumentation

All specimens were tested as simply supported beams subjected to a four-point load as illustrated in Figure (3-4).

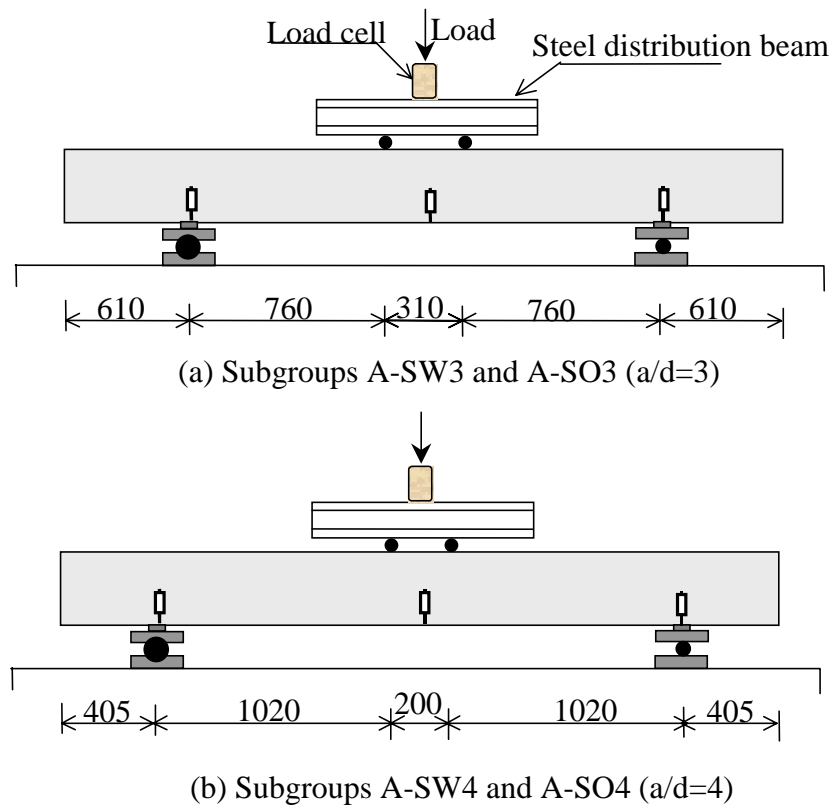


**Figure 3-4.** Schematic representation of test set-up for Series A

A universal testing machine with 1800 kN capacity was used to apply a concentrated load on a steel distribution beam used to generate the two concentrated loads. A photo showing the test setup of Specimen A-SO4-2 is given in Figure (3-5).

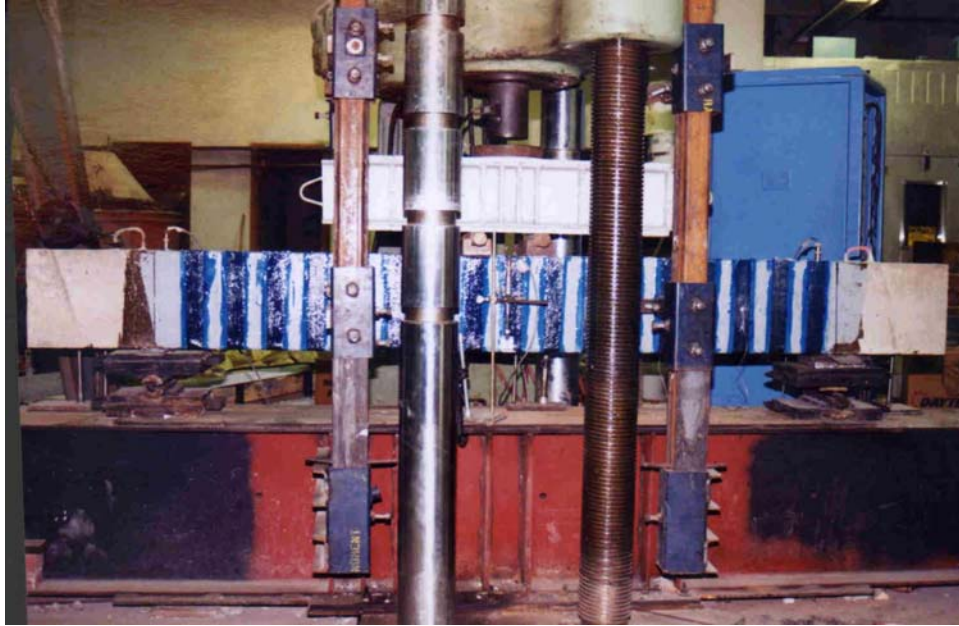


**Figure 3-5.** Test set-up of Specimen A-SO4-2

Four linear variable differential transformers (LVDTs) were used for each test to monitor vertical displacements at various locations as shown in Figure (3-4). Two LVDTs were located at mid-span on each side of the specimen. The other two LVDTs were located at the specimen supports to record support settlement.

For each specimen of Group A-SW, six strain gauges were attached to three stirrups to monitor the stirrup strain during loading as illustrated in Figure (3-1(a)). In addition, three strain gauges were attached directly to the FRP sheet on the sides of each strengthened beam to monitor strain variation in the FRP. The strain gauges were oriented in the vertical direction and located at the section mid-height with distances of 175-mm, 300-mm, and 425-mm from the support for Subgroups A-SW3 and A-SO3 specimens. For specimens of Subgroups A-SW4 and

A-SO4, the strain gauges were located at distance of 375-mm, 500-mm, and 625-mm from the support.

### **3-2-6 Test Procedure**

The specimens were subjected to repeated loading, usually one cycle before cracking followed by three cycles with the last one up to ultimate. Note that, the applied load versus deflection curves shown in this study are the envelopes of these load cycles.

The data generated from the load cell, the LVDTs, and the strain gauges were collected by a data acquisition system at a frequency of 1 HZ. This data acquisition system included a Data General Conditioner Rack and LABTECH (Laboratory Technologies Corp.) data acquisition software. The system has the capability of reading up to 32 data channels.

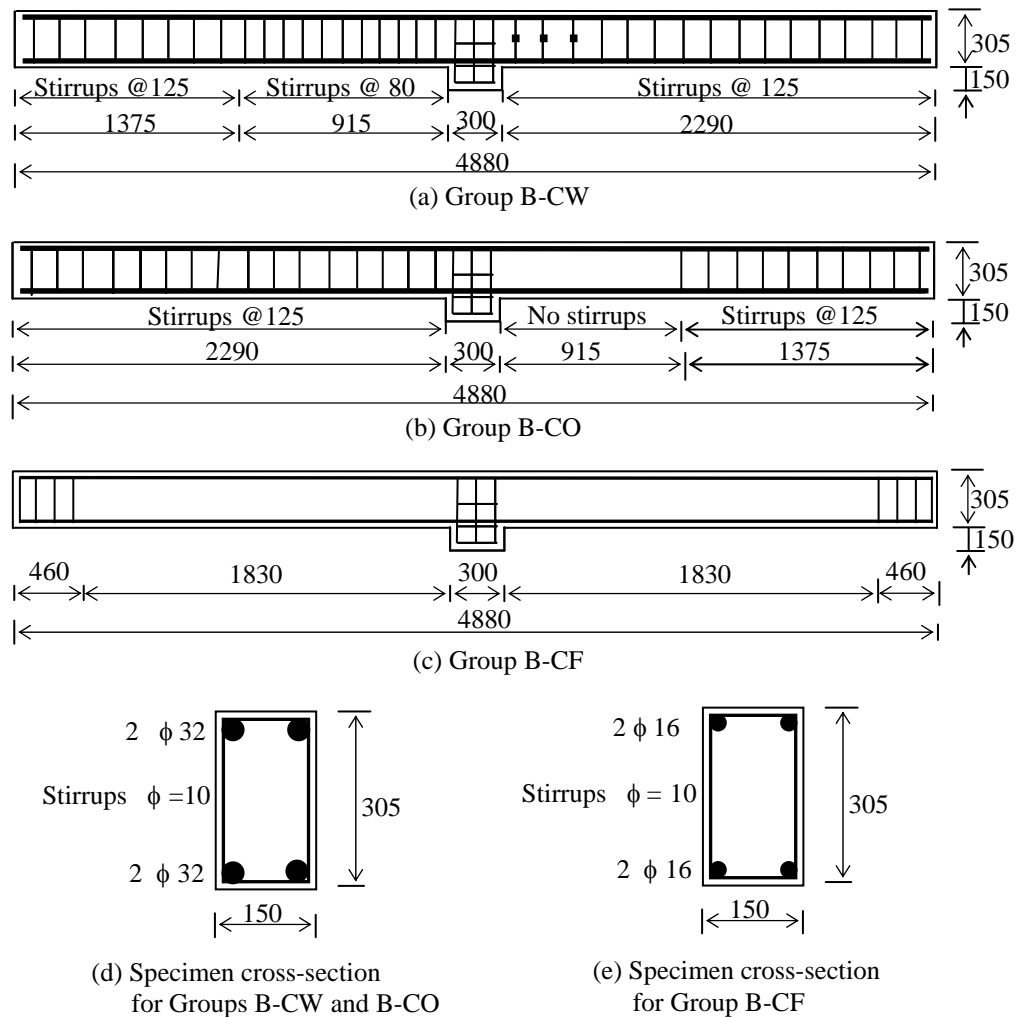
## **3-3 CONTINUOUS BEAMS WITH RECTANGULAR CROSS-SECTION**

### **3-3-1 General**

In continuous beams large shear forces are combined with large bending moments. In addition, in the negative moment regions of continuous beams, shear cracks initiates from the top of the section. In this case, the U-wrap FRP reinforcement may not be able to control the initiation of these cracks, and may have less effectiveness to enhance shear capacity. However, most of the research studies have dealt with shear strengthening of simply supported beams (strengthening in positive moment regions) and shear strengthening in negative moment regions is not yet clear. To fill this gap, nine full-scale, two-span, continuous rectangular beam specimens were investigated. The variables studied in this test series included steel stirrups, CFRP amount and distribution, and CFRP wrapping schemes.

### **3-3-2 Test Specimens and Materials**

The beam specimens of Series B were subdivided into three groups designated as B-CW, B-CO, and B-CF (Fig. 3-6). Each group had different longitudinal and shear steel reinforcement ratios.



Dimensions in mm

■ Strain gauge location

**Figure 3-6.** Configuration and reinforcement details for beam specimens of Series B

Group B-CW consisted of two beam specimens tested over a total span of 4,880 mm as illustrated in [Figure \(3-6\(a\)\)](#). The central support consisted of a 300-mm offset intended to represent the intersection with a column. The concrete strength at testing was 27.5 MPa. In this series, four 32-mm bars were used as longitudinal reinforcement with two at top and two at bottom face of the cross section. The specimens were reinforced with 10-mm stirrups throughout. The stirrup spacing in the shear span of interest was selected to force failure in that span.

Group B-CO consisted of three beam specimens, and had similar longitudinal reinforcement as that of group B-CW (Fig. 3-6(b)). No steel stirrups were provided in the tested shear span. The concrete strength at testing for this series was 20.5 MPa.

Four beam specimens were included in Group B-CF (Fig. 3-6(c)). The concrete strength at testing for this series was 50 MPa. The specimens were reinforced with four 16-mm longitudinal steel bars with two at top and two at bottom faces of the cross-section with no shear reinforcement provided.

The engineering properties of the materials used for manufacturing the test specimens are listed in Table (3-3). Fabrication of the specimens including surface preparation and CFRP installation is similar to that of beam specimens of Series A.

**Table 3-3** Materials properties of Series B specimens

Material	Specifications	Compressive strength (MPa)	Yield point (MPa)	Ultimate tensile strength (MPa)	Modulus of elasticity (GPa)
Concrete	Group B-CW	27.5	----	----	25
	Group B-CO	20.5	----	----	22
	Group B-CF	50.0	----	----	33
Steel reinforcing	$\phi = 32$ mm	----	460	730	200
	$\phi = 16$ mm	----	430	700	200
	$\phi = 10$ mm	----	350	530	200
CFRP sheet*	$t_f = 0.165$ mm	----	----	3,500	228

\* Fiber only

### 3-3-3 Strengthening Schemes

One specimen from each Group (B-CW1, B-CO1, and B-CF1) was not strengthened and was considered as a control specimen, whereas six specimens were strengthened with externally bonded CFRP sheets following different schemes. The strengthening schemes as well as the test setup are illustrated in Figure (3-7).

In Group B-CW, Specimen B-CW2 was strengthened with two CFRP plies having perpendicular fiber directions ( $90^0/0^0$ ) similar to Specimen A-SW3-2.

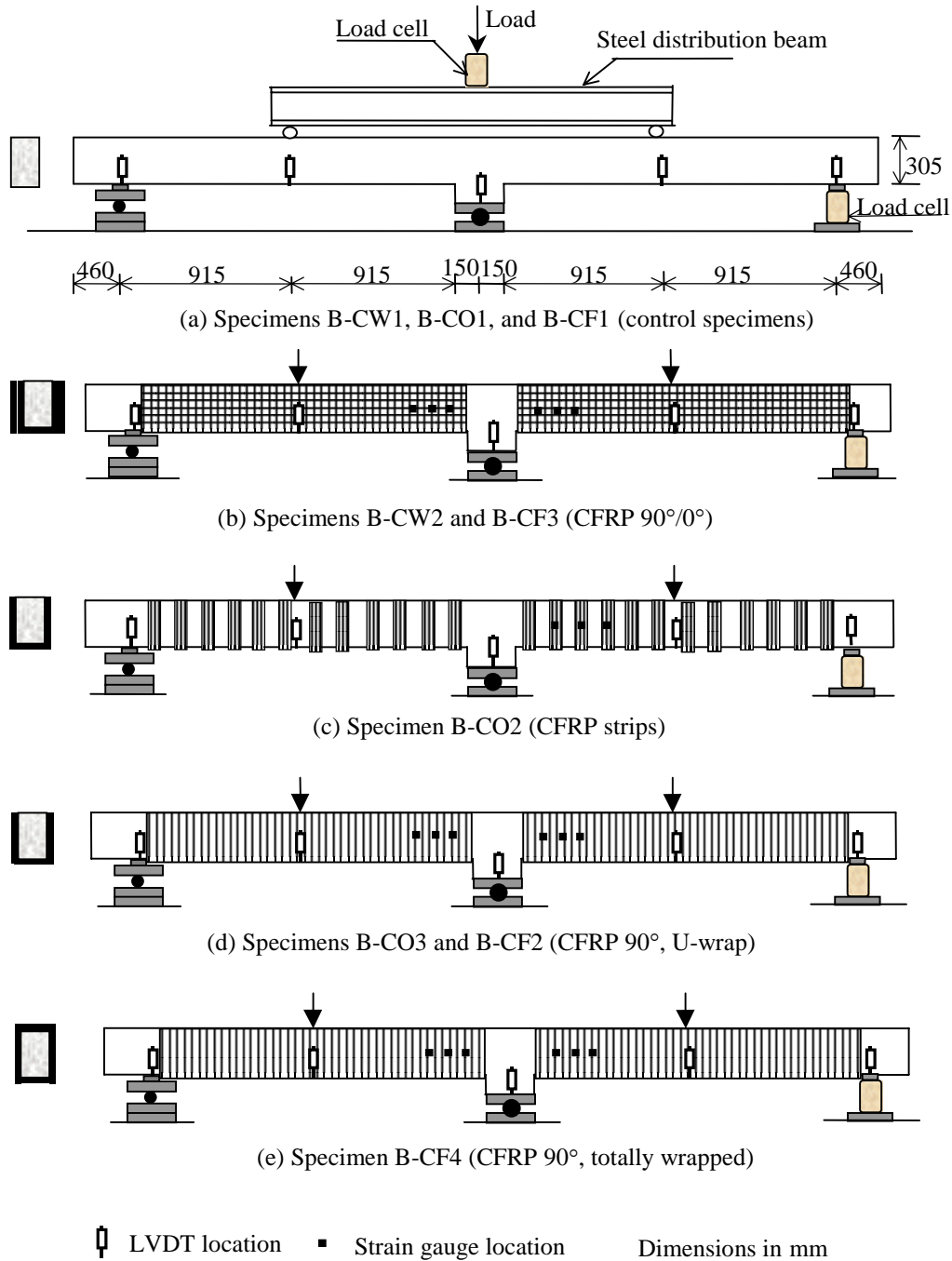


**Figure 3-7.** Strengthening schemes and test set-up for beam specimens of Series B

Two specimens were strengthened in Group B-CO. Specimen B-CO2 was strengthened with one-ply CFRP strips in the form of a U-wrap with  $90^0$  fiber orientation. The strip width was 50 mm with center-to-center spacing of 125 mm. Specimen B-CO3 was strengthened with one-ply continuous U-wrap.

In Group B-CF, three specimens were strengthened. Specimen B-CF2 was strengthened with one-ply continuous U-wrap. Specimen B-CF3 was strengthened with two CFRP plies having perpendicular fiber directions ( $90^0/0^0$ ). Specimen B-CF4 was totally wrapped with one-ply CFRP sheets. The sheets were attached to the four sides of the specimen with an overlap of 50 mm on the topside. Even though total wrapping may not be possible in the field, this case is somehow a representation of the upper threshold.

### 3-3-4 Test Setup and Instrumentation

The specimens were tested as continuous beams under concentrated loads applied to the mid-point of each span. Two load cells were used to monitor total applied load and reaction at the span of interest (Fig. 3-7). This allowed the computation of the exact shear force in the span of interest, independently of re-distribution phenomena. The load was applied progressively in few cycles, usually one cycle before cracking followed by three cycles to ultimate. The shear force versus deflection curves shown in this study are the envelopes of these load cycles.

Five LVDTs were used for each test to monitor the vertical displacement at various locations as illustrated in Figure (3-7). Of these five LVDTs, one was placed at each support to monitor support movement.

For each specimen of Group B-CW, six strain gauges were attached to three stirrups to monitor the strain in the stirrups during loading. Three strain gauges were attached directly to the FRP on the sides of each strengthened specimen of Groups B-CW and B-CO, and six in specimens of Group B-CF as illustrated in Figure (3-7). The strain gauges were oriented in vertical direction and located at mid-height with distances of 175, 300, and 425 mm from the face of the central support. A photo showing the test setup of specimen B-CO2 is given in Figure (3-8).



**Figure 3-8.** Test set-up of Specimen B-CO2

### **3-4 SIMPLY SUPPORTED BEAMS WITH T-CROSS-SECTION**

#### **3-4-1 General**

At present, most of the studies have specifically addressed shear strengthening of rectangular beams. However, T-section beams are of great importance because they are the most commonly used in practice. Also, they represent a more challenging case than rectangular beams due to the flange that reduces the FRP bonded length over the diagonal shear cracks.

In this research study, six full-scale, T-section RC beams designed to fail in shear were strengthened with different CFRP configurations and tested. One specimen was kept without strengthening whereas five specimens were strengthened with different CFRP configurations. The selected parameters were; (a) CFRP amount and distribution (i.e., continuous wrap versus strips); (b) bonded surface (i.e., lateral sides versus U-wrap); (c) fiber orientation (i.e.,  $90^{\circ}$ - $0^{\circ}$  fiber combination versus  $90^{\circ}$  direction); and (d) end anchorage (i.e., U-wrap with and without end anchor).

### 3-4-2 Test Specimens and Materials

The materials used for manufacturing the test specimens and their engineering properties are listed in [Table \(3-4\)](#).

**Table 3-4** Materials properties for Series C specimens

Material	Specifications	Compressive strength (MPa)	Yield point (MPa)	Ultimate tensile strength (MPa)	Modulus of elasticity (GPa)
Concrete	----	35	----	----	28
Steel Reinforcing	$\phi = 28$ mm	----	470	730	200
	$\phi = 13$ mm	----	350	530	200
	$\phi = 10$ mm	----	350	530	200
CFRP sheets*	$t_f = 0.165$ mm	----	----	3,790	228

\* Fiber only

The test specimens were reinforced with two 28-mm bars as longitudinal steel reinforcement and no steel stirrups were provided in the test region. Configuration and reinforcement details for beam specimens of Series C are illustrated in [Figure \(3-9\)](#). A photo showing the beam specimens during casting is given in [Figure \(3-10\)](#).

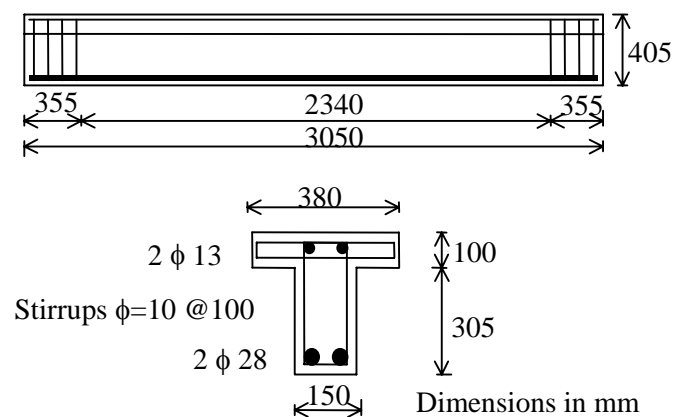


**Figure 3-9.** Configuration and reinforcement details for beam specimens of Series C



**Figure 3-10.** Casting of beam specimens of Series C

### 3-4-3 Strengthening Schemes

Strengthening schemes and test setup of the beam specimens are illustrated in [Figure \(3-11\)](#). Specimen C-BT1 was referred as the control specimen. Specimen C-BT2 was strengthened with one-ply continuous U-wrap throughout the beam span and no end anchors were used. Specimen C-BT3 was strengthened with two CFRP plies having perpendicular fiber direction ( $90^0/0^0$ ). Specimen C-BT4 was strengthened with one-ply CFRP strips in form of a U-wrap with  $90^0$ -fiber orientation. The strip width was 50 mm with center-to-center spacing of 125 mm. Specimen C-BT5 was strengthened with CFRP strips attached only on the two beam sides with  $90^0$ -fiber orientation. The strips width and spacing were similar to specimen C-BT4. Specimen C-BT6 was strengthened with continuous U-wrap with end anchor. The purpose, details, and installation procedure of the end anchor are discussed in the following section.

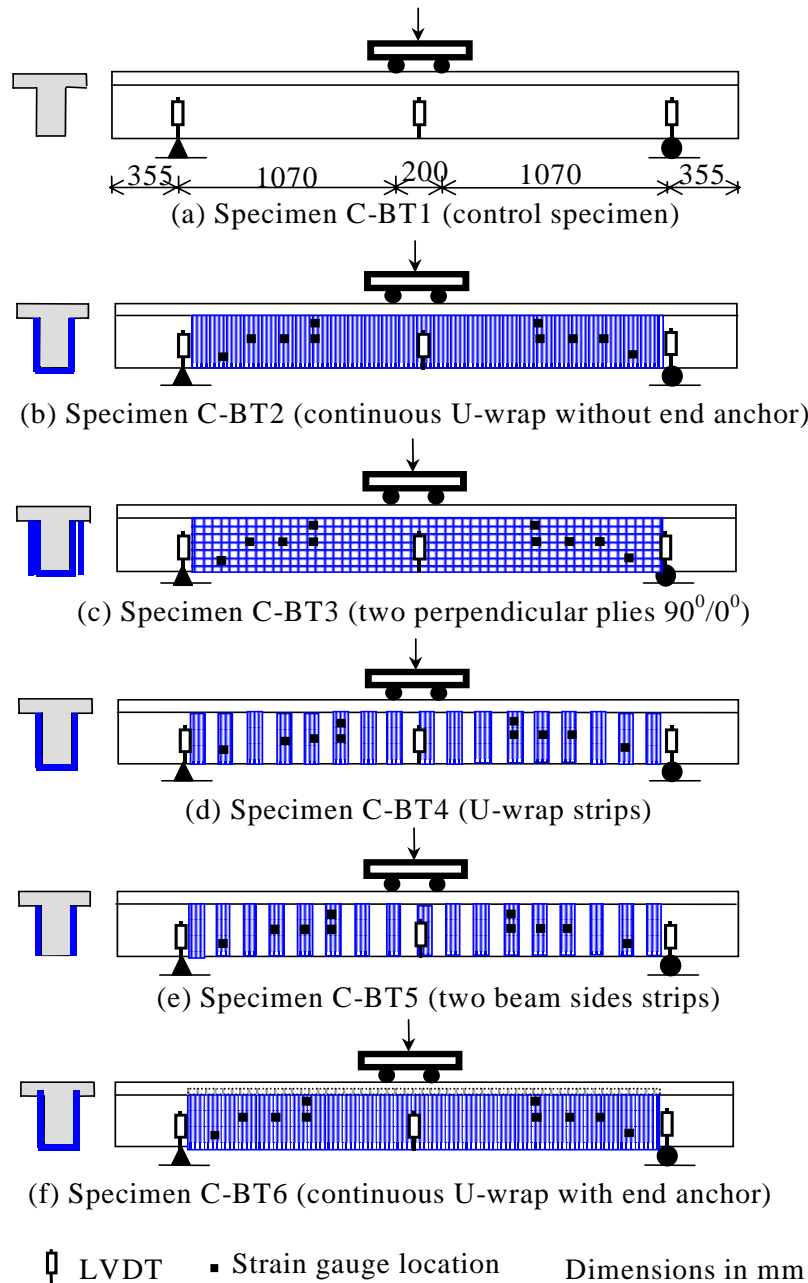


**Figure 3-11.** Strengthening schemes and test set-up for beam specimens of Series C

### 3-4-3-1 U-Wrap with End Anchor

In order to address the problems associated with the debonding of FRP from the concrete surface, and to eliminate the shortcomings of traditional anchors as discussed earlier in Section 2-5-3, an innovative anchoring system was proposed and developed at UMR.<sup>30</sup> The idea is to bent portion of the end of FRP sheet into a preformed groove in the concrete flange at the corner. The

groove is then filled with epoxy paste and includes an FRP rod. The system is called U-anchor. A cross-section showing details of the U-anchor system is given in [Figure \(3-12\)](#).

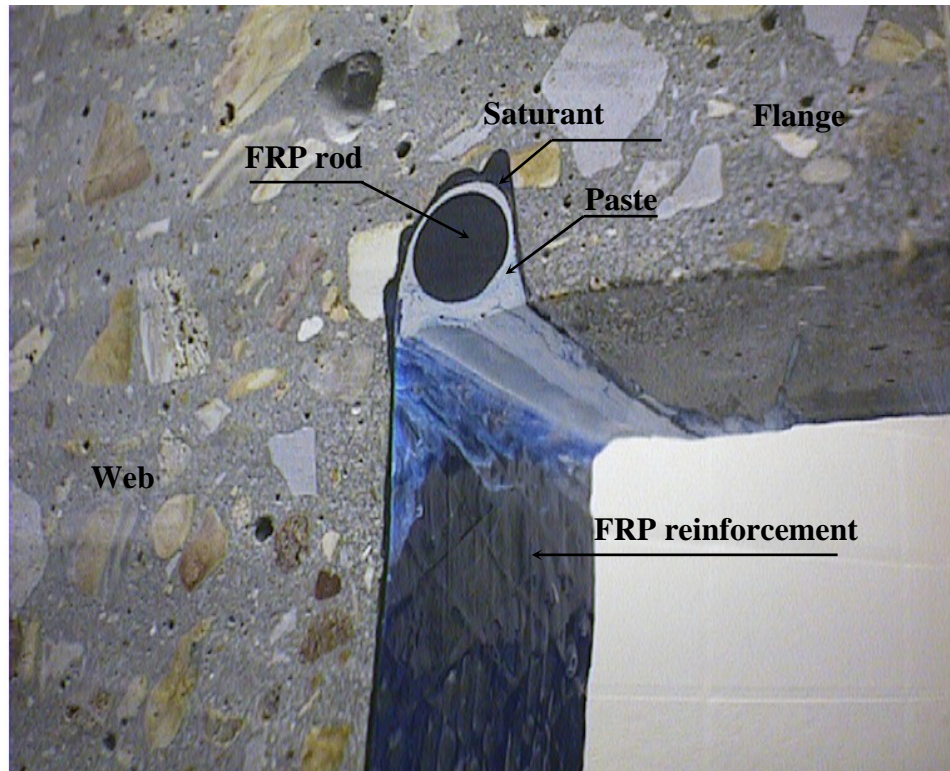


**Figure 3-12.** Details of the U-anchor obtained by slicing a beam

To validate the effectiveness of the U-anchor system, Specimen C-BT6 was strengthened with continuous U-wrap in a manner similar to that of Specimen C-BT2. The ends of the U-wraps in Specimen C-BT6 were anchored to the flanges on both sides of the beam using the U-anchor system.

The anchoring was attained by grooving the concrete flanges at the corner. The groove dimensions was approximately  $15\text{mm} \times 15\text{mm}$  and extended throughout the strengthened length of the specimen. The strengthening work started with concrete surface preparation and priming that included the walls of the groove. The CFRP sheets were bonded to the concrete surface and to the walls of the groove. After the resin impregnating the sheet (saturant) had set, the groove

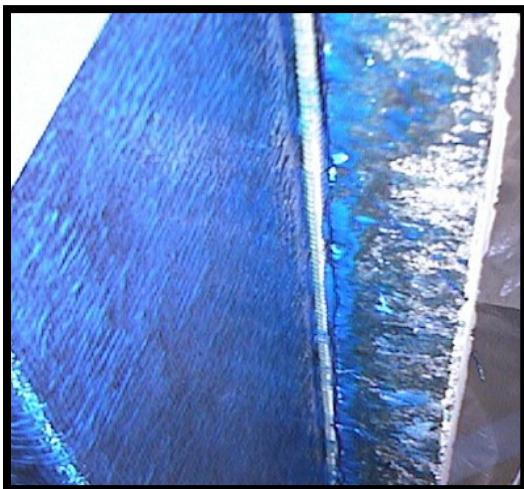
was filled half way with the epoxy paste. The high viscosity paste ensured easy execution. A 10 mm-diameter glass FRP rod was then placed into the groove and was lightly pressed in place. This action forced the paste to flow around the sheet and to cover simultaneously part of the rod and the sides of the sheet. The rod was held in place using wedges. The groove was then filled with the same paste and the surface was leveled. Photographs showing the sequence of steps for CFRP sheet and anchor installation are given in [Figure \(3-13\)](#).



(a) Cutting a groove in the beam flange



(b) Applying CFRP sheet



(c) Inserting a glass FRP rod



(d) Filling the groove with epoxy paste

**Figure 3-13.** End anchor details for Specimen C-BT6

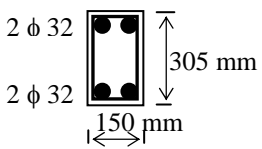
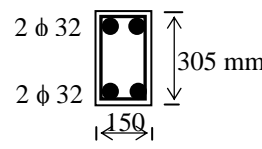
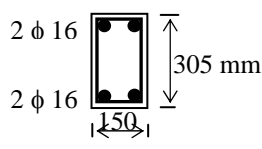
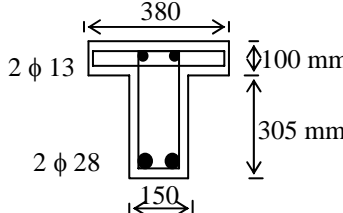
#### **3-4-4 Test Setup and Instrumentation**

All specimens were tested as simply supported beams using a four-point loading with shear span-to-effective depth ratio ( $a/d$ ) equals to 3. A steel distribution beam used to generate the two concentrated loads. The load was applied progressively in cycles as discussed earlier. Four LVDTs were used for each test to monitor vertical displacements at various locations as shown in [Figure \(3-11\)](#). For each specimen, ten strain gauges were attached directly to the FRP on the sides of the strengthened specimens and oriented in the vertical direction to monitor the strain in the FRP. The strain gauges were mounted at the locations of expected shear cracks (as observed in control specimen C-BT1 during testing). Strain gauges positions are shown in [Figure \(3-11\)](#).

#### **3-5 SUMMARY OF THE TEST SPECIMENS**

A summary of structural system, cross-section dimensions and details, shear span-to-depth ratio ( $a/d$ ), concrete strength, steel shear reinforcement, and CFRP strengthening configurations is listed in [Table \(3-5\)](#).

Table 3-5 Summary of test specimens

No.	Specimen designation	Structural system and cross-section details	a/d ratio	Concrete strength ( $f'_c$ ) (MPa)	Shear reinforcement	
					Steel stirrups in test region	CFRP
1	A-SW3-1	Simply supported beams 	3	19.3	$\phi 10 @ 125 \text{mm}$	----
2	A-SW3-2		3	19.3	$\phi 10 @ 125 \text{mm}$	Two plies (90°/0°)
3	A-SW4-1		4	19.3	$\phi 10 @ 125 \text{mm}$	----
4	A-SW4-2		4	19.3	$\phi 10 @ 125 \text{mm}$	Two plies (90°/0°)
5	A-SO3-1		3	27.5	----	----
6	A-SO3-2		3	27.5	----	U-wrap strips, 50 @ 125mm
7	A-SO3-3		3	27.5	----	U-wrap strips, 75 @ 125mm
8	A-SO3-4		3	27.5	----	One ply continuous U-wrap
9	A-SO3-5		3	27.5	----	Two plies (90°/0°)
10	A-SO4-1		4	27.5	----	----
11	A-SO4-2		4	27.5	----	U-wrap strips, 50 @ 125mm
12	A-SO4-3		4	27.5	----	One ply continuous U-wrap
13	B-CW1	Continuous beams	3.6	27.5	$\phi 10 @ 125 \text{mm}$	----
14	B-CW2	Continuous beams 	3.6	27.5	$\phi 10 @ 125 \text{mm}$	Two plies (90°/0°)
15	B-CO1		3.6	20.5	----	---
16	B-CO2		3.6	20.5	----	U-wrap strips, 50 @ 125mm
17	B-CO3	3.6	20.5	----	One ply continuous U-wrap	
18	B-CF1	Continuous beams	3.6	50	----	----
19	B-CF2	Continuous beams 	3.6	50	----	One ply continuous U-wrap
20	B-CF3		3.6	50	----	Two plies (90°/0°)
21	B-CF4		3.6	50	----	One ply, totally wrapped
22	C-BT1		Simply supported beams	3	35	----
23	C-BT2	Simply supported beams 	3	35	----	One ply continuous U-wrap
24	C-BT3		3	35	----	Two plies (90°/0°)
25	C-BT4		3	35	----	U-wrap strips, 50 @ 125mm
26	C-BT5		3	35	----	Two sides strips 50 @ 125
27	C-BT6		3	35	----	U-wrap with end anchor

## **CHAPTER 4**

### **EXPERIMENTAL RESULTS**

#### **4-1 GENERAL**

In the following section, the results obtained from testing twenty-seven, full-scale, RC beams included in this experimental program are presented and discussed. The results recorded for each test included measurements of deflection, stirrup strains (when available), and CFRP strain at various load stages. The observed crack pattern and mode of failure at ultimate are reported. In addition, comparisons of test results to investigate the factors affecting shear strength of strengthened beams are included.

The beam specimens were grouped into three main series designated as A, B, and C. In Series A, twelve rectangular beam specimens were tested as simply supported beams. In Series B, nine rectangular beam specimens were tested as two span continuous beams. In Series C, six T-beam specimens were tested as simply supported beams.

#### **4-2 TEST RESULTS OF SERIES A**

In this series, twelve rectangular beam specimens were tested as simply supported beams. The variable investigated in this test series included steel stirrups, shear span-to-depth ratios, CFRP amount and distribution. The specimens were grouped into four subgroups designated as A-SW3, A-SW4, A-SO3, and A-SO4 depending on the shear reinforcement and shear span-to-depth ratios ( $a/d$  ratios).

##### **4-2-1 Subgroup A-SW3**

Subgroup A-SW3 consisted of two beam specimens had steel stirrups throughout their span. The  $a/d$  ratio of the specimens was taken as 3. In Specimen A-SW3-1, which is referred as the control specimen, shear cracks were formed close to the middle of the shear span when the

load reached approximately 90 kN (corresponding to a shear force of 45 kN and shear stress of 1.2 MPa). As the load increased, additional shear cracks formed throughout, widening and propagating until failure that occurs by shear compression at a total applied load of 253 kN. **Figure (4-1) shows** the crack pattern of Specimen A-SW3-1 at ultimate load.



**Figure 4-1.** Crack pattern at ultimate failure of Specimen A-SW3-1

In Specimen A-SW3-2, which was strengthened with CFRP ( $90^0/0^0$ ), no cracks were visible on the sides or bottom of the test specimen due to the FRP wrapping. However, a longitudinal splitting crack initiated on the top surface of the specimen at a high load of approximately 320 kN. The crack initiated at the location of applied load and extended towards the support. The specimen failed by concrete splitting, as shown in **Figure (4-2)**, at total load of 354 kN. This was an increase of 40% in ultimate capacity compared to the control Specimen A-SW3-1. The splitting failure was due to the relatively high longitudinal compressive stress developed at top of the specimen, which created a transverse tension, led to the splitting failure. In addition, the relatively large amount of longitudinal steel reinforcement combined with over-strengthening for shear by CFRP wrap probably caused this mode of failure. The load versus mid-span deflection curves for Specimens A-SW3-1 and A-SW3-2 are illustrated in **Figure (4-3)** to show the additional capacity gained by CFRP.

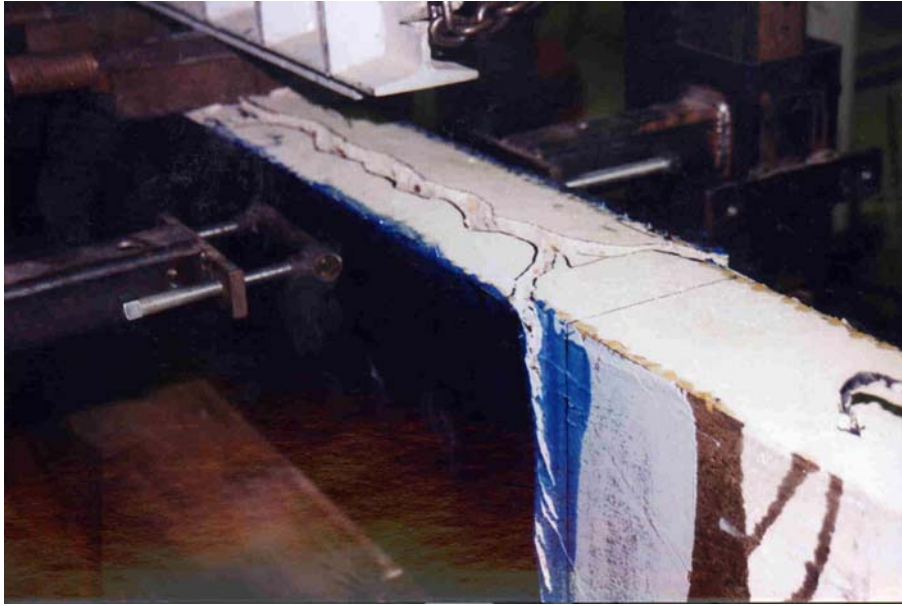


**Figure 4-2.** Splitting failure of Specimen A-SW3-2

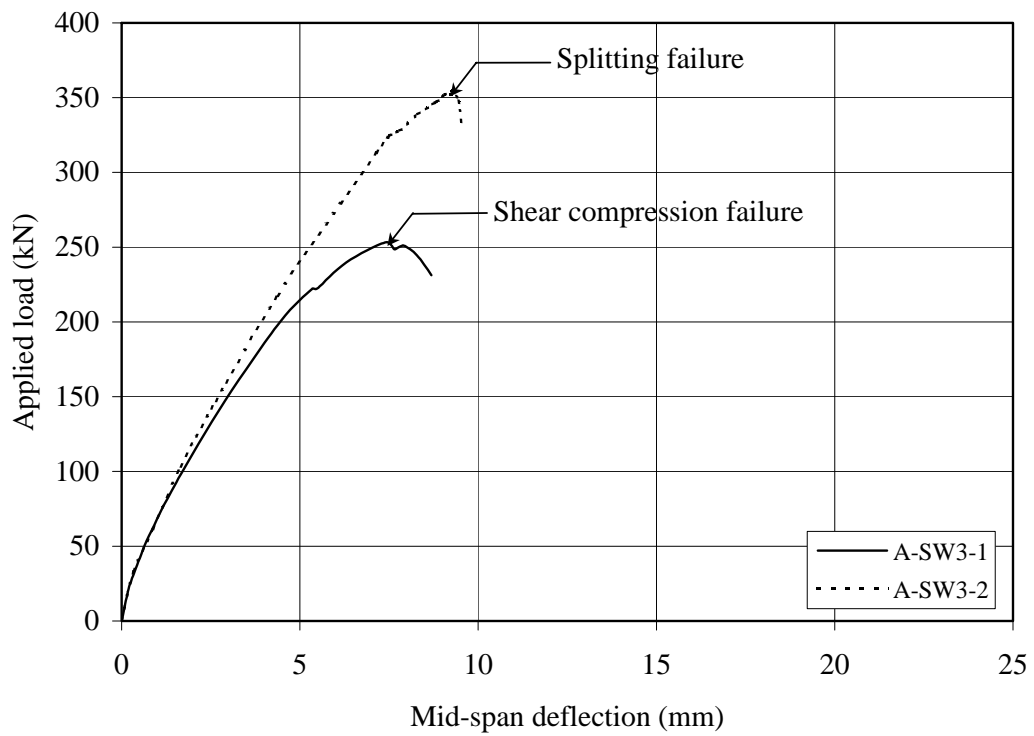


**Figure 4-3.** Experimental load-deflection relationship of Specimens A-SW3-1 and A-SW3-2

The maximum CFRP vertical strain measured at failure in Specimen A-SW3-2 was approximately 0.0023 mm/mm, which corresponded to only 14% of the reported CFRP ultimate strain. This value is not absolute because it greatly depends on the location of the strain gauges with respect to a crack. However, the recorded strain indicates that if the splitting did not occur, the shear capacity could have reached higher load.

Comparison between measured local stirrup strains in Specimens SW3-1 and SW3-2 are shown in **Figure (4-4)**. The stirrups 1, 2, and 3 were located at distance of 175-mm, 300-mm, and 425-mm from the support, respectively. The results showed that the stirrups 2 and 3 did not yield at ultimate for both specimens. The strains (and the forces) in the stirrups of Specimen A-SW3-2 were, in general, smaller than those of Specimen A-SW3-1 at the same level of loading due to the effect of CFRP.

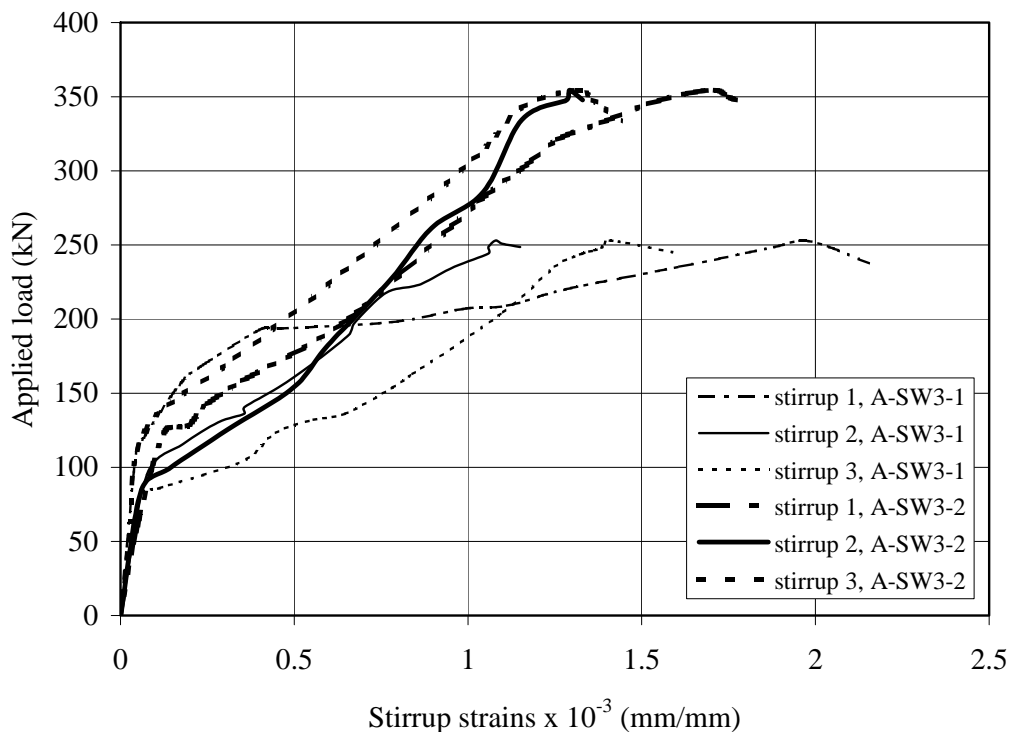


**Figure 4-4.** Applied load versus strains in the stirrups for Specimens A-SW3-1 and A-SW3-2

#### 4-2-2 Subgroup A-SW4

Subgroup A-SW4 consisted of two specimens similar to that of Subgroup A-SW3 except that  $a/d$  ratio was selected to be 4 instead of 3. In Specimen A-SW4-1, the first diagonal crack was formed in the member at a total applied load of 75 kN. As the load increased, additional shear cracks formed throughout the shear span. Failure of the specimen occurred when the total applied load reached 200 kN. This was a decrease of 20% in shear capacity compared to the Specimen A-SW3-1 with  $a/d$  ratio equal to 3. Photos of the ultimate failure for Subgroup A-SW4 specimens are illustrated in [Appendix A](#).

In Specimen A-SW4-2, the failure was controlled by concrete splitting similar to test Specimen A-SW3-2. The total applied load at ultimate was 361 kN with an 80% increase in ultimate capacity compared to the control Specimen A-SW4-1. In addition, the measured strains in the stirrups for Specimen A-SW4-2 were less than those of Specimen A-SW4-1. The applied load versus mid-span deflection curves for beam Specimens A-SW4-1 and A-SW4 are illustrated in [Figure \(4-5\)](#). It may be noted that Specimen A-SW4-2 resulted in greater deflection when compared to Specimen A-SW4-1.

When comparing the test results of Subgroup A-SW3 specimens to that of Subgroup A-SW4, the ultimate failure load of Specimen A-SW3-2 and A-SW4-2 was almost the same. However, the enhanced capacity of Specimen A-SW3-2 ( $a/d = 3$ ) due to the addition of the CFRP reinforcement was 101 kN, while in Specimen A-SW4-2 ( $a/d = 4$ ) was 161 kN. This indicates that the contribution of external CFRP reinforcement may be influenced by the  $a/d$  ratio and appears to decrease with a decreasing  $a/d$  ratio. Further, for both strengthened Specimens (A-SW3-2 and A-SW4-2) CFRP sheets did not fracture or debond from the concrete surface at ultimate and this indicates that CFRP could provide additional strength if the beams did not failed by splitting.

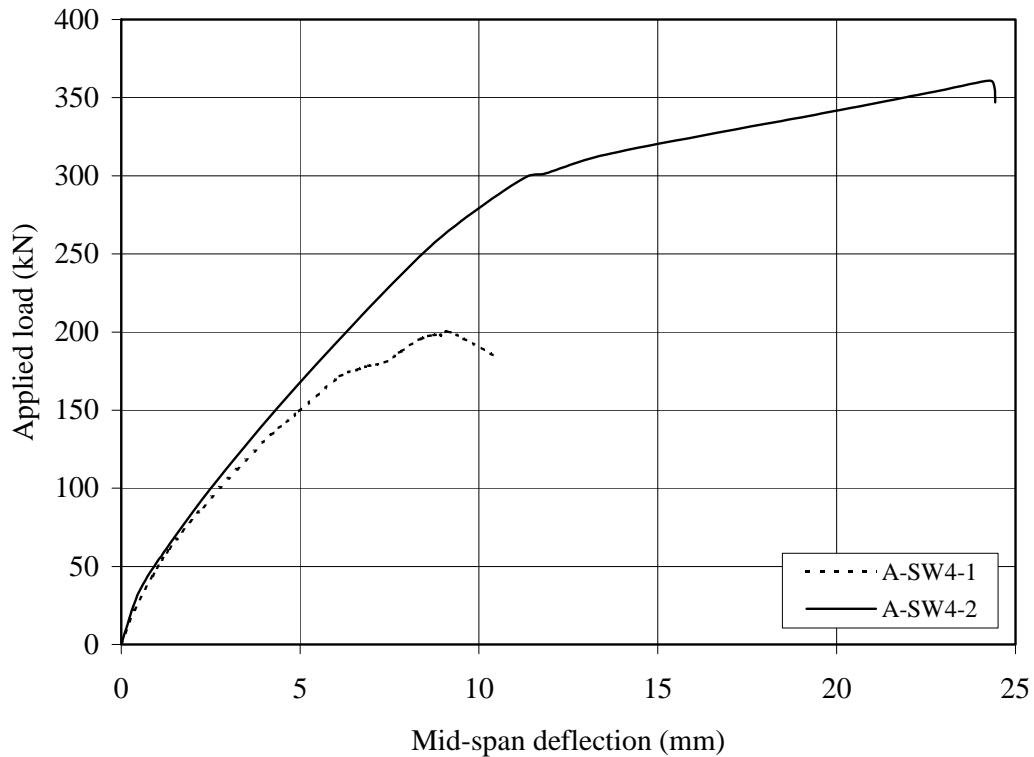


**Figure 4-5.** Experimental load-deflection relationship for Specimens A-SW4-1 and A-SW4-2

#### 4-2-3 Subgroup A-SO3

Subgroup A-SO3 consisted of five beam specimens, which had the same cross section dimensions and longitudinal steel reinforcement as for Groups A-SW. No steel stirrups were provided in the test shear span and the  $a/d$  ratio was 3.

The failure mode of control Specimen A-SO3-1 was described as shear compression (Fig. 4-6). Failure of the specimen occurred at a total applied load of 154 kN (corresponding to shear force of 77 kN). This load was a decrease of shear capacity by 54.5 kN compared to the Specimen A-SW3-1 due to the absent of the steel stirrups. In addition, the crack pattern in Specimen A-SW3-1 was different from that of Specimen A-SO3-1. In Specimen A-SW1, the presence of stirrups provided a better distribution of diagonal cracks throughout the shear span.



**Figure 4-6.** Crack pattern at ultimate failure of Specimen A-SO3-1

In Specimen A-SO3-2, which was strengthened with 50-mm CFRP strips spaced at 125-mm, the first diagonal shear crack was formed at an applied load of 100 kN. The crack propagated as the load increased in a similar manner to that of Specimen A-SO3-1. Sudden failure occurred due to debonding of the CFRP strips over the diagonal shear crack, with spalled concrete attached to the CFRP strips, as shown in [Figure \(4-7\)](#). The total ultimate recorded load was 262 kN with a 70% increase in shear capacity over the control specimen A-SO3-1. The maximum local CFRP vertical strain measured at failure in Specimen A-SO3-2 was 0.0047 mm/mm (i.e. 28% of the ultimate strain) which indicated that the CFRP did not reach its ultimate strength. The applied load versus mid-span deflection curves for beam specimens of Subgroup A-SO3 are illustrated in [Figure \(4-8\)](#).

Specimen A-SO3-3, strengthened with 75-mm CFRP strips failed as a result of CFRP debonding at a total applied load of 266 kN ([see Fig. 4-9](#)). No significant increase in shear capacity was noted compared to Specimen A-SO3-2. The maximum-recorded vertical CFRP strain at failure was 0.0052 mm/mm (i.e. 31% of the ultimate strain).



**Figure 4-7.** Ultimate failure of Specimen A-SO3-2

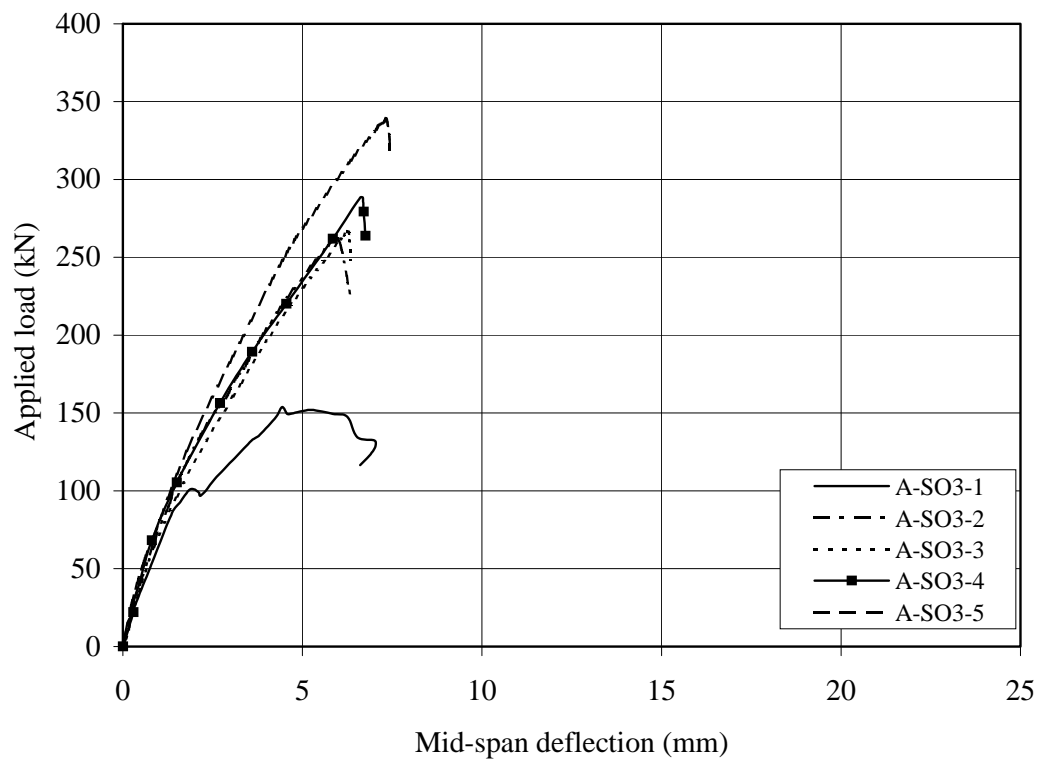


**Figure 4-8.** Experimental load-deflection relationships for Subgroup A-SO3 specimens



**Figure 4-9.** Ultimate failure of Specimen A-SO3-3

Specimen A-SO3-4, which was strengthened with a continuous CFRP U-wrap ( $90^{\circ}$ ), failed as a result of CFRP debonding at an applied load of 289 kN (see Fig. 4-10). Results show that Specimen A-SO3-4 exhibited increase in shear capacity of 87%, 10%, and 8.5% over Specimens A-SO3-1, A-SO3-2, and A-SO3-3 respectively.

Applied load versus vertical CFRP strain for Specimen A-SO3-4 is illustrated in Figure (4-11) in which strain gauges; sg1, sg2, and sg3 were located at mid-height with distances of 175 mm, 300 mm, and 425 mm from the support, respectively. Figure (4-11) shows that the CFRP strain was nil prior to diagonal crack formation, then increased slowly until the specimen reached a load in the neighborhood of the ultimate strength of the control specimen. At this point, the CFRP strain increased significantly until failure. The maximum local CFRP vertical strain measured at failure was about 0.0045 mm/mm.

When comparing the results of Specimens A-SO3-4 and A-SO3-2, the CFRP amount used to strengthen Specimen A-SO3-4 was 250% of that used for Specimen A-SO3-2. However, only a 10% increase in shear capacity was achieved for the additional amount of CFRP used. In case of continuous U-wrap, debonding of FRP sheets is a progressive failure starting at top of a



Figure 4-10. Ultimate failure of Specimen A-SO3-4

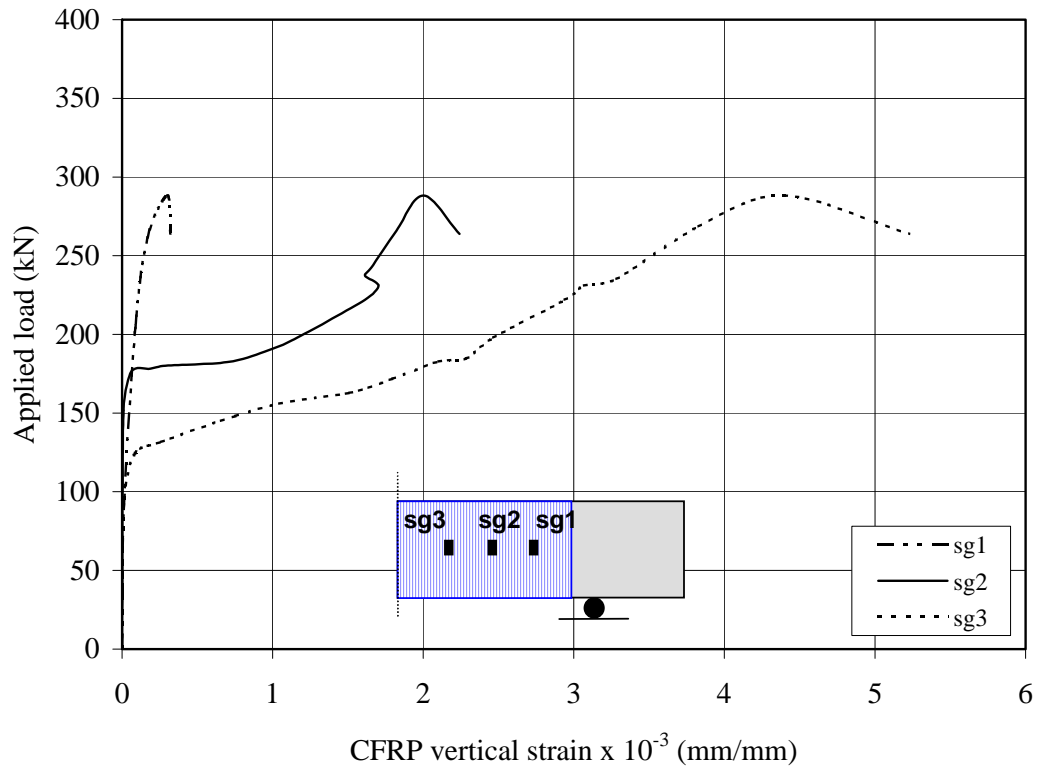


Figure 4-11. Applied Load versus measured vertical CFRP strain for Specimen A-SO3-4

Diagonal shear crack, where the development length is not sufficient. This means that, if FRP debonding failure is not prevented, there is an optimum FRP quantity, beyond which the capacity does not increase with increasing amount of FRP. This observation is consistent with reported findings from other study,<sup>16</sup> which indicates that the contribution of FRP to the shear capacity increases almost linearly with FRP axial rigidity expressed by  $\rho_f E_f$  ( $\rho_f$  is the FRP area fraction and  $E_f$  is the FRP elastic modulus) up to approximately 0.4 GPa. Above this value the effectiveness of FRP ceases to be positive.

In Specimen A-SO3-5, strengthened with two perpendicular plies (i.e.,  $90^0/0^0$ ) of CFRP, The failure occurred at a total applied load of 339 kN with a 120% increase in the shear capacity compared to the control Specimen A-SO3-1. The final failure was controlled by concrete splitting as shown in Figure (4-12). By comparing to the specimen with only one CFRP ply in  $90^0$  orientation (i.e., Specimen A-SO3-4), the shear capacity was increased by 17% as a result of the horizontal restraint provided by the added  $0^0$  ply. In addition, the failure mode was changed from CFRP debonding to concrete splitting.



**Figure 4-12.** Splitting failure of Specimen A-SO3-5

By comparing the test results of Specimens A-SW3-2 and A-SO3-5, having the same  $a/d$  ratio and strengthening schemes but with different steel shear reinforcement, the shear strength (i.e., 177 kN and 169.5 kN for Specimens A-SW3-2 and A-SO3-5, respectively) and the ductility are almost identical. One may conclude that the contribution of CFRP benefits the beam capacity to a greater degree for beams without steel shear reinforcement than for beams with adequate shear reinforcement.

#### **4-2-4 Subgroup A-SO4**

Subgroup A-SO4 consisted of three beam specimens similar to Subgroup A-SO3 specimens except the  $a/d$  ratio, which was selected to be 4. Subgroup A-SO4 strengthened specimens exhibited the largest increase in shear capacity compared as to the other three subgroups.

The control Specimen A-SO4-1 failed as a result of shear compression at a total load of 130 kN. This was a decrease in shear capacity of 18% compared to the Specimen A-SO3-1 with  $a/d$  ratio equal to 3. Comparing with the Specimen A-SW4-1, a decrease in shear capacity of 35 kN was recorded due to absence of the steel stirrups. Photos of the ultimate failure for Subgroup A-SO4 specimens are illustrated in [Appendix A](#). The experimental results in terms of applied load versus mid-span deflection for this subgroup specimens are illustrated in [Figure \(4-13\)](#).

In Specimen A-SO4-2, strengthened with CFRP strips, the failure was controlled by CFRP debonding at a total load of 255 kN with 96% increase in shear capacity over the control Specimen A-SO4-1. The maximum local CFRP strain measured at failure was 0.0062 mm/mm.

When comparing the test results of Specimen A-SO4-2 to that of Specimen A-SO3-2, the enhanced shear capacity of Specimen A-SO4-2 ( $a/d=4$ ) due to addition of CFRP strips was 62.5 kN, while Specimen A-SO3-2 ( $a/d=3$ ) resulted in added shear capacity of 54 kN. As expected, the contribution of CFRP reinforcement to resist the shear appeared to decrease with decreasing  $a/d$  ratio.

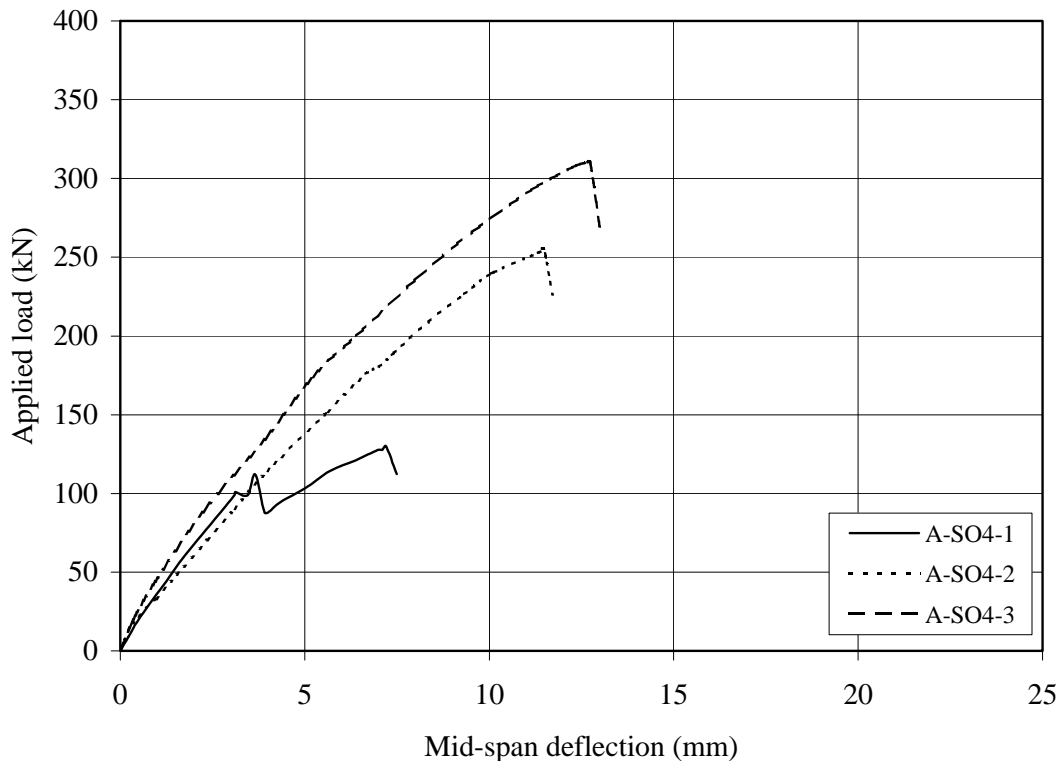


**Figure 4-13.** Experimental load-deflection relationship for Subgroup A-SO4 specimens

Specimen A-SO4-3, strengthened with continuous U-wrap, failed as a result of concrete splitting at an applied load of 310 kN with a 138% increase in capacity compared to that of Specimen A-SO4-1. The maximum local CFRP strain measured at failure was 0.0037 mm/mm.

#### 4-2-5 Summary and Results Evaluation of Series A

In series A, an experimental investigation was conducted to study the shear performance and the modes of failure of simply supported rectangular beams with shear deficiencies, strengthened with CFRP sheets. The variables investigated in this test series included steel stirrups, shear span-to-depth ratio ( $a/d$  ratio), CFRP amount and distribution. The results reveal that the strengthening technique using CFRP sheets can be used to increase significantly shear capacity, with efficiency that varies depending on the tested variables. For the beams tested in this series, increases in shear strength ranged from 40 to 138%.

Prior to inclined cracking, the strain in the externally bonded CFRP reinforcement is equal to the corresponding strain of the concrete. Since concrete cracks at a very small strain, CFRP will not prevent inclined cracks from forming and becomes efficient only after performing of the cracks (the measurements of CFRP strain show that the CFRP reinforcement is practically free of stress prior to crack formation). CFRP reinforcement enhances the shear resistance of a beam in two ways. First, part of shear force is resisted by CFRP reinforcement that traverses a particular crack similar to stirrups. Secondly, CFRP slow the growth of diagonal cracks and reduces their progression into the compression zone. This lead to a more uncracked concrete section available at the head of the crack in the compression zone to enhance the shear resistance provided by concrete contribution.

The recorded CFRP strain of the tested beams show that the failure of CFRP system occurs at an average stress level below nominal strength due to debonding of CFRP from concrete surface or concrete splitting in the cases of over strengthened beams. The test results indicate that contribution of CFRP benefits the shear capacity to a greater degree for beams without shear reinforcement than for beams with adequate shear reinforcement.

When comparing the test results of specimens with  $a/d$  ratio equal 4 to the corresponding specimens with  $a/d$  equal 3, the contribution of CFRP reinforcement to the shear capacity appears to decrease with decreasing value of  $a/d$  ratio. The effectiveness of CFRP for shear resistance of beams with short shear spans in which the arch action rather than beam action governs the failure still needs to be investigated. When arch action behavior governs, and failure is attained by splitting or crushing of concrete, the occurring deformations do not allow for the formation of the truss mechanism due to CFRP reinforcement and the contribution of CFRP in this case needs to be addressed.

Based upon the test results of Subgroup A-SO3 specimens, increasing the amount of CFRP may not result in a proportional increase in the shear strength especially if the failure controls by debonding of CFRP. The CFRP amount used to strengthen Specimen A-SO3-4 was 250% of that used in Specimen A-SO3-2, which resulted in a minimal (10%) increase in shear

capacity. Proportional increases in shear capacity with increases CFRP amount may be achieved when debonding is prevented such as in the case of the use of end anchor.

Moreover, the results of Subgroup A-SO3 specimens indicate that the added 0<sup>0</sup> ply improve the beam capacity by providing horizontal restraint. In addition, it may be reduce the propagation of vertical cracks starting at the bottom of the section in the case positive moment regions.

The summary of the test results of Series A specimens is detailed in Table (4-1). Note that, the proposed design model presented in Chapter 5 can predict the shear capacity and failure mode of the strengthened beams. A comparison between test results and calculated values is listed in Table (5-2).

**Table (4-1)** Summary of the test results of Series A

Test No.	Specimen designation	a/d ratio	Shear reinforcement		Failure mode	Total applied shear force at ultimate (kN)	Contribution of CFRP to the shear capacity (kN)	CFRP strengthening effectiveness ratio %
			Steel stirrups in test region	CFRP				
1	A-SW3-1	3	φ10@125mm	----	Shear	126.5	0.0	----
2	A-SW3-2	3	φ10@125mm	Two plies (90°/0°)	Splitting	177.0	> 50.5	> 40
3	A-SW4-1	4	φ10@125mm	----	Shear	100.0	0.0	----
4	A-SW4-2	4	φ10@125mm	Two plies (90°/0°)	Splitting	180.5	> 80.5	> 80
5	A-SO3-1	3	----	----	Shear	77.0	0.0	----
6	A-SO3-2	3	----	U-wrap strips, 50 @ 125mm	Debonding	131.0	54.0	70
7	A-SO3-3	3	----	U-wrap strips, 75 @ 125mm	Debonding	133.5	56.5	73
8	A-SO3-4	3	----	One ply continuous U-wrap	Debonding	144.5	67.5	87
9	A-SO3-5	3	----	Two plies (90°/0°)	Splitting	169.5	>92.5	>120
10	A-SO4-1	4	----	----	Shear	65.0	0.0	----
11	A-SO4-2	4	----	U-wrap strips, 50 @ 125mm	Debonding	127.5	62.5	96
12	A-SO4-3	4	----	One ply continuous U-wrap	Splitting	155.0	>90.0	> 138

### 4-3 TEST RESULTS OF SERIES B

Series B consisted of nine two span continuous beam specimens with rectangular cross section. The specimens of this series were subdivided into three groups designated as B-CW, B-CO, and B-CF. Each group had a different longitudinal and transverse steel reinforcement ratio.

#### 4-3-1 Group B-CW

Group B-CW consisted of two specimens having steel stirrups throughout. A diagonal crack was formed in the control Specimen B-CW1 close to the middle of the shear span when the load was approximately 150 kN. As the load increased, more diagonal shear cracks formed throughout the shear span, widened and propagated up to failure at a load of 508 kN (corresponding to a shear force of 175kN). The crack pattern of specimen B-CW1 at ultimate is illustrated in [Appendix A](#).

In Specimen B-CW2, which was strengthened with CFRP ( $90^0/0^0$ ), longitudinal cracks were formed on the topside of the beam at an applied load of 530 kN. The cracks initiated at the location of the applied load (mid span) and extended towards the middle support. At failure, the concrete cover on the topside was extensively damaged. This probably occurred due to over strengthening of the beam for shear and flexure in conjunction with relatively high longitudinal compressive stress developed at top of the specimen, which created a transverse tension. The failure occurred at applied load of 623 kN (corresponding to a shear force of 214 kN), a 22% increase in ultimate capacity as compared to B-CW1. The ultimate failure of Specimen B-CW2 is shown in [Figure \(4-14\)](#).

The applied shear force versus mid-span deflection curves for Specimens B-CW1 and B-CW2 are shown in [Figure \(4-15\)](#). The maximum CFRP strain measured at failure in specimen B-CW2 was about 0.0027 mm/mm, which corresponded to 17% of the ultimate strain.



**Figure 4-14.** Ultimate failure of Specimen B-CW2

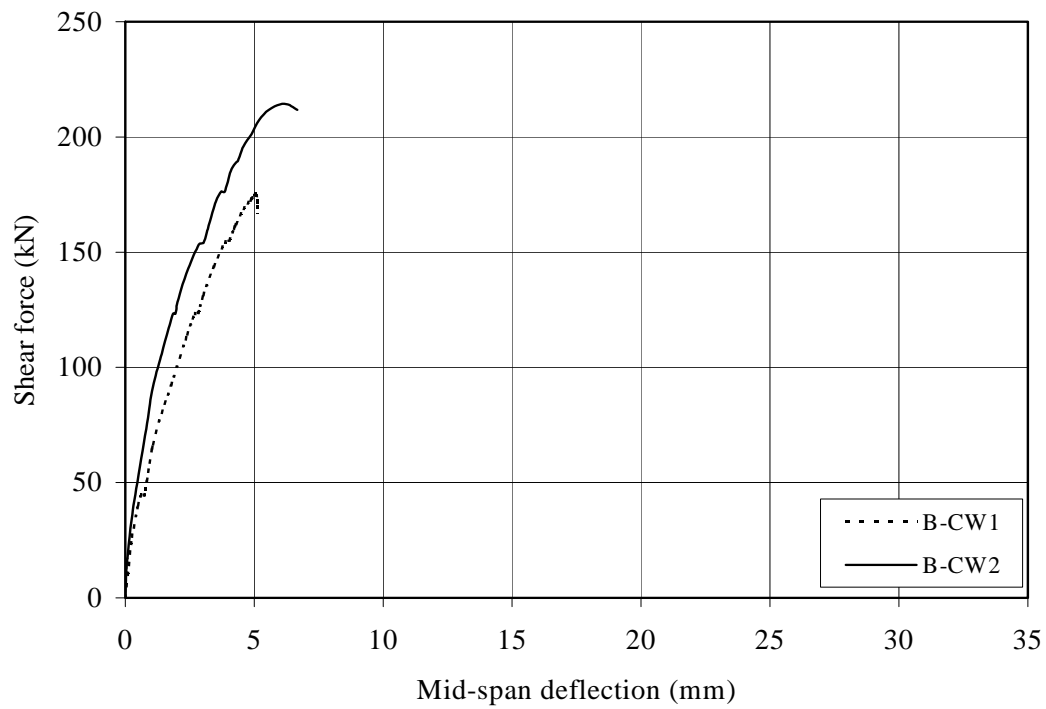


**Figure 4-15.** Experimental shear force-deflection relationship for Group B-CW specimens

In Specimen B-CW1, only stirrup number 3 located at distance of 300 mm from face of middle support yielded at ultimate. Comparisons between stirrup strains in Specimens B-CW1 and B-CW2 are shown in [Figure \(4-16\)](#). The strains of stirrups of Specimen B-CW2 were in general smaller than those in Specimen B-CW1 at the same load level. This was due to the effect of CFRP.

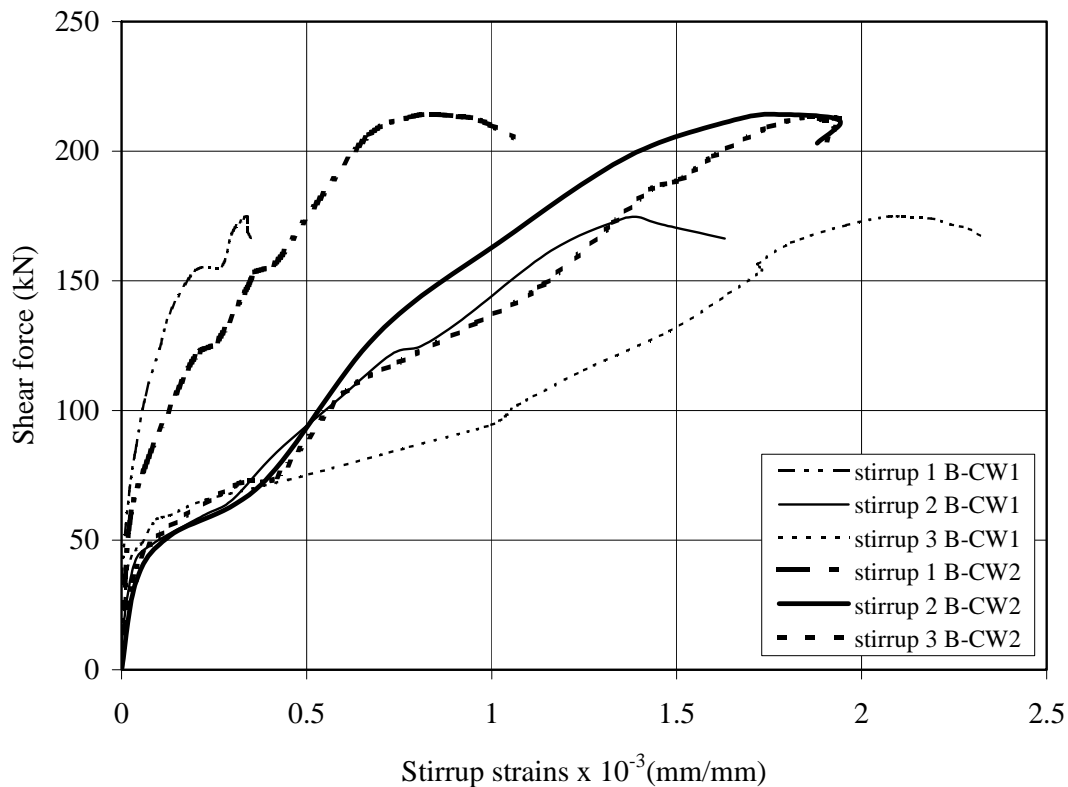


**Figure 4-16.** Applied shear force versus strains in the stirrups for Specimens B-CW1 and B-CW2

#### 4-3-2 Group B-CO

Group B-CO consisted of three specimens with no stirrups provided in the test shear span. The strengthened specimens of Group B-CO showed the largest increase in shear capacity compared to the other two groups (i.e., Groups B-CW and B-CF). In control Specimen B-CO1, the first diagonal shear crack initiated at a total load of about 90 kN. As the load increased, more

shear cracks formed throughout the shear span. When the total load reached 145 kN, the corresponding shear force of 45 kN reach its peak and remained constant thereafter, while the total load increased to its maximum of 220 kN. The relatively large amounts of top and bottom longitudinal steel reinforcement kept the beam integral until total damage of concrete occurred. Photos of the ultimate failure for Group B-CO specimens are illustrated in [Appendix A](#).

In Specimen B-CO2, strengthened with CFRP strips, the first diagonal shear crack was formed at a load of 140 kN. Failure occurred at the total load of 265 kN due to debonding of the CFRP strips over the main shear crack. The applied shear force at ultimate was 88 kN, an 83% increase in shear capacity over the control Specimen B-CO1. The maximum local vertical CFRP strain at beam failure was 0.0047 mm/mm. Experimental results in terms of applied shear force versus mid-span deflection for specimens of Group B-CO are shown in [Figure \(4-17\)](#).

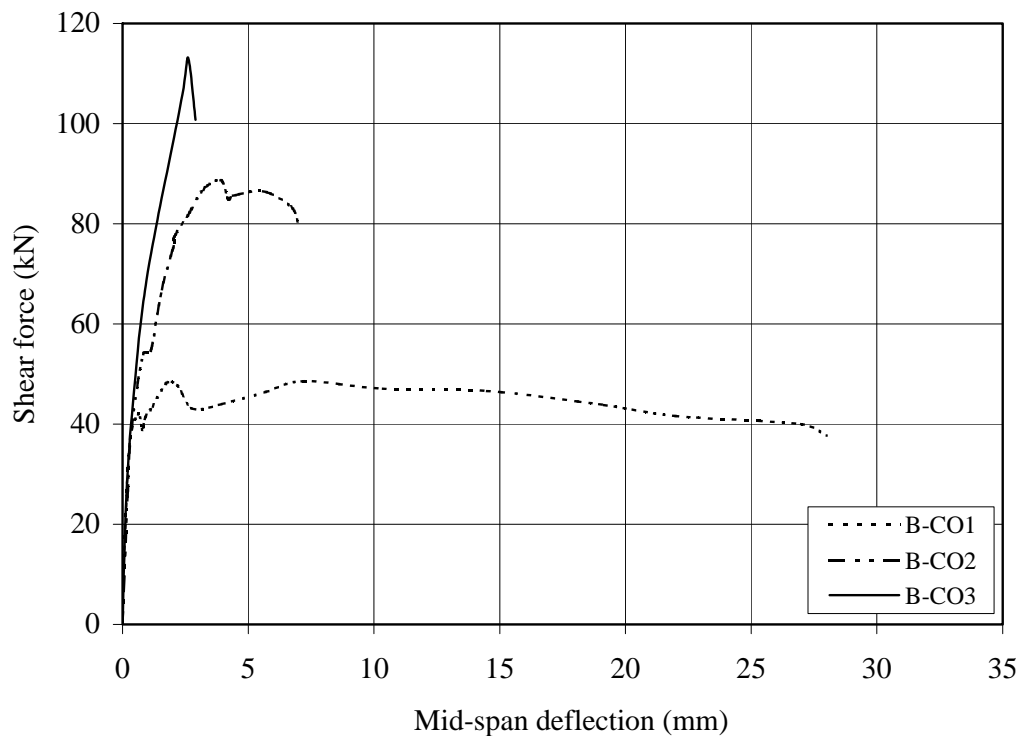


**Figure 4-17.** Experimental shear force-deflection relationship for Group B-CO specimens

Specimen B-CO3, strengthened with CFRP continuous U-wrap, failed by CFRP debonding at a total load of 330 kN (corresponding to a shear of 113 kN). The specimen showed an increase in shear capacity of 135% and 28% over Specimen B-CO1 and B-CO2, respectively.

In this specimen, longitudinal cracks were observed on the topside of the beam before failure similar to Specimen B-CW2.

The applied shear force versus vertical CFRP strain for Specimen B-CO3 is shown in **Figure (4-18)**. The strain gauges sg1, sg2, and sg3 were located at mid-height at distances of 175 mm, 300 mm, and 425 mm from the face of the middle support, respectively. **Figure (4-18)** shows that the CFRP strain was nil prior to diagonal crack formation then increased until failure occurred. Strain gage number 2 shows larger strain and this may be due to a diagonal crack located nearby this gage. The maximum vertical strain in CFRP was about 0.0037 mm/mm which corresponding to only 22% of CFRP ultimate strain. However, the recorded strain indicated that if the debonding of CFRP could be prevented, a higher increase in shear capacity of the beam would be attained.

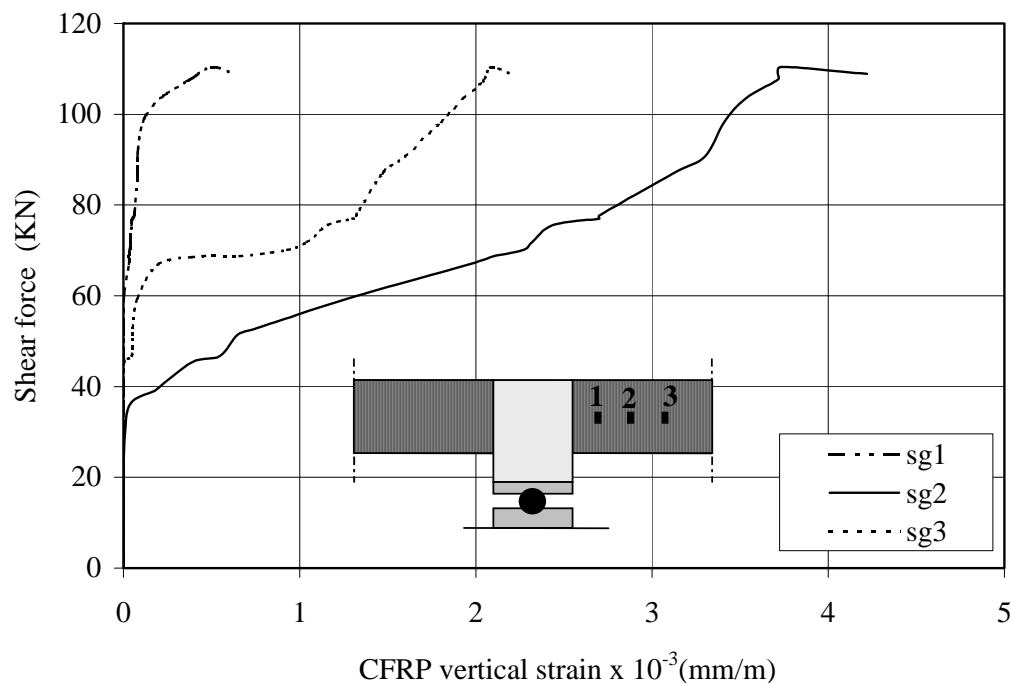


**Figure 4-18.** Applied shear force versus measured vertical CFRP strain for Specimen B-CO3

#### 4-3-3 Group B-CF

Group B-CF consisted of four beam specimens with no web reinforcement being provided. The longitudinal steel reinforcement ratio of Group B-CF specimens was less than

that of Group B-CO specimens. The control Specimen B-CF1 exhibited a shear compression failure mode as shown in Figure (4-19). Failure occurred at total load of 268 kN with a corresponding shear force of 93 kN.



**Figure 4-19.** Ultimate failure of Specimen B-CF1

The use of continuous U-wrap oriented at  $90^0$  in specimen B-CF2 caused a change in the final failure mode from shear to flexural. In Specimen B-CF2 debonding of CFRP sheets was observed close to the middle support after failure. The recorded load at failure was 337 kN, corresponding to a shear force of 119 kN, showing an increase of 28% over the control Specimen B-CF1.

In Specimen B-CF3, strengthened with CFRP ( $90^0/0^0$ ) exhibited a flexural mode of failure. The maximum total applied load was 394 kN, corresponding to a shear force of 131 kN, indicating an increase of 40 % and 10% over B-CF1 and B-CF2, respectively. Spalling of the concrete cover was observed in the topside similar to Specimen B-CW2.

In Specimen B-CF4, strengthened with totally wrapped CFRP sheet, flexural failure occurred at an applied load of 400 kN corresponding to a shear force of 140 kN. Figure (4-20) shows the experimental results of series B-CF in terms of shear force versus mid-span deflection. The final failure of Specimen B-CF4 is shown in Figure (4-21). In comparison to the control

Specimen B-CF1, the beam capacity increased by 50 percent. In addition, a large non-linear phase was recorded showing a notable increase in ductility as compared to other specimens.

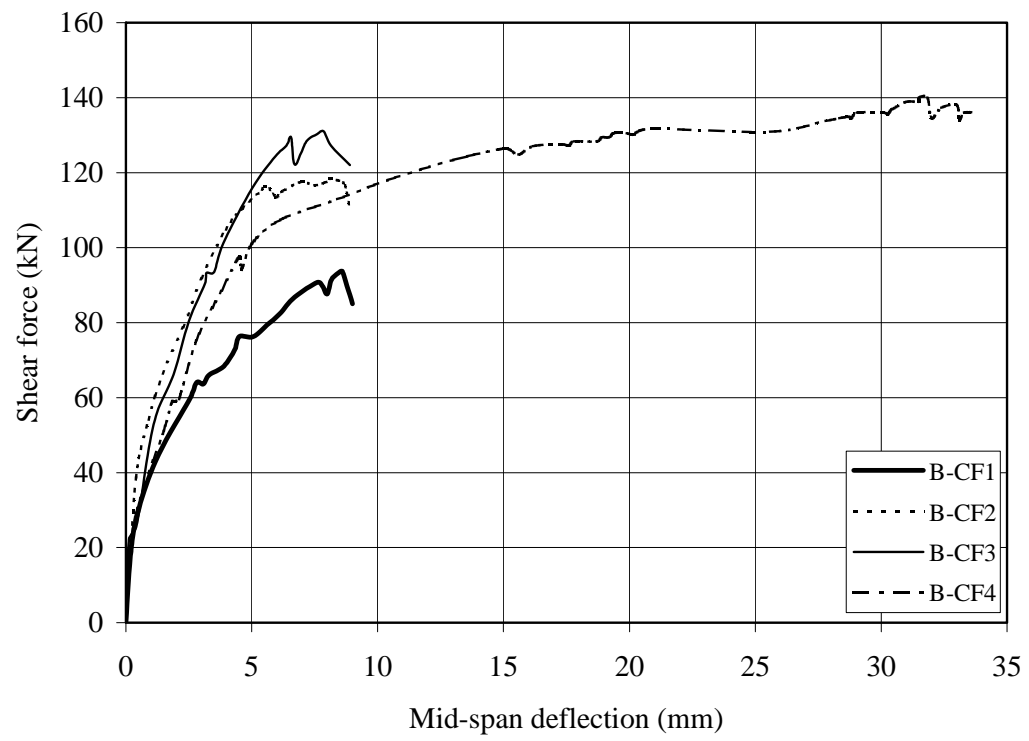


Figure 4-20. Experimental shear force-deflection relationship for Group B-CF specimens



Figure 4-21. Ultimate failure of Specimen B-CF4

#### 4-3-4 Summary and Results Evaluation of Series B

In the negative moment regions of continuous beams, shear cracks initiate from the top of the cross section. In this case, the U-wrap FRP reinforcement may not be able to control the initiation of these cracks, and may have less effectiveness to enhance shear capacity. In this test series, the capability of CFRP reinforcement to increase the shear capacity of two-span continuous RC beams strengthened with CFRP sheets was investigated. The variables investigated in this test series included steel stirrups, CFRP amount and distribution, and CFRP wrapping schemes.

The test results indicate that the externally bonded CFRP reinforcement can be used to enhance the shear capacity of the beams in positive and negative moment regions. For the specimens included in this series, increase in shear strength ranged from 22 to 135%. Test results also indicate that the contribution of CFRP benefits the shear capacity to a large degree for beams without stirrups than for beams with adequate steel shear reinforcement. As reported before in series A, the results of Group B-CO specimens show that increasing the amount of CFRP may not result in a proportional increase in the shear capacity.

Based upon the test results of Group B-CF specimens, the strengthening with bi-axial reinforcement (i.e. two plies  $90^0/0^0$ ), Specimen B-CF3, resulted in 10 % increase in the ultimate capacity compared to Specimen B-CF2 strengthened with continuous one ply U-wrap ( $90^0$ ). For the specimen strengthened with totally wrapped CFRP, an increase in ultimate capacity of 17% over the specimen strengthened with U-wrap was achieved. Even though total wrap configuration provides an excellent end anchorage and may increase concrete confinement, it is not practical from a constructability standpoint. The summary of the test results of series B specimens is detailed in Table (4-2).

**Table (4-2)** Summary of the test results of Series B

Test No.	Specimen designation	Shear reinforcement		Failure mode	Total applied shear force at ultimate (kN)	Contribution of CFRP to the shear capacity (kN)	CFRP strengthening effectiveness ratio %
		Steel stirrups in test region	CFRP				
13	B-CW1	φ10@125mm	----	Shear	175.0	0.0	----
14	B-CW2	φ10@125mm	Two plies (90°/0°)	Splitting	214.0	> 39.0	> 22
15	B-CO1	----	----	Shear	48.0	0.0	----
16	B-CO2	----	U-wrap strips, 50 @ 125mm	Debonding	88.0	40.0	83
17	B-CO3	----	One ply continuous U-wrap	Debonding	113.0	65.0	135
18	B-CF1	----	----	Shear	93.0	0.0	----
19	B-CF2	----	One ply continuous U-wrap	Flexural	119.0	> 26.0	> 28
20	B-CF3	----	Two plies (90°/0°)	Flexural	131.0	> 38.0	> 40
21	B-CF4	----	One ply, totally wrapped	Flexural	140.0	> 47.0	> 50

#### 4-4 TEST RESULTS OF SERIES C

In Series C, six beam specimens with T cross-section were tested as simply supported beam. The variables investigated in this series were CFRP amount and distribution, CFRP bonded area, fiber orientation, and CFRP end anchorage.

##### 4-4-1 Test Results and discussions

During loading of Specimen C-BT1, diagonal shear cracks formed at a load of 110 kN. The shear cracks initiated at the center of both shear spans simultaneously. The first shear crack was the critical crack in the specimen. As the load increased, this crack started to widen and propagated leading to the eventual failure at a load of 180 kN. The ultimate failure of Specimen C-BT1 is shown in [Figure \(4-22\)](#).

In Specimen C-BT2, strengthened with continuous U-wrap at 90°, failure was initiated by debonding of the CFRP sheet (with a thin layer of concrete adhered to it) over the main shear crack at the same location observed in Specimen C-BT1 ([Fig. 4-23](#)). It was followed by shear compression failure at a load of 310 kN.



**Figure 4-22.** Ultimate failure of Specimen C-BT1



**Figure 4-23.** Ultimate failure of Specimen C-BT2

Strengthening of Specimen C-BT2 with CFRP U-wraps resulted in a 72% increase in the shear capacity. The maximum FRP strain was 0.0045 mm/mm (corresponding to 28% of the reported ultimate strain of the CFRP). If debonding could be prevented, a better utilization of the strengthening material and consequently a higher increase in shear capacity of the beam would have been attained. The experimental results in terms of total applied load versus mid span deflection for the tested beam specimens of this series are shown in Figure (4-24).

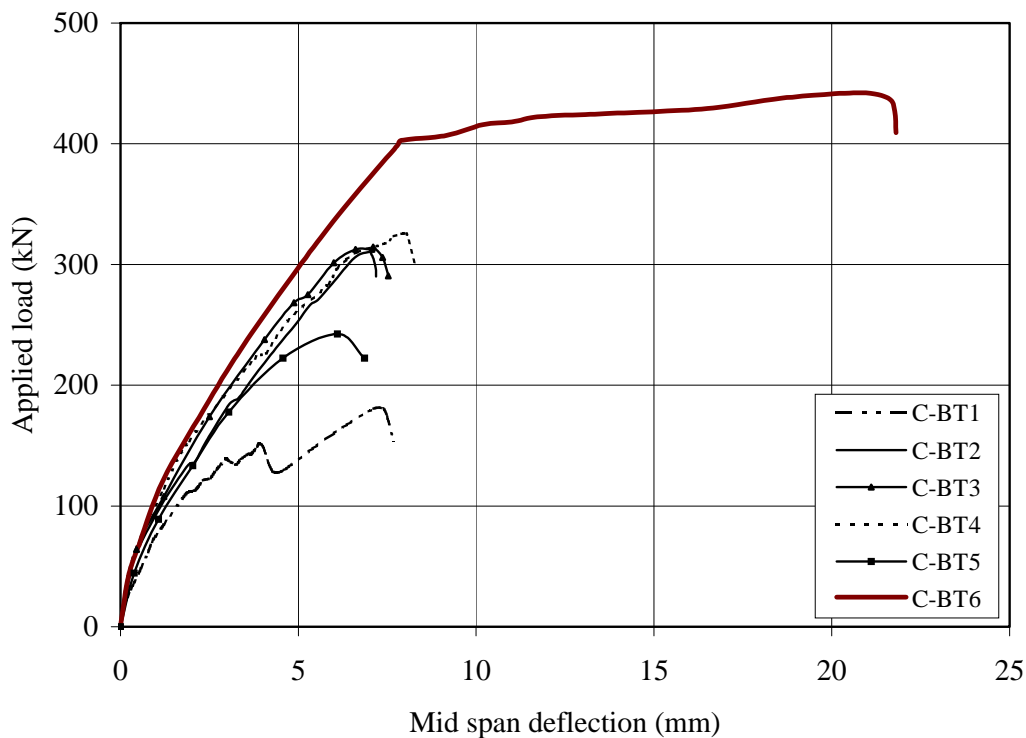


**Figure 4-24.** Experimental load-deflection relationship for Series C specimens

In Specimen C-BT3 with  $90^0/0^0$  CFRP, the failure mode was similar to that of Specimen C-BT2 (see Fig. 4-25). The failure occurred at a total applied load of 315 kN with no significant increase in shear capacity compared to Specimen C-BT2. Adding a ply in the  $0^0$  direction over a ply in the  $90^0$  direction had no effect on shear capacity because the failure mode was mainly controlled by FRP debonding.



**Figure 4-25.** Ultimate failure of Specimen C-BT3

In Specimen C-BT4 with CFRP strips in a form of U-wraps, the diagonal shear crack was formed at a total load of 140 kN. The crack propagated as the load increased similarly to Specimen C-BT1. The failure initiated due to debonding of one CFRP strip, with a thin concrete layer attached to it, over the main diagonal shear crack, in the area between the center of the shear crack and its upper end. This led to an instantaneous increase in the load carried by the adjacent strips resulting in the fracture of two of them followed directly by shear compression failure. The Ultimate failure of Specimen C-BT4 is shown in Figure (4-26).

Applied load versus vertical CFRP strain for Specimen C-BT4 is shown in Figure (4-27). The strain gauges sg6, sg7, sg8, sg9, and sg10 were located at distances of 200, 450, 575, 700, and 700 mm from support, respectively. The maximum-recorded local vertical strain in CFRP at ultimate was approximately 0.01 mm/mm, which is close to twice the value recorded in the case of continuous sheets (i.e., Specimen C-BT2). The sudden failure of Specimen C-BT4 occurred at a load of 324 kN. The load carrying capacity of Specimen C-BT4 with CFRP strips is slightly higher than that of Specimen C-BT2 with continuous sheets. As discussed earlier in Section (4-2-3), there is an optimum amount of FRP, beyond which the strengthening effect becomes inefficient.



**Figure 4-26.** Ultimate failure of Specimen C-BT4

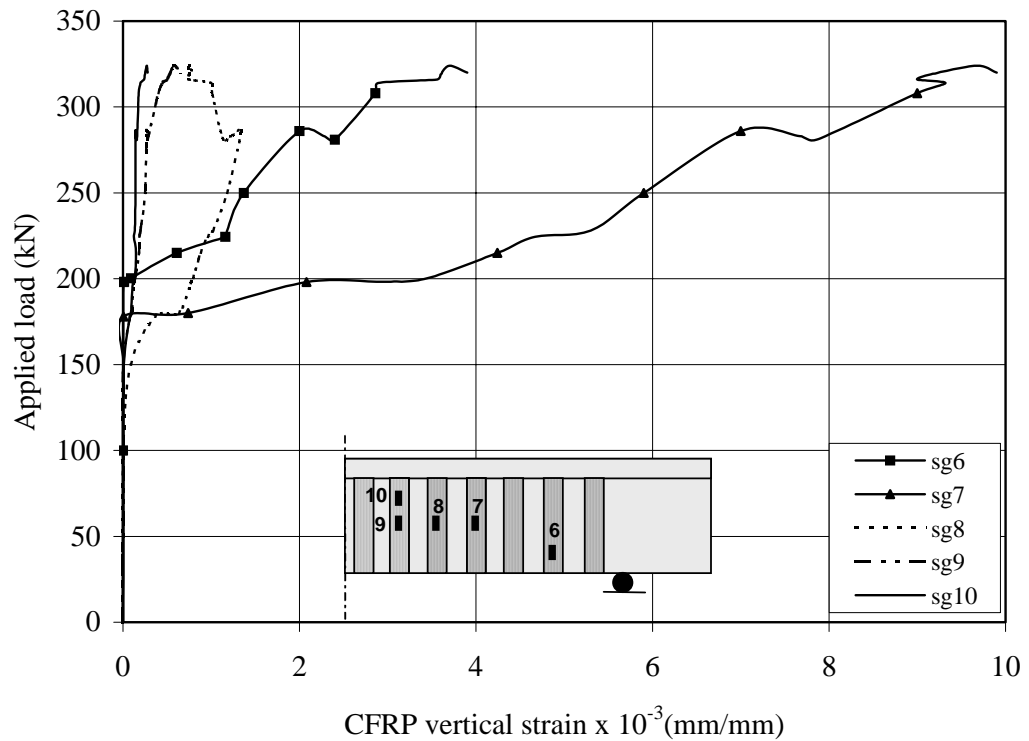


**Figure 4-27.** Applied load versus measured vertical CFRP strain for Specimen C-BT4

In Specimen C-BT5 with CFRP strips attached to the beam sides only, a diagonal shear crack formed at total applied load of 140 kN and propagated as the load increased in a similar manner to Specimens C-BT1 and C-BT4. Brittle failure occurred at a total applied load of 243 kN by debonding of the CFRP strips followed directly by shear compression failure. The location of the debonding area is different from that of Specimen C-BT4. In this case, it was below the main shear crack between its center and its lower end as shown in [Figure \(4-28\)](#). Strengthening of Specimen C-BT5 with CFRP strips on the two beam sides resulted in a 35% increase in the shear capacity. Unfortunately, the strain gauges results were not reliable and not discussed herein.



**Figure 4-28.** Ultimate failure of Specimen C-BT5

As a result of the use of U-anchors, a significant increase in the shear capacity was achieved in Specimen C-BT6. Also, the failure mode was changed from CFRP debonding (as observed in Specimen C-BT2) to flexural failure mode. The measured local maximum vertical strain of the CFRP wrap was 0.0063 mm/mm or 40% of ultimate. This value is not absolute because it greatly depends on the location of the strain gage with respect to a crack. Load versus CFRP strain curves for the two strengthened Specimens C-BT2 and C-BT6 are shown in [Figure](#)

(4-29). For both beams, shear cracking at different locations started at the same load level (e.g., approximately 150 kN for location 9, and 200 kN for location 7 and 10), however, a much higher ultimate load and strain were reached in Specimen C-BT6. No debonding of CFRP wrap was observed up to the ultimate load in Specimen C-BT6. After the beam failed in flexure, the CFRP wrap ruptured at the end of the shear crack near the support, as shown in Figure (4-30).

The load carrying capacity of Specimen C-BT6 was 442 kN, which is 145% and 42% higher than the load carrying capacity of the control Specimen C-BT1 and the similarly strengthened Specimen C-BT2, respectively. Figure (4-24) indicates that the response of Specimen C-BT6 was initially stiffer and later more ductile than response of Specimen C-BT2. The additional ductility was a result of change the failure mode from CFRP debonding to flexural failure. Therefore, the mid-span deflection of Specimen C- BT6 at failure was about 3 times the deflection of Specimen C-BT2 at failure.

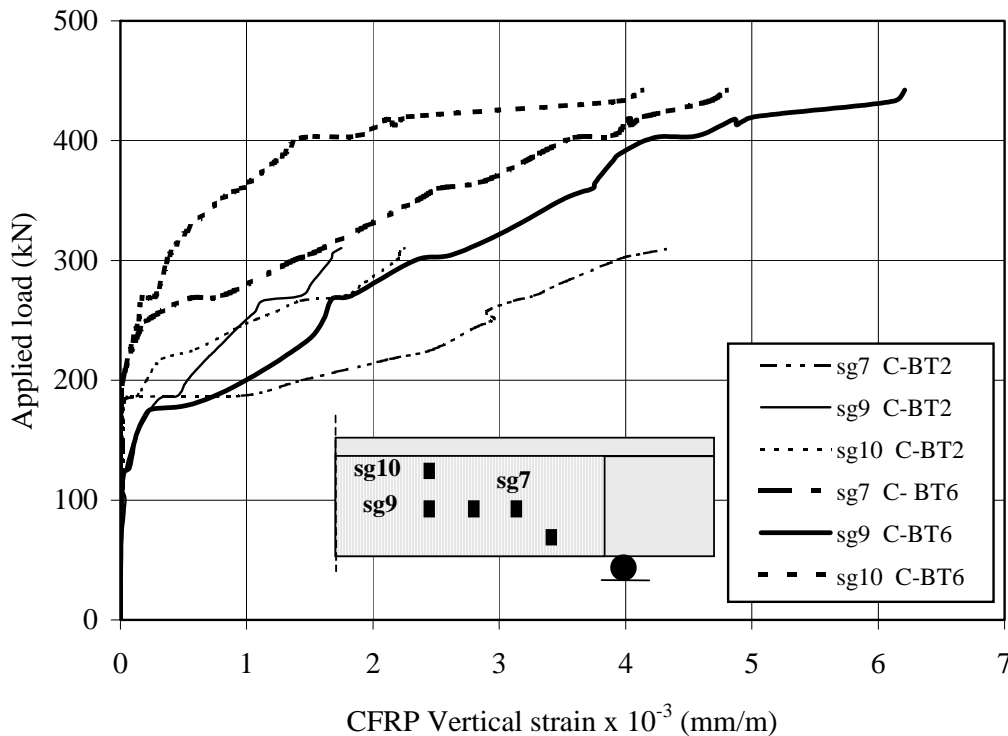


**Figure 4-29.** Applied load versus vertical CFRP strain for Specimens C-BT2 and C-BT6



**Figure 4-30.** Ultimate failure of Specimen C-BT6

#### **4-4-2 Summary and Results Evaluation of Series C**

Beams with T-cross-section are of great importance because they are the most commonly used in practice. Also, they represent a more challenging case than rectangular beams because of reduced area for placement of FRP. In this test series, the shear performance of T-beams with shear deficiencies strengthened with different configurations of CFRP sheets was investigated. The test parameters were CFRP end anchorage, bonded area, CFRP amount and distribution.

The test results indicate that the externally bonded CFRP reinforcement can be used to enhance the shear capacity of T-beams. For the specimens included in the test series, an increase in shear strength ranged from 35 to 145% was achieved. The test results show that the performance of CFRP can be improved significantly if adequate end anchorage is provided. The U-anchor system is easy to apply, compatible with any external FRP strengthening system, and avoids high stress concentration and durability concern compared to the traditional mechanical anchors made of steel plates and bolts. This anchor is recommended where bond and/or development length of FRP are critical according to the design procedure.

The test result of Specimen C-BT5 indicate that applying CFRP to the beam sides only is less effective than a U-wrap due to lack of FRP bonded length under the diagonal shear crack. As reported in the earlier two series (i.e. series A and B), the results of this series also indicate that, if an effective end anchor to control FRP debonding is not used, there exists an optimum amount of FRP, beyond which the strengthening effectiveness can not be increased. The summary of the test results of Series C specimens is detailed in Table (4-3).

**Table (4-3)** Summary of the test results of Series C

Test No.	Specimen designation	CFRP reinforcement	Failure mode	Total applied shear force at ultimate (kN)	Contribution of CFRP to the shear capacity (kN)	CFRP strengthening effectiveness ratio %
22	C-BT1	----	Shear	90.0	0.0	----
23	C-BT2	One ply continuous U-wrap without end anchor	Debonding	155.0	65.0	72
24	C-BT3	Two plies (90°/0°)	Debonding	157.5	67.5	75
25	C-BT4	U-wrap strips, 50 @ 125mm	Debonding	162.5	72.0	80
26	C-BT5	Two sides strips, 50 @ 125mm	Debonding	121.5	31.5	35
27	C-BT6	One ply continuous U-wrap with end anchor	Flexural	221.0	> 131.0	> 145

## CHAPTER 5

### DESIGN APPROACH

#### 5-1 GENERAL

The proposed design approach for computing the shear capacity of RC beams strengthened with externally bonded CFRP sheets is provided in this section. The design approach is expressed in ACI design code format, Egyptian code format, and Eurocode format. The main factors affecting the additional strength that may be achieved by the externally bonded CFRP reinforcement have been considered. The first version of the proposed design approach in ACI Code format was published in 1998.<sup>36</sup> The proposed model described two possible failure mechanisms of CFRP reinforcement, namely: CFRP fracture and CFRP debonding. Furthermore, two limits on the contribution of CFRP shear were proposed. The first limit was set to control the shear crack width and loss of aggregate interlock, and the second was to preclude web crushing. In this section, attempts were made to improve the 1998 shear design approach. Modifications were proposed<sup>34</sup> to include results of a new study on bond mechanism between CFRP sheet and concrete surface. The proposed design algorithms give satisfactory and conservative results when compared with all available test results up to date.

#### 5-2 FACTORS AFFECTING THE SHEAR CONTRIBUTION OF FRP

Based upon the results of the experimental program and the data collected from other research studies, the contribution of externally bonded FRP to the shear capacity is influenced by the following parameters:

- Type of FRP, and its unidirectional rigidity
- Amount and distribution of FRP reinforcement
- Fiber orientation

- Wrapping schemes (total wrap, U-wrap, or fiber attached on the two web sides of the beam)
- Presence of FRP end anchor
- Concrete strength
- Concrete surface preparation and surface roughness
- Steel shear reinforcement index
- Loads and support conditions (i.e., strengthening in negative or positive moment regions)
- Shear span-to-depth ratio

The proposed design algorithms focused on CFRP sheets and included some of the above factors. However, further modification to the shear design approach is recommended to account for all factors when a sufficient database of suitable test results becomes available.

## 5-3 SHEAR DESIGN OF RC STRENGTHENED BEAMS IN ACI CODE FORMAT

### 5-3-1 ACI Code Provision for Shear

In the ACI Code,<sup>37</sup> the basic design equation for the shear capacity of a concrete member is.

$$V_u \leq \phi V_n \quad (5-1)$$

(ACI Eq. 11-1)

where  $V_u$  is the total shear force applied at a given section due to the factored loads;  $\phi$  is the strength reduction factor, taken equal to 0.85; and  $V_n$  is the nominal shear strength equal to:

$$V_n = V_c + V_s \quad (5-2)$$

(ACI Eq. 11-2)

where,  $V_c$  is the nominal shear strength provided by concrete (which for a cracked section is attributable to aggregate interlock, dowel action of longitudinal reinforcement, and the diagonal tensile strength of the uncracked portion of concrete), and  $V_s$  is the nominal shear strength provided by steel shear reinforcement.

The nominal shear strength provided by concrete,  $V_c$ , is assumed to be the same for beams with or without shear reinforcement and is taken as the shear causing significant inclined cracking:

$$V_c = \left( 0.168 \sqrt{f'_c} + 17.23 \rho_w \frac{V_u d}{M_u} \right) b_w d \leq 0.29 \sqrt{f'_c} b_w d \quad (5-3)$$

(ACI Eq. 11-5)

where  $\rho_w$  is the ratio of longitudinal tensile steel;  $M_u$  is the factored moment occurring simultaneously with  $V_u$  at section considered. The quantity  $V_u d/M_u$  shall not be taken greater than 1. In Equation (5-3) the second term is generally small. Therefore, ACI 318-95 allows the use of the following simplified equation.

$$V_c = \frac{1}{6} \sqrt{f'_c} b_w d \quad (5-4)$$

(ACI Eq. 11-3)

The nominal shear reinforcement contribution,  $V_s$ , is based on the 45-degree-truss model.

$$V_s = \frac{A_v f_y (\sin\alpha + \cos\alpha) d}{s} \quad (5-5)$$

(ACI Eq. 11-16)

where,  $A_v$  is the area of shear reinforcement,  $f_y$  is the yield stress,  $\alpha$  is the angle between inclined stirrups and longitudinal axis of the beam, and  $s$  is the spacing of the stirrups.

To avoid shear failure initiated by web crushing before utilizing the full capacity of the shear reinforcement, the ACI 318-95 limits  $V_s$  to  $0.67 \sqrt{f'_c} b_w d$ . In addition, a minimum amount of web reinforcement,  $A_{v(\min.)}$ , has to be provided if the applied shear force,  $V_u$ , exceeds half of the factored inclined cracking shear,  $\phi(0.5V_c)$ .

$$A_{v(\min.)} = \frac{b_w s}{3f_y} \quad (5-6)$$

The stirrups are unable to resist shear failure unless they are crossed by an inclined crack. For this reason, ACI Section-11-5-4-1 sets the maximum spacing of vertical stirrups as the smaller of  $d/2$  or 610 mm if  $V_s \leq \frac{1}{3} \sqrt{f'_c} b_w d$  and the smaller of  $d/4$  or 305mm if  $V_s > \frac{1}{3} \sqrt{f'_c} b_w d$ .

### 5-3-2 Shear Capacity of a CFRP Strengthened Section

In traditional shear design approaches (including the ACI Code), the nominal shear strength of an RC section, is the sum of the shear strengths of concrete and steel shear reinforcement. For beams strengthened with externally bonded FRP reinforcement, the shear strength may be computed by the addition of a third term to account of the FRP contribution. This is expressed as follows:

$$V_n = V_c + V_s + V_f \quad (5-7)$$

where  $V_f$  is the shear contribution of externally bonded FRP. The design shear strength is obtained by multiplying the nominal shear strength by a strength reduction factor,  $\phi$ . It is suggested that the strength reduction factor  $\phi = 0.85$  given in ACI 318-95 be maintained for the concrete and steel terms. However, the reduction factor for CFRP reinforcement may require an adjustment, as discussed later.

#### 5-3-2-1 Contribution of CFRP Reinforcement ( $V_f$ ) to the Shear Capacity

**General:** To compute the nominal shear strength as given in Equation (5-7), it is necessary to quantify the contribution of CFRP reinforcement to the shear capacity ( $V_f$ ). At the ultimate limit state for the member in shear, it is not possible to attain the full strength of the FRP. Failure is governed by either fracture of the FRP sheet at average stress levels well below FRP ultimate capacity due to stress concentrations, debonding of the FRP sheet from the concrete surface, or a significant decrease in the post-cracking concrete shear strength from a loss of aggregate interlock. The design procedure takes all of these possible failure modes into consideration.

**Basic Design Equation:** The proposed expression to compute CFRP sheet contribution is given in Equation (5-8). This equation is similar to that for shear contribution of steel stirrups and consistent with ACI format. The shear contribution is computed by assuming a shear crack angle of 45 degrees, computing the area of reinforcement that crosses this potential crack, and multiplying the area by the strength of the material.

$$V_f = \frac{A_f f_{fe} (\sin\beta + \cos\beta) d_f}{s_f} \quad (5-8)$$

In Equation (5-8),  $A_f$  is the area of one strip of transverse FRP reinforcement covering two sides of the beam. This area may be expressed as follows:

$$A_f = 2 t_f w_f \quad (5-9)$$

where  $t_f$  is the FRP reinforcement thickness and  $w_f$  is the width of the strip. The dimensions used to define the area of CFRP are shown in Figure (5-1). The spacing between the strips,  $s_f$ , is defined as the distance from the centerline of one strip to the centerline of an adjacent strip. Note that, for continuous vertical FRP reinforcement, the spacing of the strip,  $s_f$ , and the width of the strip,  $w_f$ , are equal. The angle  $\beta$  is angle between principal fiber orientation and longitudinal axis of the beam.

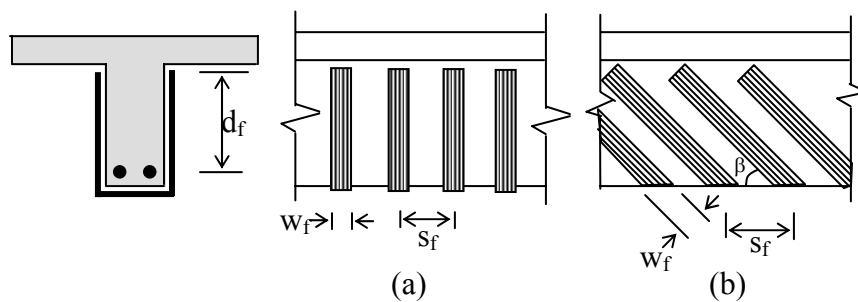


**Figure 5-1.** Definition of area of FRP in shear reinforcement

(a) Vertical FRP strips (b) Inclined strips

The effective depth of FRP strip,  $d_f$ , is the vertical projection of the shear crack (assumed to be  $45^\circ$ ) minus the distance from the top of the crack to the end of the sheet. Because shear cracks typically initiate as vertical cracks until they reach the depth of longitudinal steel reinforcement, the effective depth,  $d_f$ , should be measured from the centroid of the steel at the bottom section. Typically, the strips extend only to the soffit of the slab. Therefore, the effective depth of FRP strip,  $d_f$ , may be computed by subtracting the slab depth from the depth of the steel,  $d$ .

The other variable in Equation (5-8) is the effective average stress in the FRP sheet at ultimate,  $f_{fe}$ . The effective average FRP stress, taken smaller than its ultimate strength, is computed by applying a reduction coefficient,  $R$ , to the ultimate FRP tensile strength,  $f_{fu}$ , as expressed in Equation (5-10).

$$f_{fe} = R f_{fu} \quad (5-10)$$

The proposed reduction coefficient is determined based on the possible failure modes. The failure can be expressed in terms of fracture of the CFRP sheet (failure mode 1), or debonding of CFRP sheet from concrete substrate (failure mode 2). In either case, an upper limit of reduction coefficient is established to control the shear crack width and the loss of aggregate interlock. The nominal shear capacity of the CFRP reinforcement relating to these failure modes is function of the reduction coefficient. The controlling failure mode is determined by taking the lowest reduction coefficient.

**Reduction Coefficient based on CFRP Sheet Fracture Failure:** Based on the review of the available experimental results, Traintafillou<sup>16</sup> observed that the effective average FRP strain,  $\epsilon_{fe}$ , at ultimate is a function of  $\rho_f E_f$ , where  $\rho_f$  is the FRP area fraction and equal to  $(2t_f / b_w)(w_f / s_f)$  and  $E_f$  is the elastic modulus of FRP. Adopting this model with some modifications to incorporate the shortcomings discussed earlier in Section 2-4, the author proposed a refined model.<sup>36</sup>

Because CFRP is linearly elastic until failure, the effective average strain,  $\varepsilon_{fe}$ , at ultimate limit state, may be computed by Equation (5-11).

$$\varepsilon_{fe} = R \varepsilon_{fu} \quad (5-11)$$

where  $\varepsilon_{fu}$  is the ultimate tensile strain of CFRP. Equation (5-8) may be rewritten as follows:

$$V_f = \rho_f E_f \varepsilon_{fe} b_w (\sin\beta + \cos\beta) d_f \quad (5-12)$$

Here, the effective average stress,  $f_{fe}$ , is replaced with the effective average strain times the modulus of elasticity.

To establish the reduction coefficient,  $R$ , all of available experimental results in which failure is controlled by CFRP fracture were used to calibrate Equation (5-12). In this study, the results of twenty-two tests listed in Table (5-1) were used. For each test specimen, the effective average strain is determined by equating the experimentally determined CFRP contribution to Equation (5-12) and back calculating  $\varepsilon_{fe}$ . Then, the ratio of effective average strain to the ultimate strain,  $R = \varepsilon_{fe} / \varepsilon_{fu}$ , is plotted versus  $\rho_f E_f$  as shown in Figure (5-2). A polynomial function is used to fit the data for the case of  $\rho_f E_f \leq 0.7$  GPa. This polynomial is given in Equation (5-13) after multiplying by a safety factor equal to 0.85.

$$R = 0.56 (\rho_f E_f)^2 - 1.22 (\rho_f E_f) + 0.78 \quad (5-13)$$

Further adjustment of Equation (5-13) may be suggested when more data become available especially for  $\rho_f E_f > 0.7$  GPa.

**Table (5-1).** Experimental data on shear strengthening using CFRP

No. (1)	Reference and Test specimen Designation (2)	$f'_c$ (MPa) (3)	Section Dimensions			CFRP Properties and Wrapping Schemes				$\beta^\circ$ (11)	$\rho_f$ ( $\times 10^{-3}$ ) (12)	$V_{f,exp}$ (kN) (13)	$\varepsilon_{fe}$ ( $\times 10^{-3}$ ) (14)	Failure Mode (15)
			$b_w$ (mm) (4)	$d$ (mm) (5)	$d_f$ (mm) (6)	$t_f$ (mm) (7)	$E_f$ (GPa) (8)	$f_{fu}$ (MPa) (9)	Wra. Sch. (10)					
1	SA(S2)	45.2	200	260	260	0.11	230	3,480	S	90	0.55	68.4	11.6	Debonding
2	SA(S3)	41.3	200	260	260	0.11	230	3,480	U	90	0.55	110	15.1	Debonding
3	SA(S4)	37.5	200	260	260	0.11	230	3,480	S	90	1.1	64.2	5.4	Debonding
4	SA(S5)	39.7	200	260	260	0.11	230	3,480	U	90	1.1	106.1	8.9	Debonding
5	SA1(2)	35.7	150	240	140	0.11	230	3,480	U	90	1.46	24	3.79	Debonding
6	SA1(3)	35.3	150	240	140	0.11	230	3,480	A	90	1.46	65	10.26	Debonding
7	UJ(5)	24	100	170	170	0.097	230	2,650	S	90	1.94	20.1	2.94	Debonding
8	UJ(6)	27	100	170	170	0.097	230	2,650	S	45	1.94	32.3	3.34	Debonding
9	UJ(7)	27	100	170	170	0.194	230	2,650	S	90	3.9	20.1	1.47	Debonding
10	UJ(3)	24	100	170	170	0.097	230	2,650	W	90	1.94	33.8	4.95	Fracture
11	TK(BS2)	35.1	200	420	420	0.11	280	3,494	U	90	0.17	41.2	11.4	Debonding
12	TK(BS5)	36.8	200	420	420	0.11	280	3,494	U	90	0.13	33.4	12.1	Debonding
13	TK(BS6)	35.8	200	420	420	0.11	280	3,494	U	90	0.088	30.1	12.5	Debonding
14	TK(BS7)	34.7	200	420	420	0.11	280	3,494	W	90	0.13	98.9	12.5	I
15	C(G)	46	63	152	89	0.58	21	185	U	90/0	18.2	17.1	5.14	Fracture
16	C(45G)	46	63	152	89	0.58	21	185	U	$\pm 45$	18.2	23.5	5.0	Fracture
17	T(S1a)	30	70	100	100	--	235	3,300	S	90	2.2	13.55	4.1	Debonding
18	T(S1b)	30	70	100	100	--	235	3,300	S	90	2.2	11.25	3.4	Debonding
19	T(S2a)	30	70	100	100	--	235	3,300	S	90	3.3	15.85	3.2	Debonding
20	T(S2b)	30	70	100	100	--	235	3,300	S	90	3.3	12.9	2.6	Debonding
21	T(S3a)	30	70	100	100	--	235	3,300	S	90	4.4	13.2	2.0	Debonding
22	T(S3b)	30	70	100	100	--	235	3,300	S	90	4.4	10.55	1.6	Debonding
23	T(S1-45)	30	70	100	100	--	235	3,300	S	45	2.2	14.05	3.0	Debonding
24	T(S2-45)	30	70	100	100	--	235	3,300	S	45	3.3	15.45	2.0	Debonding
25	T(S3-45)	30	70	100	100	--	235	3,300	S	45	4.4	12.15	1.3	Debonding
26	F(S-2)	30	600	510	510	0.167	240	3,834	W	90	0.56	243	6.58	II
27	F(S-3)	30	600	510	510	0.334	240	3,834	W	90	1.11	346	4.7	II
28	F(S-4)	30	600	510	510	0.501	240	3,834	W	90	1.67	493	4.4	Fracture
29	O(BS12)*	27.8	180	360	360	--	230	--	W	90	1.2	--	8.4	Fracture
30	O(BS24)*	27.8	180	360	360	--	230	--	W	90	2.4	--	6.2	Fracture
31	O(BM06)*	27.8	180	360	360	--	230	--	W	90	0.6	--	11.7	Fracture

**Table (5-1).** Experimental data on shear strengthening using CFRP (continued)

No. (1)	Reference and Test specimen Designation (2)	$f'_c$ (MPa) (3)	Section Dimensions			CFRP Properties and Wrapping Schemes				$\beta^\circ$ (11)	$\rho_f$ ( $\times 10^{-3}$ ) (12)	$V_{f,exp}$ (kN) (13)	$\epsilon_{fe}$ ( $\times 10^{-3}$ ) (14)	Failure Mode (15)
			$b_w$ (mm) (4)	$d$ (mm) (5)	$d_f$ (mm) (6)	$t_f$ (mm) (7)	$E_f$ (GPa) (8)	$f_{fu}$ (MPa) (9)	Wra. Sch. (10)					
32	O(BM12)*	27.8	180	360	360	--	230	--	W	90	1.2	--	9.3	Fracture
33	O(BM18)*	27.8	180	360	360	--	230	--	W	90	1.8	--	7.8	Fracture
34	O(BM24)*	27.8	180	360	360	--	230	--	W	90	2.4	--	6.0	Fracture
35	O(BL06)*	27.8	180	360	360	--	230	--	W	90	0.6	--	8.4	Fracture
36	O(BL12)*	27.8	180	360	360	--	230	--	W	90	1.2	--	7.8	Fracture
37	O(BMW06)*	21	180	360	360	--	230	--	W	90	0.6	--	8.4	Fracture
38	O(BMW12)*	21	180	360	360	--	230	--	W	90	1.2	--	6.9	Fracture
39	O(BMW24)*	21	180	360	360	--	230	--	W	90	2.4	--	4.6	Fracture
40	O(2)*	27.8	400	340	340	--	230	--	W	90	0.29	--	12	Fracture
41	O(3)*	27.8	400	340	340	--	230	--	W	90	0.58	--	10.3	Fracture
42	UM(CS1)	40.5	300	257	257	0.11	244	4,280	W	90	0.74	87	6.9	II
43	UM(CS2)	40.5	300	257	257	0.11	244	4,280	W	90	0.37	32	5.12	Fracture
44	UM(CS3)	44.8	150	272	272	0.11	244	4,280	W	90	0.47	52	12.4	II
45	AR(CF045)	24.8	200	340	340	0.11	230	3,480	W	90	0.26	35	9.5	I
46	AR(CF064)	24.9	200	340	340	0.11	230	3,480	W	90	0.45	61	9.6	I
47	AR(CF097)	25.2	200	340	340	0.11	230	3,480	W	90	0.77	106	9.8	I
48	AR(CF131)	25.4	200	340	340	0.11	230	3,480	W	90	1.1	157	10.3	I
49	AR(CF243)	25.6	200	340	340	0.22	230	3,480	W	90	2.2	206	6.6	I
50	M(AN-1/5)	35.1	125	165	165	--	230	3,470	W	90	0.35	18.56	12.5	Fracture
51	M(AN-1/2)	32.4	125	165	165	--	230	3,470	W	90	0.88	29.43	7.85	Fracture
52	M(CN-1/2)	39.1	125	165	165	--	230	3,470	W	90	0.88	34.5	9.2	Fracture
53	OM(SB2)**	24.3	300	260	260	0.11	248	3,430	W	90	0.37	22	3.41	III
54	OM(SB3)**	24.3	300	260	260	0.11	248	3,430	W	90	0.74	113	8.8	III
55	OM(SC2)**	25.2	600	540	540	0.11	230	2,800	W	90	0.37	105	4.23	III
56	OM(SC3)**	25.2	600	540	540	0.11	230	2,800	W	90	0.73	258	5.26	III
57	OM(SC4)**	25.2	600	540	540	0.11	230	2,800	W	90	1.85	263	2.12	III
58	TA(S4)	48.5	180	460	460	0.8	70.8	860	S	45	8.8	210.5	3.23	Fracture
59	TA(SR1)	53.8	180	460	460	0.8	70.8	860	S	45	4.4	89	2.71	Debonding
60	TA(SR2)	52.7	180	460	460	0.8	70.8	860	S	45	8.8	122.5	1.86	Debonding
61	K(B-CW2)	27.5	150	255	255	0.165	228	3,500	U	90/0	2.2	39	2.26	IV
62	K(B-CO2)	20.5	150	255	255	0.165	228	3,500	U	90	0.88	40	5.81	Debonding

**Table (5-1).** Experimental data on shear strengthening using CFRP (continued)

No. (1)	Reference and Test specimen Designation (2)	$f'_c$ (MPa) (3)	Section Dimensions			CFRP Properties and Wrapping Schemes				$\beta^\circ$ (11)	$\rho_f$ ( $\times 10^{-3}$ ) (12)	$V_{f,exp}$ (kN) (13)	$\epsilon_{fe}$ ( $\times 10^{-3}$ ) (14)	Failure Mode (15)
			$b_w$ (mm) (4)	$d$ (mm) (5)	$d_f$ (mm) (6)	$t_f$ (mm) (7)	$E_f$ (GPa) (8)	$f_{fu}$ (MPa) (9)	Wra. Sch. (10)					
63	K(B-CO3)	20.5	150	255	255	0.165	228	3,500	U	90	2.2	65	3.77	Debonding
64	K(C-BT2)	35	150	355	255	0.165	228	3,790	U	90	2.2	65	3.77	Debonding
65	K(C-BT3)	35	150	355	255	0.165	228	3,790	U	90/0	2.2	67.5	3.92	Debonding
66	K(C-BT4)	35	150	355	255	0.165	228	3,790	U	90	0.88	72	10.4	Debonding
67	K(C-BT5)	35	150	355	255	0.165	228	3,790	S	90	0.88	31.5	4.57	Debonding
68	K(C-BT6)	35	150	355	267	0.165	228	3,790	A	90	2.2	131	7.26	Flexural
69	K(A-SW3-2)	19.3	150	255	255	0.165	228	3,790	U	90/0	2.2	50.5	2.93	IV
70	K(A-SW4-2)	19.3	150	255	255	0.165	228	3,790	U	90/0	2.2	80.5	4.67	IV
71	K(A-SO3-2)	27.5	150	255	255	0.165	228	3,790	U	90	0.88	54	7.84	Debonding
72	K(A-SO3-3)	27.5	150	255	255	0.165	228	3,790	U	90	1.32	56.5	5.47	Debonding
73	K(A-SO3-4)	27.5	150	255	255	0.165	228	3,790	U	90	2.2	67.5	3.92	Debonding
74	K(A-SO3-5)	27.5	150	255	255	0.165	228	3,790	U	90/0	2.2	92.5	5.37	IV
75	K(A-SO4-2)	27.5	150	255	255	0.165	228	3,790	U	90	0.88	62.5	9.07	Debonding
76	K(A-SO4-3)	27.5	150	255	255	0.165	228	3,790	U	90	2.2	90	5.22	IV

In column 2, SA= Sato et al<sup>6</sup>. ; SA1=Sato et al<sup>7</sup>. ; UJ= Uji<sup>2</sup> ; TK= Taewe et al<sup>10</sup>. ; C=Chajes et al.<sup>5</sup>; T= Triantafillou<sup>16</sup> ; F=Funakawa et al<sup>11</sup>. ; O=Ohuchi et al<sup>4</sup>. ; U=Umezu et al<sup>8</sup>. ; AR=Araki et al<sup>9</sup>. ; M=Miyauchi et al<sup>12</sup>. ; OM=Ono et al<sup>13</sup>. ; TA=Taljsten<sup>14</sup> ; K=Khalifa et al.(test results are reported in chapter 3 and 4).

\* Data collected from Triantafillou. <sup>16</sup>

\*\* Axial stress = 0.062  $f'_c$ .

In column 10, S=CFRP sheet bonded to beam sides only; U=CFRP sheet in the form of U-wrap; A= CFRP U-wrap provided with end anchor; W= CFRP sheet wrapped around the entire beam.

In columns 7, 9, and 13 -- = value not available ( $f_{fu}$  was assumed = 2,760 MPa).

In column 15, I= Shear tension failure; II= Shear failure followed by sheet fracture; III= Shear failure (type of failure was not identified in the corresponding reference); IV= Concrete splitting on a vertical plan.

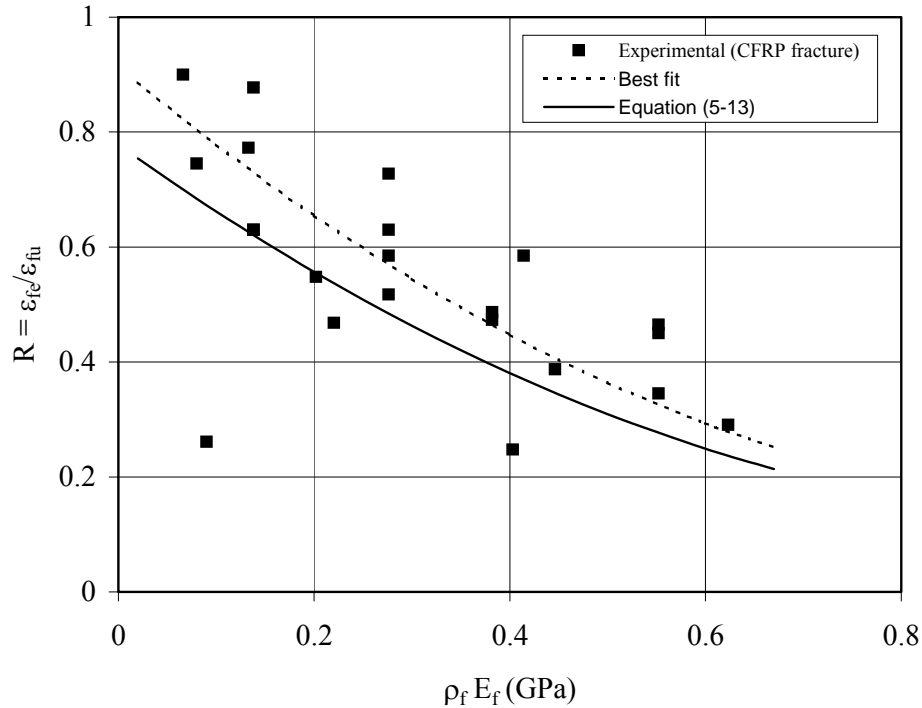


**Figure 5-2.** Strength reduction coefficient in terms of  $\rho_f E_f$  for FRP fracture

**Reduction Coefficient based on CFRP Debonding Failure:** If the CFRP sheet is U-wrapped without end anchor or bonded only to the sides of the beam, the anchorage is limited by the interfacial bond between the FRP and concrete. In these situations, a failure mode based on the bond mechanism must be investigated. Once shear forces develop inclined cracks in the concrete, high tensile stresses develop in the portions of CFRP sheet that bridge these cracks. The tensile stresses in vertically oriented CFRP sheets are a result of the vertical separation of rigid bodies of concrete on either side of the crack. These tensile stresses must be transferred to the concrete on each side of the crack by interfacial bond stresses. If this interfacial bond is compromised before fracture of the CFRP sheet, a debonding failure occurs. In order to address the debonding failure mode, another approach based on the bond characteristics of CFRP sheets with concrete is presented. The approach will, necessarily, consider the effects of concrete strength and wrapping schemes.

Bond Mechanism Models: Maeda et al.<sup>38</sup> studied the bond mechanism of CFRP sheets to concrete. The study described the concept of average bond strength and effective bond length based on experimental results and suggested empirical equations to predict bond behavior. The experiments conducted by Maeda et al. involved tensioning CFRP strips bonded to a concrete surface. Experiments were run for various CFRP sheet axial rigidity and bonded lengths. According to observations by Maeda et al., for bonded lengths over 100 mm, the ultimate tensile force that the CFRP strip carries is independent on its bonded length. The reason for this is that at an early stage of loading, load is sustained by bond in the vicinity of the loading point. If debonding occurs in this vicinity by concrete fracture, the area of active bonding is shifted to a new area. This action is repeated until debonding propagates completely through the length of the CFRP. Therefore, bond stresses are only transferred in the active bonded area. The length of CFRP that includes the active bonded area is termed the effective bond length,  $L_e$ , and presented as a function of thickness of CFRP sheet and its elastic modulus (i.e., function of axial rigidity of CFRP sheet). In addition, the bond stress at failure is presented as a linear function of CFRP stiffness. Based on the results of this study conducted by Maeda et al, the author presented a set of equations that apply the concepts of effective bond length and average bond stress to shear strengthening.<sup>36</sup> The empirical equations predict the average bond strength and effective bond length used to quantify the capacity of CFRP sheets.

However, in a recent study, experimental and analytical results by Miller<sup>39</sup> modified the model by Maeda et al. and proposed new equations to predict the effective bond length and the ultimate load at CFRP debonding. Even though both models seemed to yield similar results in terms of ultimate load, Miller's model has been adopted.

The experimental conducted by Miller involved testing of CFRP strip bonded to a concrete surface by performing simple flexural tests (Fig. 5-3). The use of this type of test to characterize bond behavior for shear strengthening is reasonable considering the mechanism of force transfer in a shear-strengthening configuration. The test variables included concrete strength, CFRP stiffness, and the bond length.

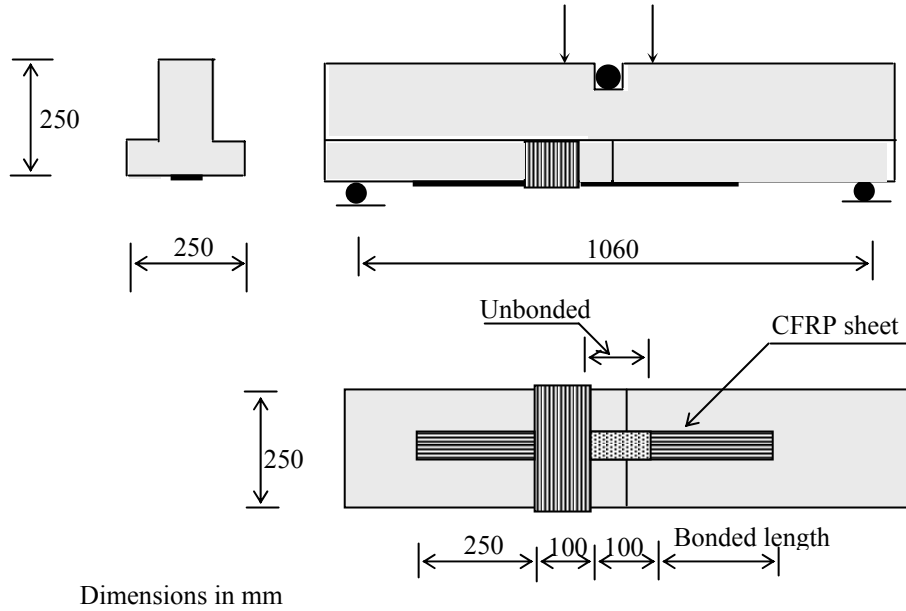


**Figure 5-3.** Layout of the bond test specimen of Miller<sup>39</sup>

Effective Bond Length and Ultimate Load Capacity: The shear capacity governed by CFRP debonding from the concrete surface was presented as a function of CFRP stiffness, concrete strength, effective depth of CFRP reinforcement, and bonded surface configurations.<sup>36</sup> In determining the reduction coefficient for bond, the effective bond length,  $L_e$ , has to be determined first. Based on analytical and experimental data from bond tests, Miller showed that the effective bond length increases as CFRP axial rigidity,  $t_f E_f$ , increases. However, he suggested a conservative value for  $L_e$  equal to 75 mm. The value may be modified when more bond tests data becomes available.

The experimental results indicated that the bond stress at failure is a function of the CFRP axial rigidity and the average bond strength,  $\tau_{bu}$  may be computed from Equation (5-14)

$$\tau_{bu} = \left( 119.06 (t_f E_f) - 0.654 (t_f E_f)^2 \right) \times 10^{-6} \quad (5-14)$$

where,  $\tau_{bu}$  is the average bond stress in GPa,  $t_f$  is the thickness of the CFRP sheet in mm, and  $E_f$  is the modulus of elasticity of CFRP sheet in GPa. Finally, considering an active bonded area

equal to the effective bond length,  $L_e$ , times the width of the bonded sheet,  $w_f$ , the ultimate load capacity of the CFRP sheet,  $P_{max}$ , may be computed from Equation (5-15).

$$P_{max} = L_e w_f \tau_{bu} \quad (5-15)$$

Equation (5-15) is applicable for CFRP axial rigidity,  $t_f E_f$ , ranging from 20 to 90 mm.GPa. Research into quantifying the bond characteristics for axial rigidity above 90 mm.GPa is being conducted at UMR.

Effect of Concrete Strength: In addition to the stiffness of the CFRP sheet, the bond strength depends on the concrete compressive strength. The concrete used in the experiments by Miller was consistently 42 MPa. For concrete of other strengths, further research is required. Although Miller concluded that the concrete strength has no significant effect on the bond mechanism between CFRP sheet and concrete surface, Horiguchi and Saeki<sup>40</sup> showed that the bond strength between the CFRP sheet and the concrete surface is a function of  $(f'_c)^{2/3}$ . Until a new study focusing on the effect of concrete strength combined with surface roughness become available, a modification to Equation (5-14) may be accomplished by multiplying by  $(f'_c/42)^{2/3}$ , where  $f'_c$  in MPa.. This modification is reflected in Equation (5-16).

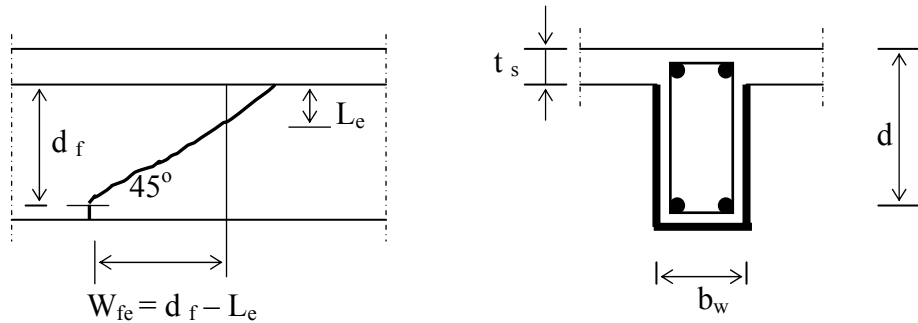
$$\tau_{bu} = \left( 119.06 (t_f E_f) - 0.654 (t_f E_f)^2 \right) (f'_c/42)^{2/3} \times 10^{-6} \quad (5-16)$$

Effect of Bonded Surface Configuration: For the case of shear strengthening, once a shear crack develops, only that portion of FRP extending past the crack by the effective bonded length will be capable of carrying shear. It is, therefore, suggested to replace the width of the FRP sheet,  $w_f$ , with an effective width,  $w_{fe}$ , in Equation (5-15). The effective width depends on the shear crack angle (assumed to be 45°) and the bonded surface configuration as illustrated in Figure (5-4). The value of  $w_{fe}$  may be computed from Equations (5-17-a) and (5-17-b).

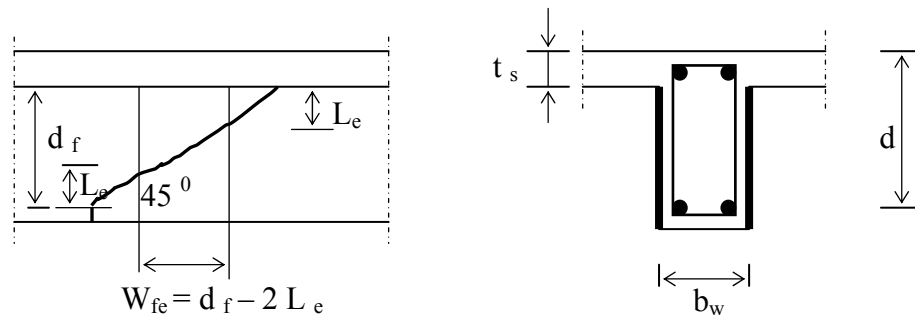
$$w_{fe} = d_f - L_e \quad \text{If the sheet is in the form of a U-wrap without end anchor} \quad (5-17-a)$$

$$w_{fe} = d_f - 2 L_e \quad \text{If the sheet is bonded only to the sides of the beam} \quad (5-17-b)$$

For the cases of those totally wrapped or U-wrap with end anchor, the failure mode of CFRP debonding is not considered.



(a) FRP sheet in the form of U-wrap



(b) FRP sheet bonded only on the two beam sides

**Figure 5-4.** Effective width of FRP reinforcement

Proposed Bond-Based Design Algorithms: The design equations for computing the shear contribution of CFRP based on the bond mechanism may be written in a similar form as Equation (5-8). For the case of bond, the total force that can be developed in the sheet on one side of the beam is  $P_{max}$  given in Equation (5-15). This force may be used to develop an

expression for the effective average stress (or reduction coefficient on the ultimate stress) similar to that used in Equation (5-8). The development of such an expression shown next.

The force  $P_{\max}$  is developed on both sides of the beam, therefore the effective stress may be determined from the following equality.

$$2P_{\max} = A_f f_{fe} \quad (5-18)$$

Using Equation (5-15),

$$2L_e w_f \tau_{bu} = A_f f_{fe} \quad (5-19)$$

Using Equations (5-10) and (5-14), and expanding the term for the area of fiber, consider  $L_e=75$  mm, and rearranging we obtain:

$$R = \frac{(f_c)^{2/3}}{\varepsilon_{fu}} [738.93 - 4.06 (t_f E_f)] \times 10^{-6} \quad (5-20)$$

This expression may be used in Equations (5-8) and (5-10), except that only those strips within the width,  $w_{fe}$ , are effective. This adjustment may be made by multiplying R by the ratio of  $w_{fe}/d_f$ . Thus, the final expression for R is given in Equation (5-21).

$$R = \frac{(f_c)^{2/3} w_{fe}}{\varepsilon_{fu} d_f} [738.93 - 4.06 (t_f E_f)] \times 10^{-6} \quad (5-21)$$

***Validity of the Proposed Bond-Based Design Algorithms:*** To validate the proposed shear design algorithms based on debonding control, all of the available test results up to date (25 tests) collected from various experimental programs and included the results of this study are used. The comparison is shown in Figure (5-5). The factored design datum shown in Figure (5-5) is based on the suggested strength reduction factor for CFRP contribution,  $\phi=0.7$ , as discussed later. The proposed design approach tends to underestimate the actual shear strength determined from experimental results, but gives conservative results. The tests used in the comparison are



This limit is such that the average strain in CFRP materials at ultimate can not be greater than 0.006 mm/mm (without the strength reduction factor). The suggested value of the upper limit is mainly based on evaluation of the available test results and it gives conservative results. However, an analytical study to link the allowable shear crack width with the effective average strain in both external shear reinforcement (CFRP sheet) and the internal one (steel stirrups) is needed, and a further adjustment to that upper limit may be suggested.

### **5-3-2-2 Design Considerations**

The proposed equations allow for the computation of the nominal shear contribution of CFRP sheets in RC beams. There are further considerations that must be made when designing these systems; this section seeks to address those issues.

**Strength Reduction Factor:** Due partly to the novelty of this repair technique, it is advisable to apply more stringent reduction factor to the FRP shear reinforcement than to the concrete shear strength and steel shear reinforcement. Based on the available experimental data, the author suggest a reduction factor of  $\phi = 0.70$  (ACI format) applied to  $V_f$  in Equation (5-8). A comparison of the experimental data with the shear contribution of CFRP computed using this value is given in Figure (5-5) for the case of failure controlled by CFRP debonding and in Figure (5-6) for failure controlled by CFRP fracture. Note that, the upper limit shown in Figure (5-6) is corresponding to  $\epsilon_{fu} = 0.015$  mm/mm. The figures show this recommendation to be conservative for nearly all cases.

**Spacing Requirements:** Similar to steel shear reinforcement, the spacing of FRP strips should not be so wide as to allow the full formation of a diagonal crack without intercepting a strip. ACI sections 11-5-4-1 and 11-5-4-3 set a limit on the maximum spacing of steel shear reinforcement as the smaller of  $d/2$  or 610 mm if  $V_u/\phi - V_c \leq 1/3\sqrt{f'_c} b_w d$  and the smaller of  $d/4$  or 305 mm if  $V_u/\phi - V_c > 1/3\sqrt{f'_c} b_w d$ . In shear strengthening situations, the value of  $V_u/\phi - V_c$  is probably exceeding  $1/3\sqrt{f'_c} b_w d$ . For this reason, if strips are used, they should not be spaced by more than the maximum given in Equation (5-23).

$$S_{f,max} = w_f + \frac{d}{4} \quad (5-23)$$

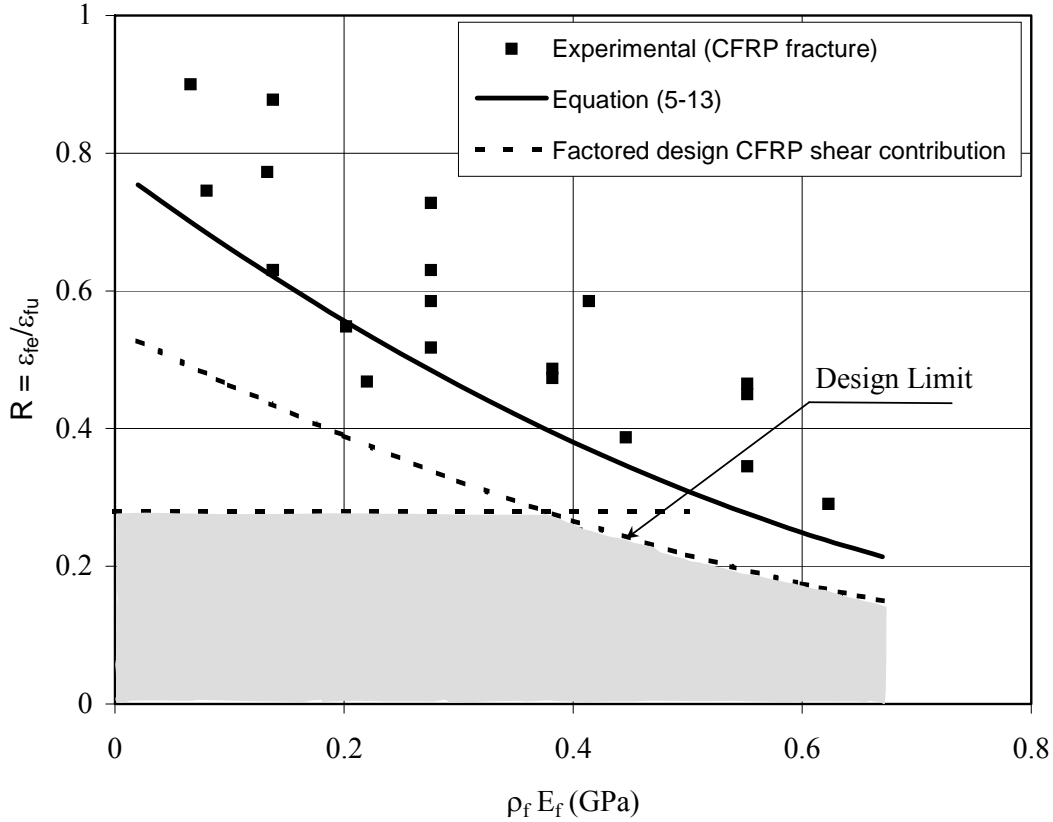


**Figure 5-6.** Effect of strength reduction factor

**Limit on Total Shear Reinforcement:** ACI 318M-95 Sections 11.5.6.7 and 11.5.6.8 set a limit on the total shear strength that may be provided by more than one type of shear reinforcement to preclude the web crushing. FRP shear reinforcement should be included in this limit. A modification to ACI 318M-95 Section 11.5.6.8 is suggested as follows:

$$V_s + V_f \leq \frac{2\sqrt{f'_c} b_w d}{3} \quad (5-24)$$

**Bi-axial CFRP Reinforcement:** The design equations presented do not address the effect of using a horizontal ply of CFRP, with fiber direction oriented parallel to the beam axis ( $\beta=0^\circ$ ),

over a vertical ply ( $\beta=90^0$ ). Adding a horizontal ply may affect shear strength contribution by providing horizontal restraint. In addition, it may slow the propagation of vertical cracks starting at the bottom of the section in positive moment regions and at the top of the section in negative moment regions. Without a quantifiable method for determining the contribution of the horizontal ply to the shear capacity, the general design approach will suffice. Research into quantifying its effect is required. However, in some situation the horizontal ply is recommended to apply over the vertical one. These situations include shear strengthening in negative moment regions if the end anchor is not provided, and shear strengthening of beams with short shear spans in which cracks tend to be steeper.

**Concrete Surface Preparation:** It is important to mention that the mechanical concrete surface preparation method (e.g., sand blasting, water blasting, or grinding mechanical) has a significant effect on the bond behavior of FRP. However, research into characterizing the roughness of the concrete surface and link the bond capacity of FRP with the degree of concrete surface roughness combining with the concrete strength is in progress at UMR. Consequently, further improvement to the shear design model is expected to include that effect.

### 5-3-3 Summary of Proposed Design Procedure

The proposed design equations for computing the shear capacity of RC beams strengthened in shear with externally bonded CFRP sheets in ACI Code format are summarized below:

The effective width of CFRP sheet,  $w_{fe}$ , may be computed first according to the suggested bonded surface configuration.

$$w_{fe} = d_f - L_e \quad \text{If the sheet is in the form of a U-wrap without end anchor} \quad (5-17-a)$$

$$w_{fe} = d_f - 2 L_e \quad \text{If the sheet is bonded to only the sides of the beam} \quad (5-17-b)$$

where  $L_e$  is the effective bonded length and equal to 75mm.

Then, the shear capacity of the section may be found by first computing the reduction coefficient,  $R$ , on the ultimate strength of the CFRP. The reduction coefficient should be taken as the *least* values determined from the three equations.

$$R = 0.56 (\rho_f E_f)^2 - 1.22 (\rho_f E_f) + 0.78 \quad (5-13)$$

$$R = \frac{(f'_c)^{2/3} w_{fe}}{\varepsilon_{fu} d_f} [738.93 - 4.06 (t_f E_f)] \times 10^{-6} \quad (5-21)$$

$$R = \frac{0.006}{\varepsilon_{fu}} \quad (5-22)$$

Note that, in Equations (5-13) and (5-21)  $E_f$  in GPa whereas  $f'_c$  in MPa, and the dimensions  $t_f$ ,  $w_{fe}$ , and  $d_f$  in mm. Equation (5-13) provides  $R$  for failure mode controlled by CFRP fraction and applicable for  $\rho_f E_f \leq 0.7$  GPa. Equation (5-21) describes the failure mode controlled by CFRP debonding and applicable for  $t_f E_f$  ranging from 20 to 90 mm.GPa. Equation (5-21) may be disregarded if the sheet is wrapped around the beam entirely or an effective end anchor is used with U-wrap.

The shear contribution of the CFRP may then be found from the following expressions:

$$f_{fe} = R f_{fu} \quad (5-10)$$

$$V_f = \frac{A_f f_{fe} (\sin\beta + \cos\beta) d_f}{s_f} \leq \left( \frac{2\sqrt{f'_c} b_w d}{3} - V_s \right) \quad \text{with } s_f \leq w_f + \frac{d}{4} \quad (5-25)$$

The shear capacity of the beam may finally be computed as:

$$\phi V_n = 0.85(V_c + V_s) + 0.70V_f \quad (5-26)$$

### 5-3-4 Model Prediction

A comparison between the computed values of CFRP contribution to the shear capacity based on the proposed design approach and all available experimental results, listed in Table (5-

1) and included the results of current study, is shown in Figure (5-8). This figure reveals that the design procedure with the recommended strength reduction factor gives conservative results for nearly all of the experimental data. Note that, data from some of the experimental programs (tests No. 15-28, 56, 57, and 68) were omitted due to unrealistic cross section dimensions. In addition, the summary and the comparison between the experimental results of this study and the calculated factored shear strength using the proposed design approach are detailed in Table (5-2). For CFRP strengthened beams, the measured contribution of concrete,  $V_c$ , and steel stirrups,  $V_s$ , (when present) were considered equal to the shear strength of a non-strengthened beam. This comparison also indicates that the design approach gives satisfactory and conservative results for the strengthened beams as illustrated in Figure (5-8).

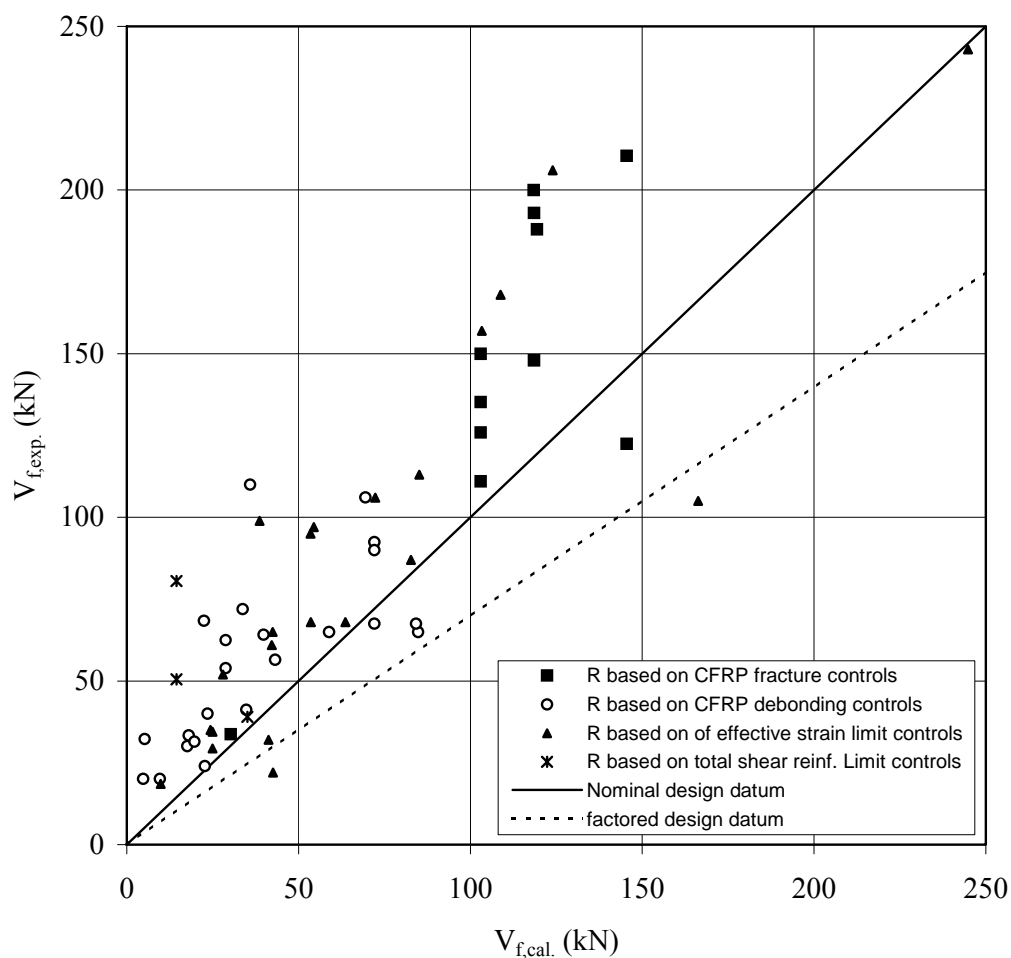


**Figure 5-7.** Comparison of experimental results with calculated values based on the proposed design procedure

**Table (5-2)** Comparison between experimental results and calculated values

No.	Specimen	Experimental results				Design approach (ACI format)					
		$V_{n,exp.}$ (kN)	$(V_c+V_s)_{exp.}$ (kN)	$V_{f,exp.}$ (kN)	Failure mode at ultimate	$(V_c+V_s)$ (kN)	$V_f$ (kN)	$V_n$ (kN)	$\phi V_f$ ( $\phi=0.7$ ) (kN)	$\phi V_n=0.85(V_c+V_s)+0.7V_f$ (kN)	Predicted failure mode
1	A-SW3-1	126.5	126.5	--	Shear	137.0	--	137.0	--	116.5	Shear
2	A-SW3-2	177.0	126.5	50.5	Splitting*	137.0	14.5	151.5	10.2	126.6	Web crashing**
3	A-SW4-1	100.0	100.0	--	Shear	134.6	--	134.6	--	114.4	Shear
4	A-SW4-2	180.5	100.0	80.5	Splitting*	134.6	14.5	149.1	10.2	124.6	Web crashing**
5	A-SO3-1	77.0	77.0	--	Shear	41.0	--	41.0	--	34.9	Shear
6	A-SO3-2	131.0	77.0	54.0	Debonding	41.0	28.8	69.8	20.3	55.2	Debonding
7	A-SO3-3	133.5	77.0	56.5	Debonding	41.0	43.2	84.2	30.3	65.1	Debonding
8	A-SO3-4	144.5	77.0	67.5	Debonding	41.0	72.0	113.0	50.4	85.3	Debonding
9	A-SO3-5	169.5	77.0	92.5	Splitting*	41.0	72.0	113.0	50.4	85.3	Debonding
10	A-SO4-1	65.0	65.0	--	Shear	38.7	--	38.7	--	32.9	Shear
11	A-SO4-2	127.5	65.0	62.5	Debonding	38.7	28.8	67.5	20.2	53.1	Debonding
12	A-SO4-3	155.0	65.0	90.0	Splitting*	38.7	72.0	110.7	50.4	83.3	Debonding
13	B-CW1	175.0	175.0	--	Shear	146.7	--	146.7	--	124.7	Shear
14	B-CW2	214.0	175.0	39.0	Splitting*	146.7	35.1	181.8	24.6	149.3	Web crashing**
15	B-CO1	48.0	48.0	--	Shear	42.8	--	42.8	--	36.4	Shear
16	B-CO2	88.0	48.0	40.0	Debonding	42.8	23.5	66.3	16.5	52.8	Debonding
17	B-CO3	113.0	48.0	65.0	Debonding	42.8	58.9	101.9	41.2	77.6	Debonding
18	B-CF1	93.0	93.0	--	Shear	59.2	--	59.2	--	50.3	Shear
19	B-CF2	119	93.0	>26.0	Flexural	59.2	44.0	103.2	30.8	81.1	Flexural
20	B-CF3	131	93.0	>38.0	Flexural	59.2	44.0	103.2	30.8	81.1	Flexural
21	B-CF4	140	93.0	>47.0	Flexural	59.2	44.0	103.2	30.8	81.1	Flexural
22	C-BT1	90.0	90.0	--	Shear	57.0	--	57.0	--	48.4	shear
23	C-BT2	155.0	90.0	65.0	Debonding	57.0	84.8	141.8	59.3	107.7	Debonding
24	C-BT3	157.5	90.0	67.5	Debonding	57.0	84.8	141.8	59.3	107.7	Debonding
25	C-BT4	162.0	90.0	72.0	Debonding	57.0	33.7	90.7	23.6	72.0	Debonding
26	C-BT5	121.5	90.0	31.5	Debonding	57.0	19.7	76.7	13.8	62.2	Debonding
27	C-BT6	221.0	90.0	>131.0	Flexural	57.0	103.5	160.5	72.0	120.4	Flexural

$V_n$  = nominal shear strength;  $V_c$  =nominal shear strength provided by concrete;  $V_s$ = nominal shear strength provided by steel stirrups;  $V_f$  = CFRP contribution

\* Concrete splitting on a vertical plane

\*\* Violate proposed limit for  $(V_s+V_f)$

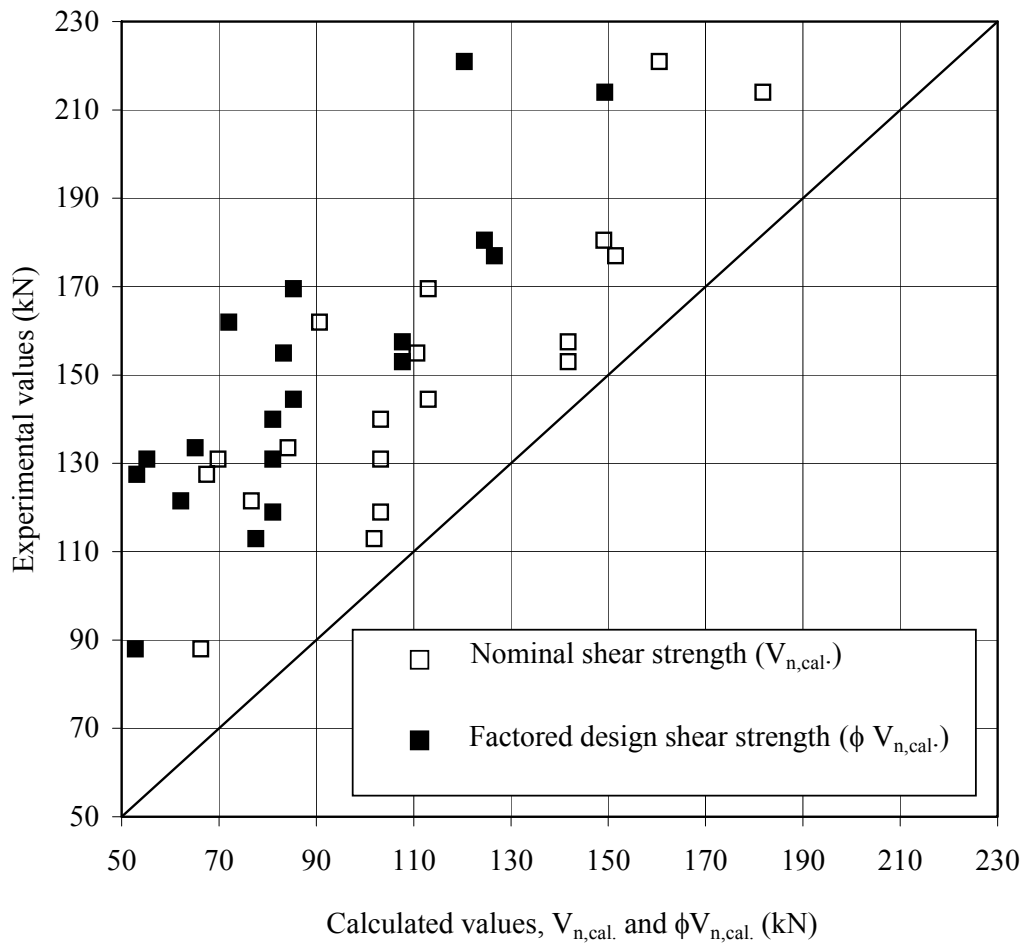


**Figure 5-8.** Comparison of experimental results with calculated values of shear strength for the strengthened beams

### 5-3-5 Design Example

Appendix D gives a design example for shear strengthening of an RC beam using externally bonded CFRP sheets according to the proposed design approach in ACI Code format.

## 5-4 SHEAR DESIGN OF RC STRENGTHENED BEAMS IN EGYPTIAN CODE FORMAT

### 5-4-1 Background and Basic Remarks

The basic equations to compute the shear capacity of RC flexural member in ultimate limit state according to the Egyptian Code<sup>41</sup> are summarized below:

The nominal ultimate shear strength at a given section of the beam,  $q_u$ , is

$$q_u = \frac{Q_u}{bd} \quad (5-27)$$

where  $Q_u$  is the ultimate shear force,  $b$  is the beam width, and  $d$  is the effective depth of the cross-section.

The nominal ultimate shear strength,  $q_u$ , must fulfill the following condition:

$$q_u \text{ (maximum)} = \text{minimum} \left[ 2.2 \sqrt{\frac{f_{cu}}{\gamma_c}} \text{ kg/cm}^2, \quad 30 \text{ kg/cm}^2 \right] \quad (5-28)$$

where  $f_{cu}$  is the characteristic cube strength of concrete in  $\text{kg/cm}^2$  ( $f_{cu}=1.25f_c$ ),  $\gamma_c$  is the strength reduction coefficient for concrete ( $\gamma_c = 1.5$ ).

The nominal shear strength provided by concrete,  $q_{cu}$ , is

$$q_{cu} = 0.75 \sqrt{\frac{f_{cu}}{\gamma_c}} \text{ kg/cm}^2 \quad (5-29)$$

If the nominal ultimate shear strength,  $q_u$ , exceed the nominal shear strength provided by concrete,  $q_{cu}$ , the web reinforcement is required. In that case, the nominal shear strength provided by shear reinforcement,  $q_{su}$ , must fulfill the following condition:

$$q_{su} \geq q_u - 0.5 q_{cu} \quad (5-30)$$

If the vertical stirrups are used without bent-up bars, the shear reinforcement should be calculated as follows:

$$q_{su} = \frac{A_{st} (f_y / \gamma_s)}{b s} \quad (5-31)$$

where  $A_{st}$  is the area of steel stirrups resisting the shearing force,  $f_y$  is the yield strength of steel,  $\gamma_s$  is the reduction factor for steel ( $\gamma_s=1.15$ ), and  $s$  is the spacing of stirrups.

If bent-up steel bars (with vertical stirrups) or inclined stirrups are used, the inclined shear reinforcement should be calculated as follows:

$$q_{sub} = \frac{A_{sb} (f_y / \gamma_s) (\sin\alpha + \cos\alpha)}{b s} \quad (5-32)$$

$$q_{su} = q_{sub} + q_{sus} \quad (5-33)$$

where  $A_{sb}$  is the area of bent-up bars or inclined stirrups,  $\alpha$  is the angle between bent-up bars or inclined stirrups and the longitudinal axis of the beam,  $q_{sub}$  is the nominal shear strength provided by the bent-up bars or inclined stirrups,  $q_{sus}$  is the nominal shear strength provided by the vertical stirrups.

#### **5-4-2 Shear Capacity of a CFRP Strengthened Section**

The following is the summary of the recommended sequence of design steps to compute the contribution of externally bonded CFRP reinforcement to the shear capacity of RC flexural member in Egyptian Code format:

1. According to the suggested bonded surface configuration (U-wrap or two beam sides), determine the effective width of CFRP sheet,  $w_{fe}$ , using Equations (5-17-a and b) with effective bonded length,  $L_e$ , equal to 75mm.

2. Determine the reduction coefficient,  $R$ , of the ultimate strength of the CFRP. The reduction coefficient should be taken as the smallest of:

- The reduction coefficient for failure mode controlled by CFRP fracture (Eq. 5-13).
- The reduction coefficient for failure mode controlled by CFRP debonding (Eq. 5-21).
- The reduction coefficient to control the shear crack width and loss of aggregate interlock (Eq. 5-22).

Note that, in Equations (5-13) and (5-21), The elastic modulus of CFRP sheet,  $E_f$  is in GPa whereas  $f'_c$  in MPa ( $f'_c$  is the cylinder compressive concrete strength ( $f_{cu}=1.25 f'_c$ )), and the dimensions  $t_f$ ,  $w_{fe}$ , and  $d_f$  are in mm. Moreover, the second expression (Eq. 5-21) may be disregarded if the sheet is wrapped around the beam entirely or an effective end anchor is used with U-wrap.

3. Determine the effective average CFRP stress,  $f_{fe}$  from Equation (5-10).

4. Compute the nominal shear strength provided by the externally bonded CFRP reinforcement,  $q_{fu}$ .

$$q_{fu} = \frac{A_f (f_{fe} / \gamma_f) (\sin\beta + \cos\beta) d_f}{s_f b d} \quad (5-34)$$

where  $\gamma_f$  is the strength reduction coefficient for CFRP, suggested to be equal to 1.4.

Note that the maximum spacing  $s_f$  has to be  $s_{f \max} = w_f + d/4$ .

5. The nominal shear strength provided by shear reinforcement,  $q_{su}$ , may be computed from Equation (5-35).

$$q_{su} = q_{sub} + q_{sus} + q_{fu} \quad (5-35)$$

where  $q_{su} = q_u - 0.5 q_{cu}$ . Note that, the nominal ultimate shear strength,  $q_u$ , must fulfill Equation (5-28).

## 5-5 SHEAR DESIGN OF RC STRENGTHENED BEAMS IN EUROCODE FORMAT

### 5-5-1 Background and Basic Remarks

In Eurocode<sup>42</sup> (EC2 1992) the design method of RC beams in shear is based on the basic assumption that the total contribution to shear capacity is the sum of the shear contributions of the concrete and steel shear reinforcement. The shear design is based on three values of shear resistance, stated as  $V_{Rd1}$ ,  $V_{Rd2}$ , and  $V_{Rd3}$ .  $V_{Rd1}$  is the design shear resistance of a concrete member without shear reinforcement. Ignoring the presence of axial force,  $V_{Rd1}$  is expressed as:

$$V_{Rd1} = \tau_{Rd} k (1.2 + 40\rho_1) b_w d \quad (5-36)$$

where  $\tau_{Rd}$  is the basic design shear strength of concrete ( $\tau_{Rd} = 0.25 f_{ctk}/\gamma_c$ ),  $f_{ctk}$  is the characteristic tensile strength of concrete,  $\gamma_c$  is the partial safety factor for concrete ( $\gamma_c=1.5$ ),  $k$  is the size effect factor ( $k = 1.6 - 0.001d \geq 1.0$ ),  $\rho_1$  is the ratio of longitudinal steel reinforcement ( $\rho_1 \leq 0.02$ ).

For a member provided with shear reinforcement, the design shear capacity,  $V_{Rd3}$  is expressed by Equation (5-37).

$$V_{Rd3} = V_{Rd1} + V_{wd} \quad (5-37)$$

where  $V_{wd}$  is the contribution of steel shear reinforcement. Eurocode gives two methods for proportioning shear reinforcement, standard method and the variable strut inclination method.

In the interests of simplicity, the standard method may be considered only in relation to shear reinforcement. The contribution of the steel shear reinforcement,  $V_{wd}$  is given by Equation (6-38).

$$V_{wd} = \frac{A_{sw} (f_{ywk} / \gamma_s) (0.9d) (1 + \cot\alpha) \sin\alpha}{s} \quad (6-38)$$

where  $A_{sw}$  is the cross-section area of shear reinforcement,  $s$  is the spacing of shear reinforcement measured along the longitudinal axis,  $f_{ywk}$  is the yield strength of shear

reinforcement,  $\gamma_s$  is the material safety factor for steel ( $\gamma_s=1.15$ ), and  $\alpha$  is the angle between steel shear reinforcement and the longitudinal axis of the beam.

Irrespective of the amount of shear reinforcement provided, an upper limit is imposed,  $V_{Rd2}$ , on the design shear resistance to preclude web crushing or compression zone failure. The following condition must be fulfilled.

$$V_{Rd1} + V_{wd} \leq V_{Rd2} \quad (5-39)$$

The design resistance  $V_{Rd2}$  is given in Equation (5-40).

$$V_{Rd2} = 0.5 v f_{cd} b_w (0.9d)(1 + \cot\alpha) \quad (5-40)$$

Where  $v$  is the efficiency factor ( $v = 0.7 - f_{ck}/200 \geq 0.5$ ),  $f_{ck} = f_c/\gamma_c$

Finally, at ultimate limit state, the applied design shear force,  $V_{sd}$ , must fulfill the following conditions:

$$V_{sd} \leq V_{Rd1} + V_{wd} \quad (5-41)$$

$$V_{sd} < V_{Rd2} \quad (5-42)$$

### 5-5-2 Shear Capacity of a CFRP Strengthened Section

The proposed design equation (Eq. 5-25) for computing the contribution of externally bonded CFRP reinforcement may be rewritten in Eurocode format as Equation (5-43).

$$V_{fd} = \frac{A_f (f_{fe}/\gamma_f)(0.9d_f)(1 + \cot\beta) \sin\beta}{s_f} \leq [V_{Rd2} - (V_{Rd1} + V_{wd})] \quad (5-43)$$

Where  $V_{fd}$  is the design shear contribution of CFRP to the shear capacity in Eurocode format,  $\gamma_f$  is the partial safety factor for CFRP materials (suggested equal to 1.3).

## CHAPTER 6

### SUMMARY, CONCLUSIONS, AND RECOMMENDATIONS

#### 6-1 SUMMARY

The main objectives of this research study were: (1) to investigate the shear performance and modes of failure of RC beams strengthened with externally bonded CFRP sheets, (2) to address the factors that influence the shear strength, and (3) to propose a design model for computing the shear capacity of the strengthened beams.

In order to fulfill these objectives, an extensive experimental program consisting of twenty-seven, full-scale, RC beams was performed at University of Missouri-Rolla (UMR). The beam specimens were grouped into three main series. The first series focused on shear strengthening of rectangular simply supported beams. The second series examined the capability of CFRP to enhance the shear capacity of continuous beams. The third series investigated the strengthening of simply supported beams with T-shaped cross-section. The variables investigated in this experimental study included steel stirrups, shear span-to-depth ratio, beam cross-section, CFRP amount and distribution, bonded surface configuration, fiber orientation, and end anchor. In addition, a novel end anchor system to allow a better exploitation of the strengthening system was described and tested.

The design approach for computing the shear capacity of RC beams strengthened with externally bonded CFRP composites was proposed. The design model considers CFRP contribution in analogy to conventional shear reinforcement and is presented according to the design format of ACI and two other design codes (Egyptian code and Eurocode). The model addresses the two possible failure mechanisms of CFRP reinforcement, namely: CFRP fracture and CFRP debonding. Furthermore, two limits on the contribution of CFRP shear reinforcement were proposed. The first limit was set to control the shear crack width and loss of aggregate

interlock by imposing a threshold strain. The second limit was to preclude web crushing and was imposed by setting a limit on the total shear strength that may be provided by the external (and internal) shear reinforcement.

## 6-2 CONCLUSIONS

Egypt is facing a growing need for effective means of repair and strengthening of RC structures. Because of their outstanding mechanical, physical, and chemical properties, in addition to simplicity and effectiveness, advanced composite materials show promise in this area. The tests results described in this study indicated that the strengthening technique based on externally bonded CFRP composites can be used to increase significantly shear capacity of RC beams, with efficiency that varies depending on the test variables. For the beams included in the experimental program, increases in shear strength ranged from 22 to 145%.

Based on the experimental and analytical results, the following conclusions are drawn:

- Externally bonded CFRP reinforcement can be used to enhance the shear capacity of RC beams in positive and negative moment regions.
- The test results confirm that the strengthening technique of FRP system is applicable and can increase the shear capacity of rectangular as well as T-beams.
- The experimental verification of the end anchor system shows its effectiveness in increasing the shear capacity of RC beams. This anchor is recommended where bond and/or development length of FRP are critical according to the design procedure.
- Existing evidence clearly indicates that the proprietary end anchor system can make FRP strengthening even more attractive and economical for concrete repair and strengthening.
- The recorded CFRP strain of the tested beams indicates that the failure of a CFRP system occurs at an average effective stress level below nominal strength due to stress concentration or debonding of CFRP from concrete surface.
- The test results show that, at the same load level, the strain in the stirrups of a strengthened beam is smaller than that of the control specimen.

- The test results indicate that the contribution of CFRP benefits the shear capacity to a greater degree for beams without steel shear reinforcement than for beams with adequate steel shear reinforcement.
- The contribution of externally bonded CFRP reinforcement to the shear capacity is influenced by the shear span-to-depth ratio ( $a/d$ ) and it appears to increase with an increase in  $a/d$  ratio.
- Increasing the amount of CFRP may not result in a proportional increase in the shear strength especially if debonding of CFRP controls the failure. A proportional increase in shear capacity with increasing CFRP amount may be achieved when debonding is prevented such in the case of beams with end anchor.
- The test results indicate that the presence of  $0^0$  ply may improve the shear capacity by providing horizontal restraint to the diagonal shear cracks.
- Applying CFRP to the beam sides only is less effective than a U-wrap configuration.
- Comparing with all available published test results to date, the proposed design approach for computing the shear capacity of the strengthened beams gives acceptable and conservative results.

### **6-3 RECOMMENDATIONS FOR FUTURE WORK**

Based on the finding and conclusions of the current study, the following recommendations are made for future research in FRP shear strengthening:

- Research is needed to develop an analytical model to predict the shear behavior and failure mode of RC members strengthened with externally bonded FRP composites and to evaluate the influence of different parameters on the overall behavior of the member. The compression field theory may be used to determine the effect of the FRP on the shear capacity and the crack inclination angle at ultimate limit state. The interfacial bond strength between FRP and concrete substrate and the stress concentration have to be considered in the model.
- Experimental and analytical investigations are required to link the shear contribution of FRP with the load condition. These studies have to consider both the longitudinal steel

reinforcement ratio and the concrete strength as parameters. Laboratory specimens should maintain practical dimensions.

- The interaction between the contribution of external FRP and internal steel shear reinforcement has to be investigated.
- The strengthening effectiveness of FRP has to be addressed in the cases of short shear spans in which arch action behavior governs failure.
- Strengthening effectiveness of U-wrap with/without end anchor in negative moment regions has to be investigated for T beams.
- In order to validate the use of U-wrap with the end anchor in seismic retrofitting situations, the strengthening effectiveness of this system needs to be tested under a cyclic load.
- An experimental program to quantify the bond characteristics of CFRP sheets for axial rigidity above 90 kN/mm is required.
- Research is needed to characterize the roughness of the concrete surface and to link the bond capacity of FRP with the degree of concrete surface roughness combining with the concrete strength.
- An experimental program is required to investigate the shear strengthening of RC beams with aramid and glass FRP composites.
- Analytical investigation to relate the effective average strain of FRP to the shear crack width is required.
- To optimize design algorithms, additional specimens need to be tested with different CFRP amount and configurations to create a large database.
- Effect of existing transverse steel reinforcement, shear span-to-depth ratio, adding a ply in the  $0^0$  direction over a ply in  $90^0$  direction, and degree of concrete surface roughness on the shear contribution of CFRP need to be considered in the proposed design algorithms.
- Shear design algorithms need to be expanded to include strengthening with aramid and glass FRP sheets in addition to CFRP. The bond mechanism between AFRP and GFRP and the concrete substrate should be investigated first.

## **APPENDIX A**

### **PHOTOS OF THE TESTED BEAMS**



**Figure A-1.** Ultimate failure of Specimen A-SW4-1 (control specimen)



**Figure A-2.** Splitting failure of Specimen A-SW4-2 (CFRP 90°/0°)

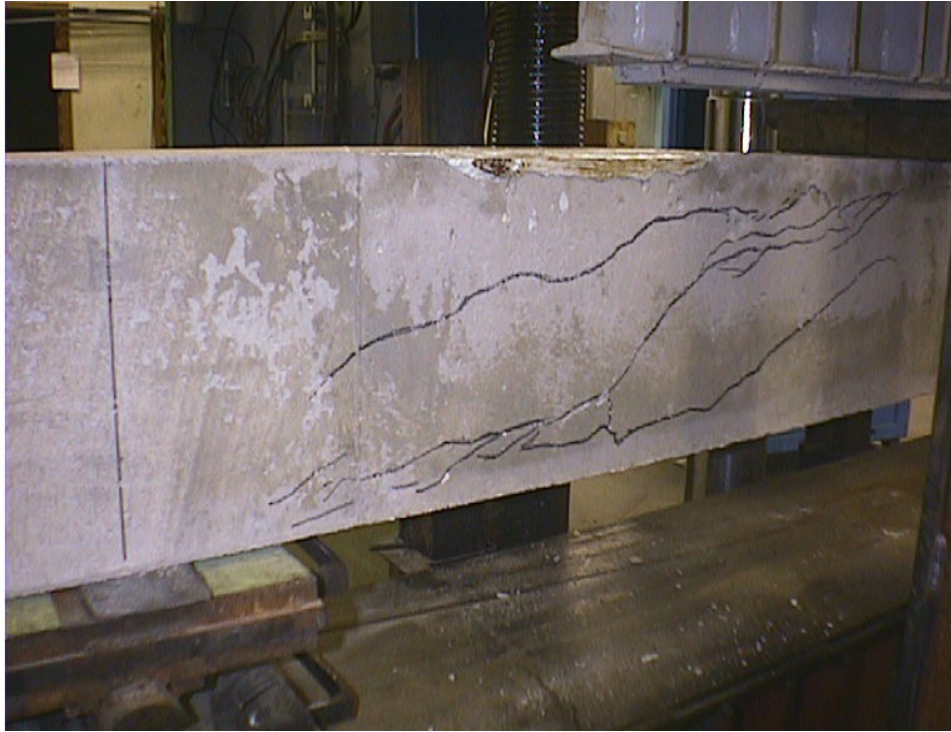


**Figure A-3.** Ultimate failure of Specimen A-SO4-1 (control specimen)

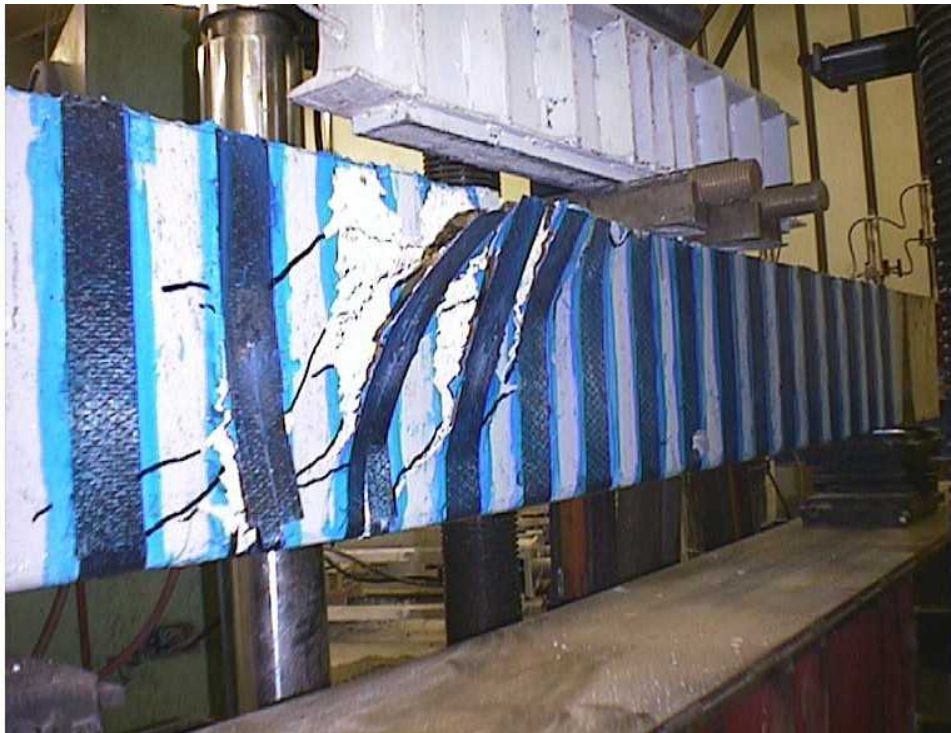


**Figure A-4.** Debonding failure of Specimen A-SO4-2 (U-wrap strips)



**Figure A-5.** Splitting failure of Specimen A-SO4-3 (Continuous U-wrap)



**Figure A-6.** Ultimate failure of Specimen B-CW1 (control specimen)



**Figure A-7.** Ultimate failure of Specimen B-CW2 (CFRP 90°/0°)



**Figure A-8.** Ultimate failure of Specimen B-CO1 (control specimen)



**Figure A-9.** Debonding failure of Specimen B-CO2 (U-wrap strips)



**Figure A-10.** Ultimate failure of Specimen B-CO3 (continuous U-wrap)



**Figure A-11.** Ultimate failure of Specimen B-CF2 (continuous U-wrap)



**Figure A-12.** Ultimate failure of Specimen B-CF3 (CFRP 90°/0°)

## **APPENDIX B**

### **LOAD VERSUS DEFLECTION VURVES**

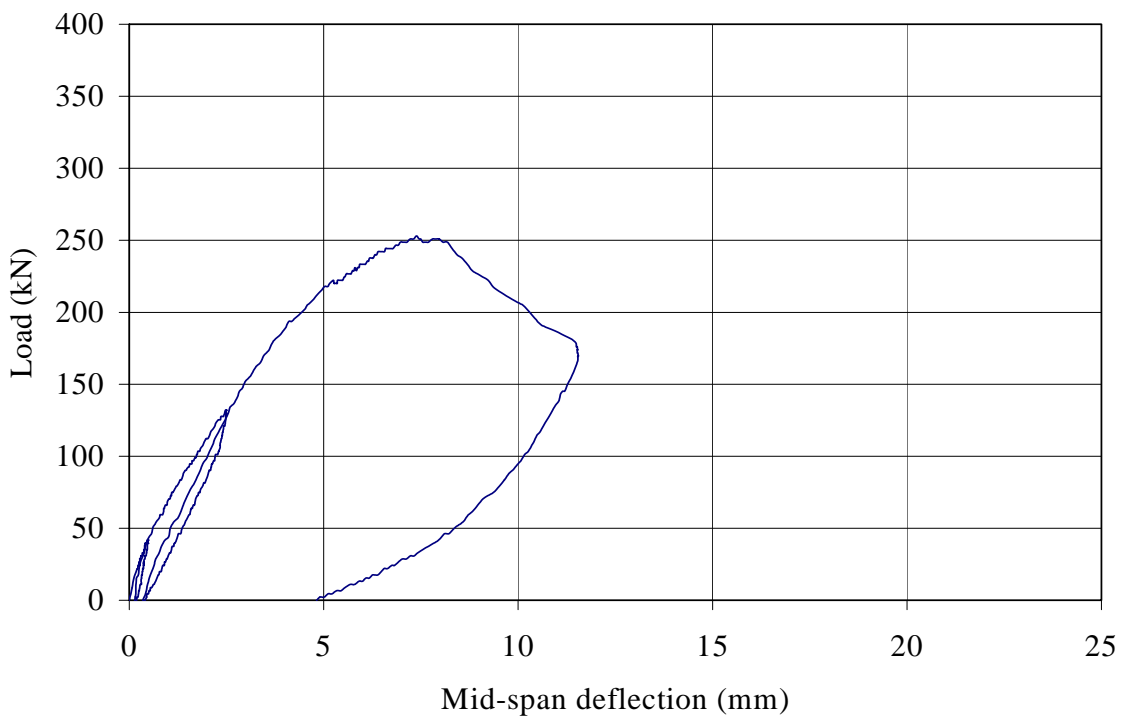


**Figure B-1.** Applied load versus mid-span deflection for Specimen A-SW3-1

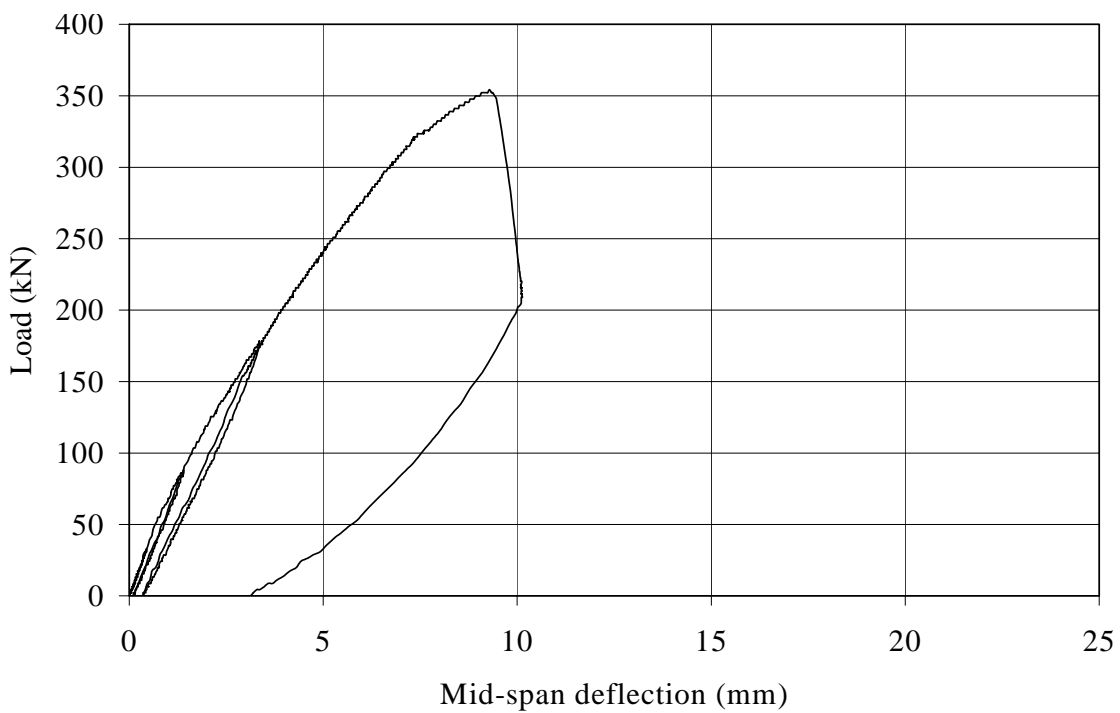


**Figure B-2.** Applied load versus mid-span deflection for Specimen A-SW3-2

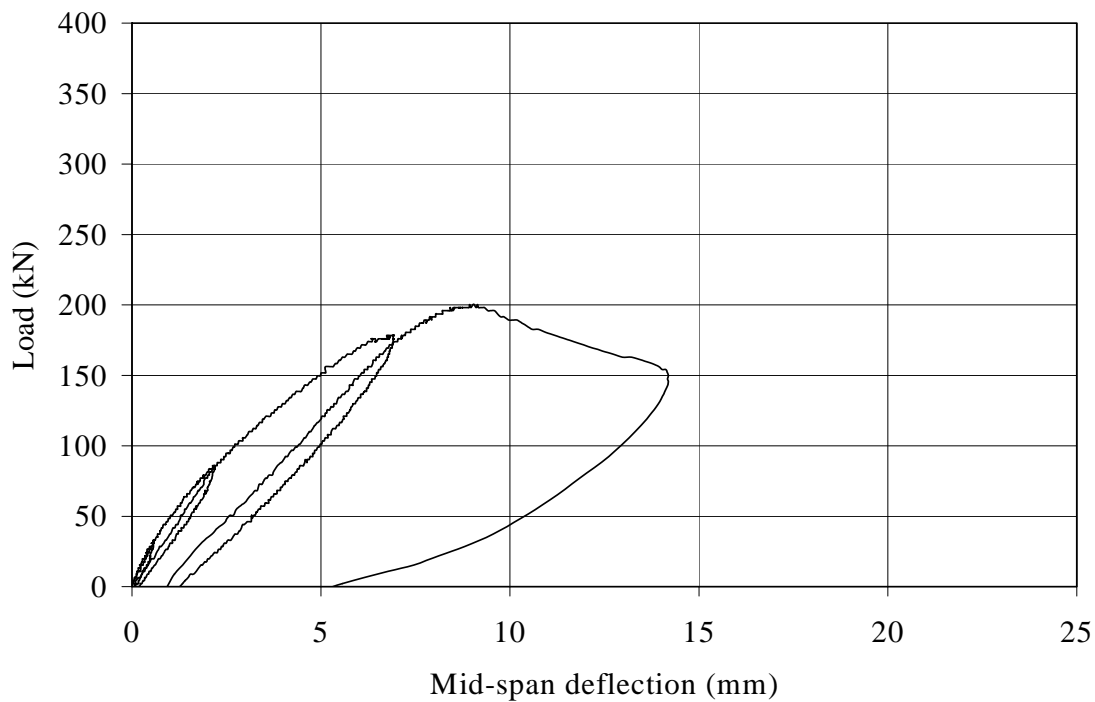


**Figure B-3.** Applied load versus mid-span deflection for Specimen A-SW4-1

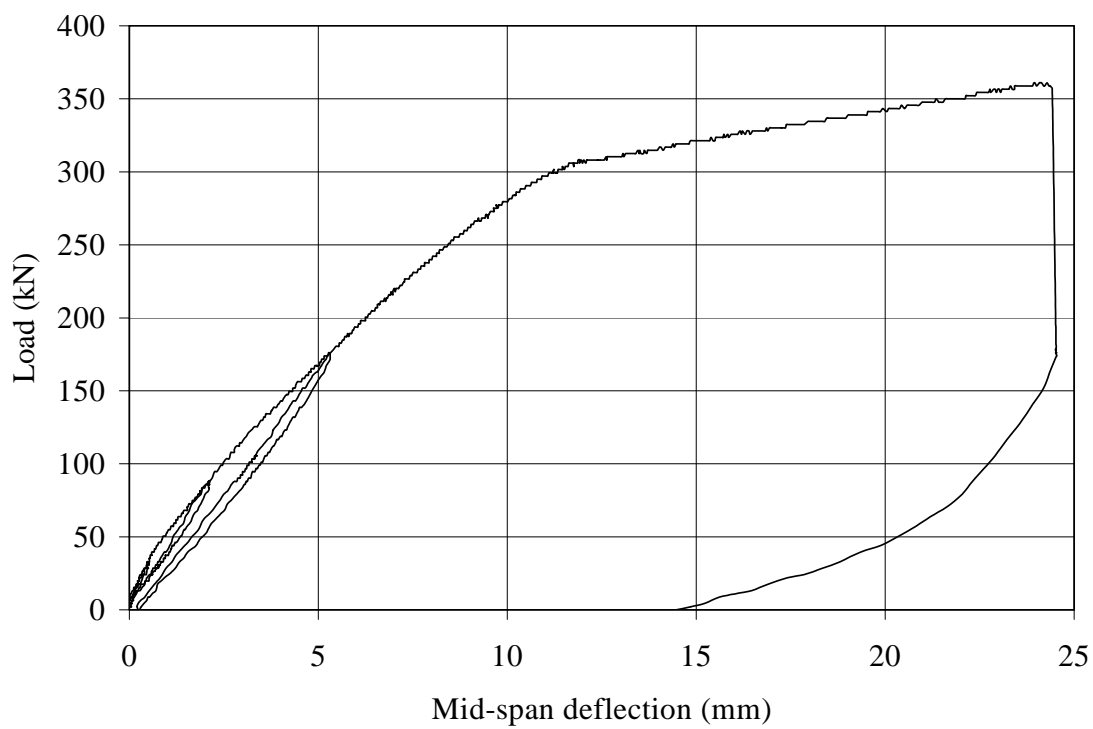


**Figure B-4.** Applied load versus mid-span deflection for Specimen A-SW4-2

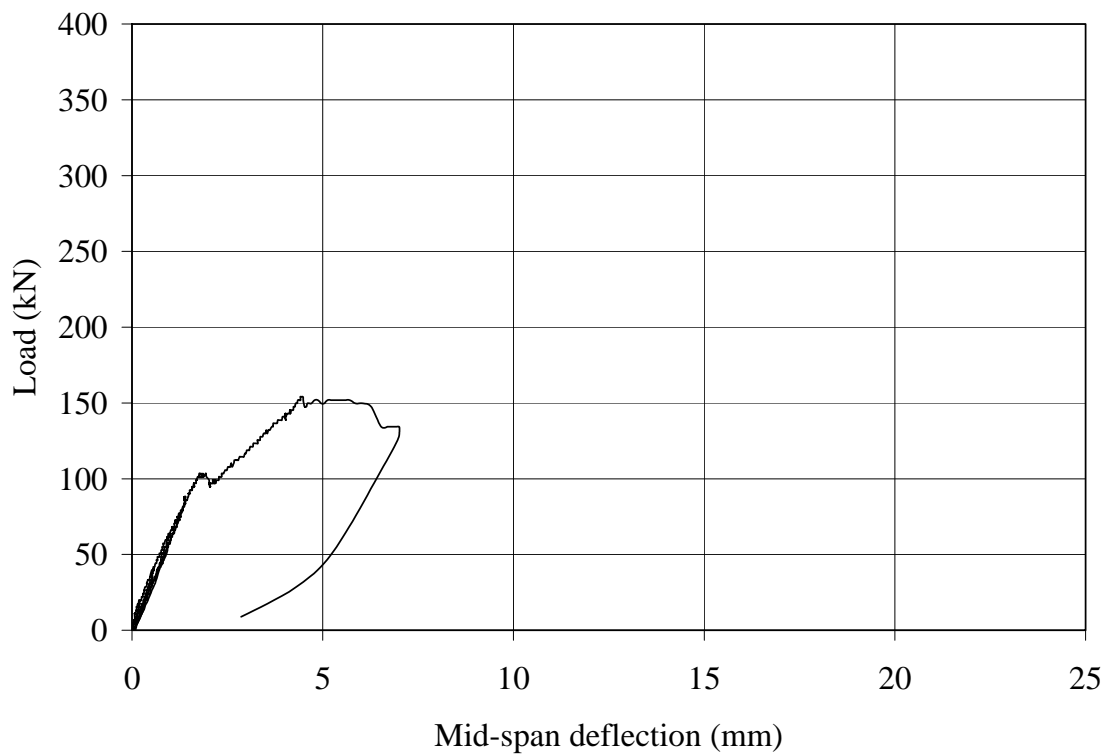


**Figure B-5.** Applied load versus mid-span deflection for Specimen A-SO3-1

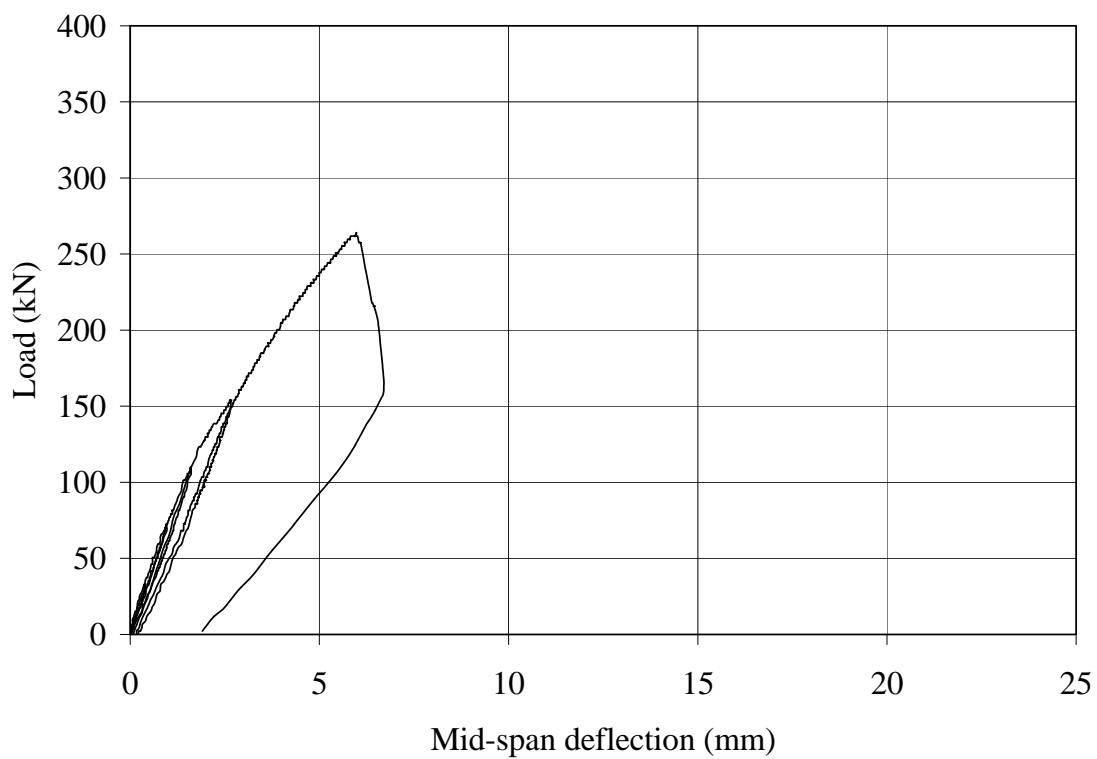


**Figure B-6.** Applied load versus mid-span deflection for Specimen A-SO3-2

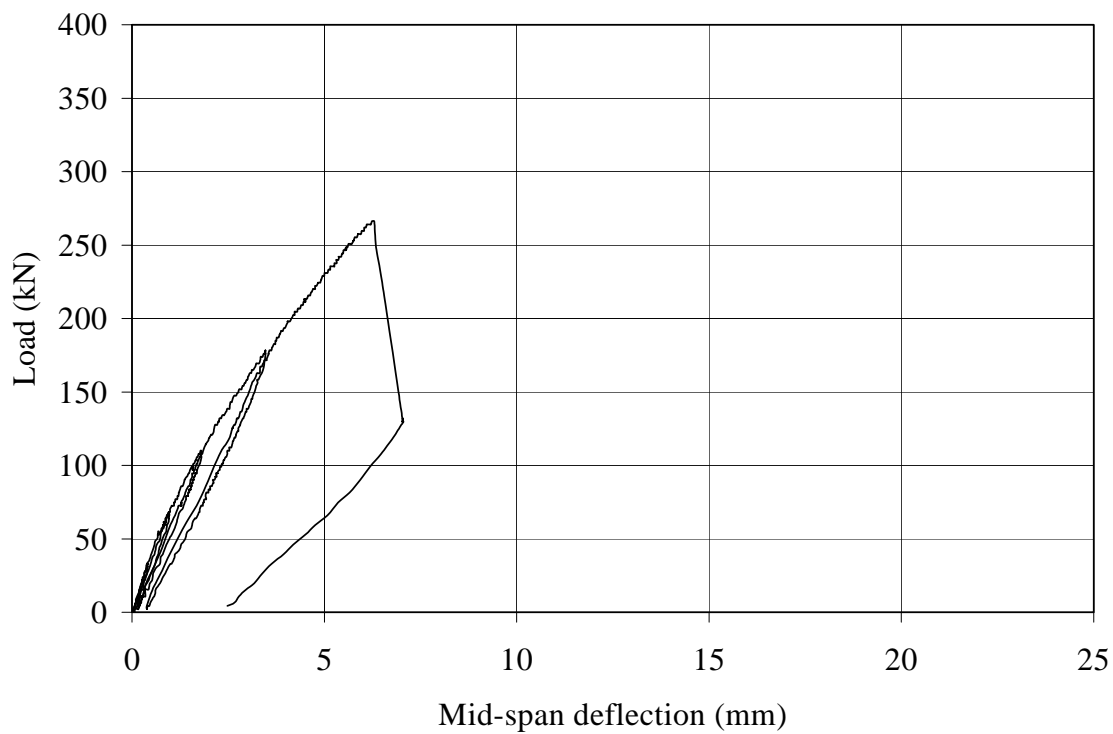


**Figure B-7.** Applied load versus mid-span deflection for Specimen A-SO3-3

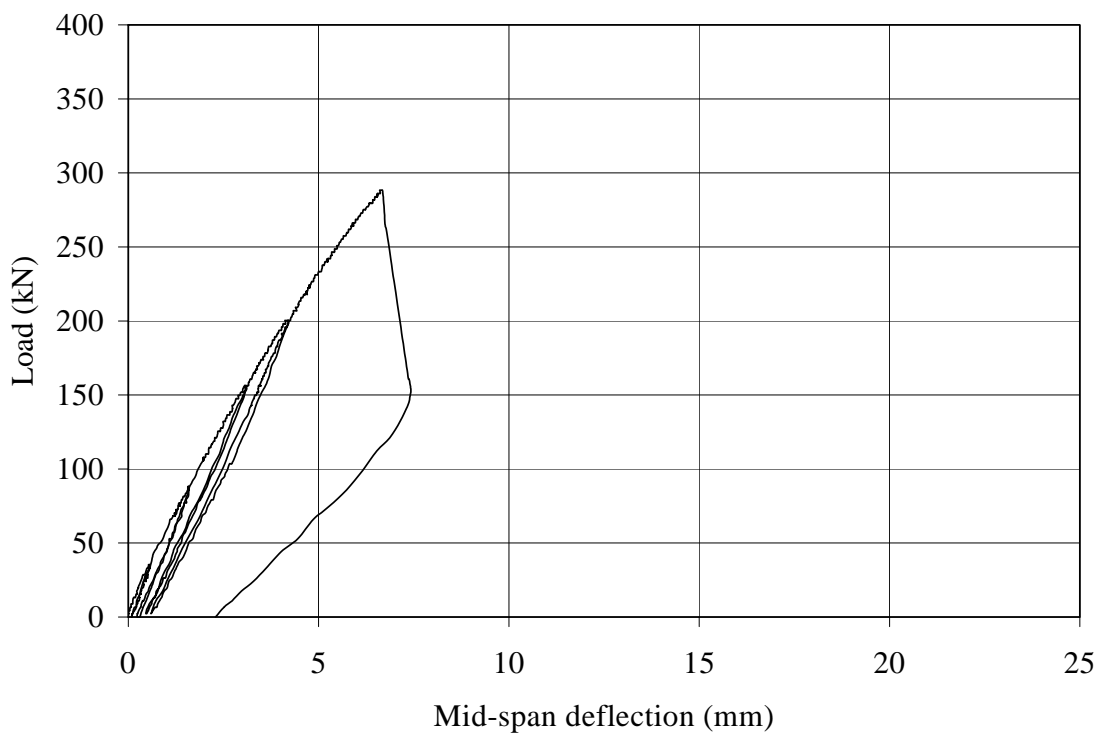


**Figure B-8.** Applied load versus mid-span deflection for Specimen A-SO3-4

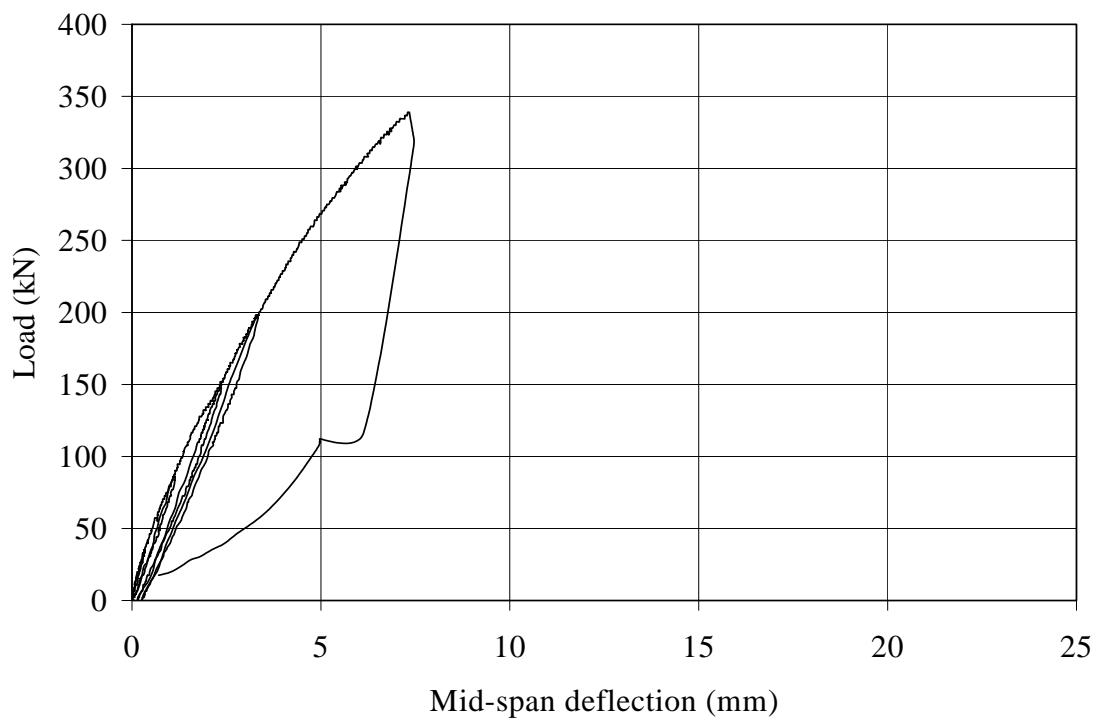


**Figure B-9.** Applied load versus mid-span deflection for Specimen A-SO3-5

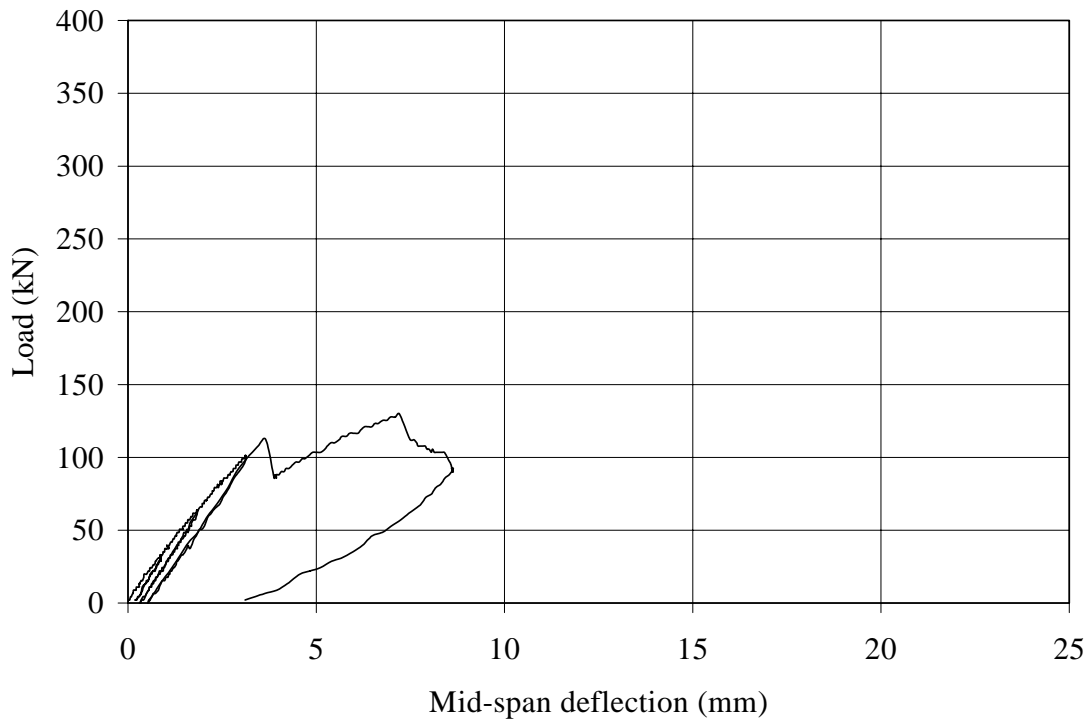


**Figure B-10.** Applied load versus mid-span deflection for Specimen A-SO4-1

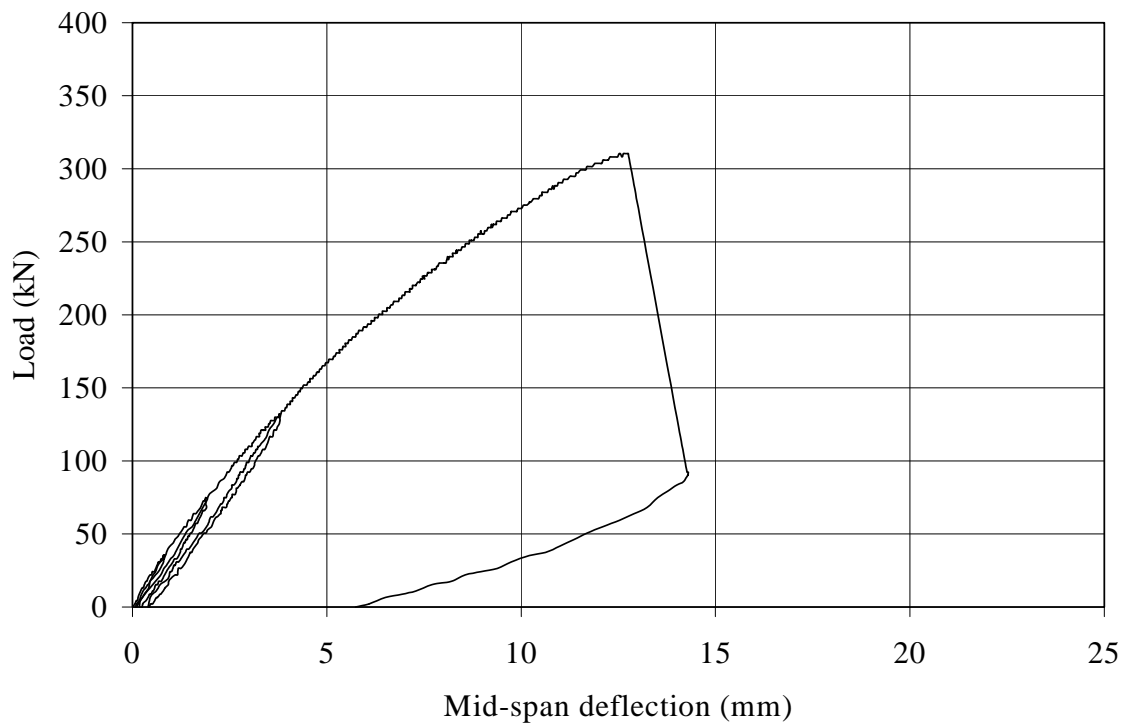


**Figure B-11.** Applied load versus mid-span deflection for Specimen A-SO4-2

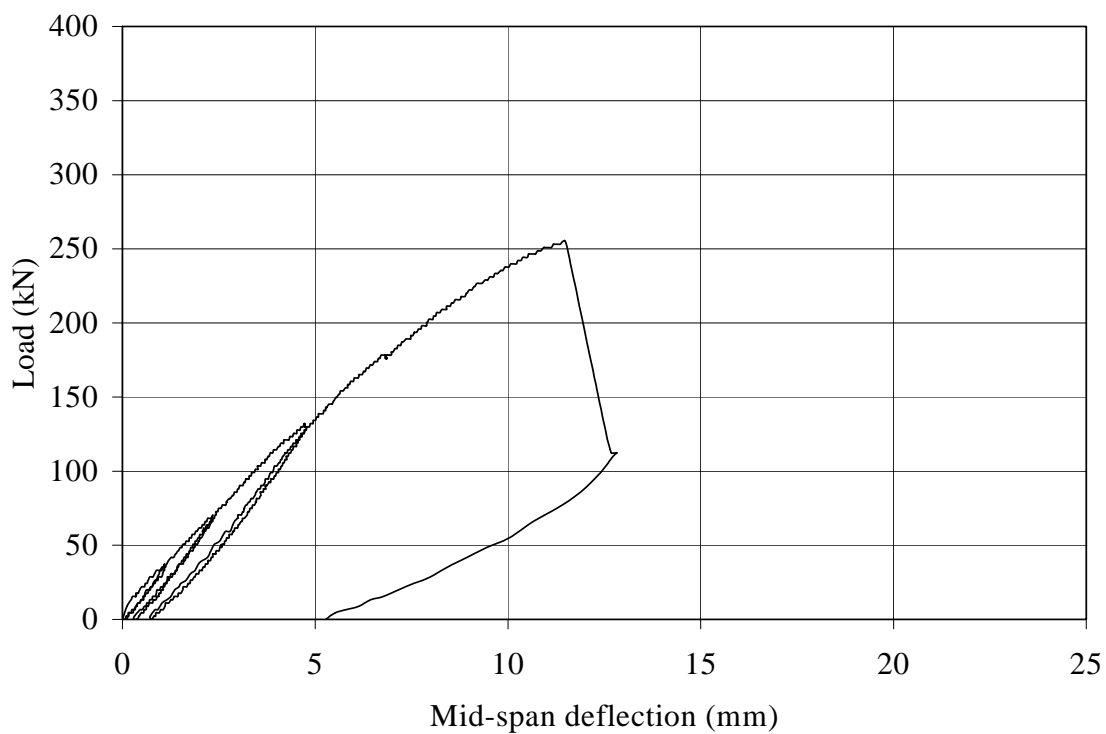


**Figure B-12.** Applied load versus mid-span deflection for Specimen A-SO4-3

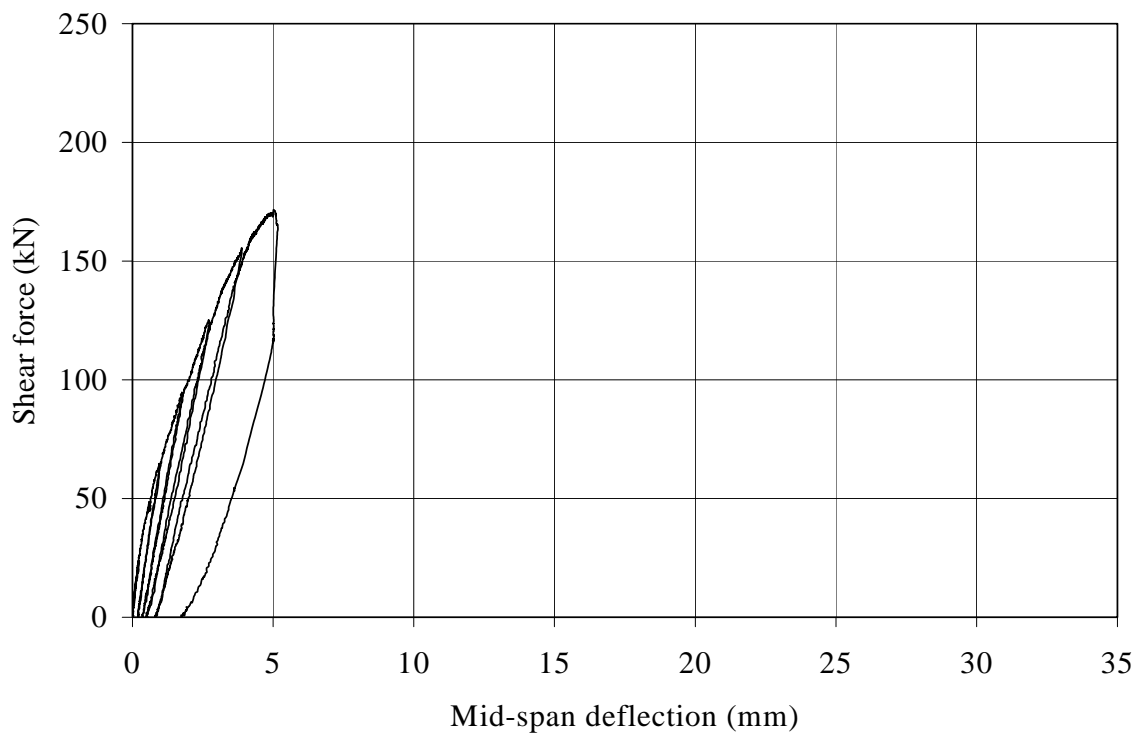


**Figure B-13.** Applied shear force versus mid-span deflection for Specimen B-CW1

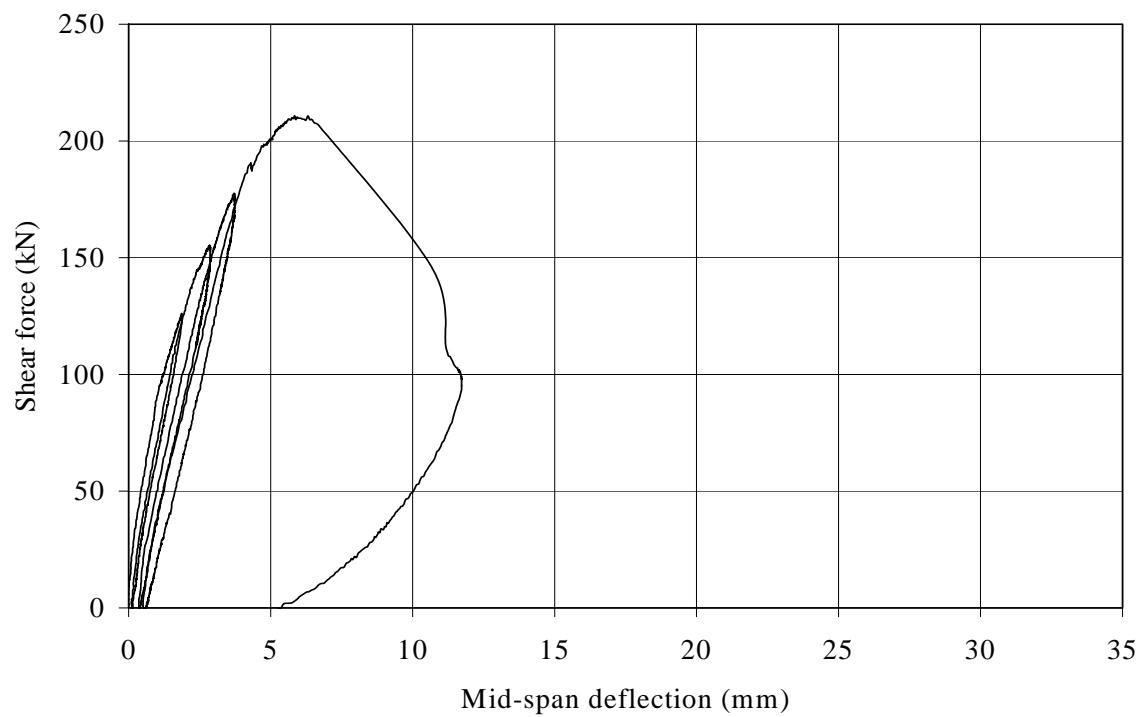


**Figure B-14.** Applied shear force versus mid-span deflection for Specimen B-CW2

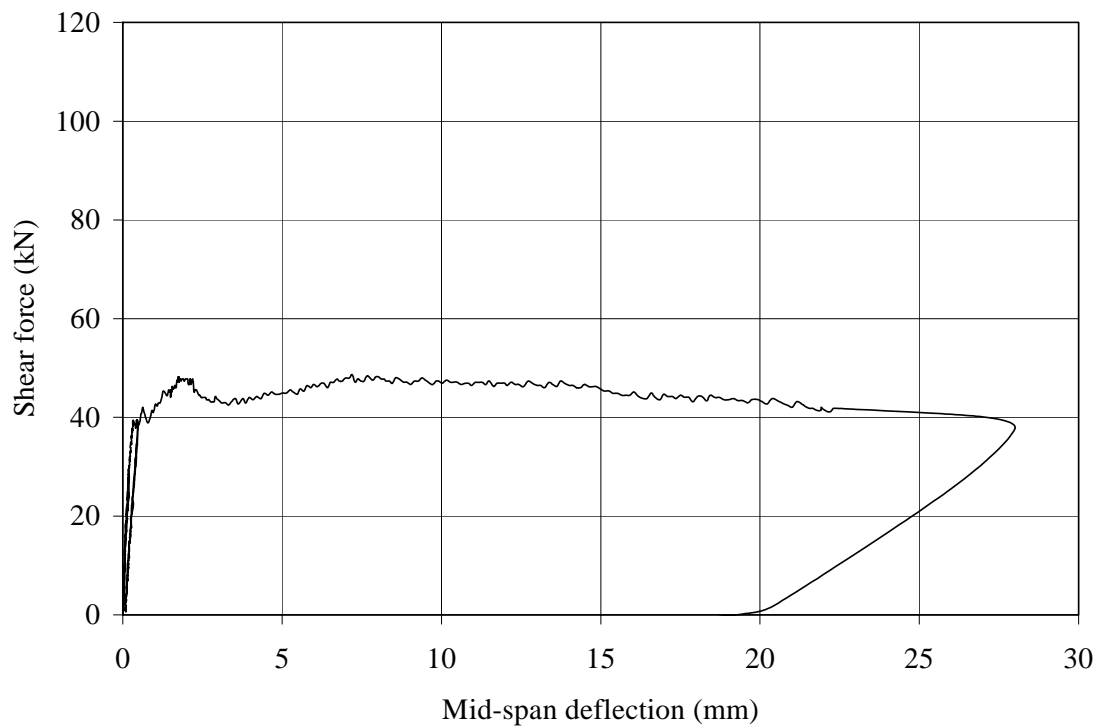


**Figure B-15.** Applied shear force versus mid-span deflection for Specimen B-CO1

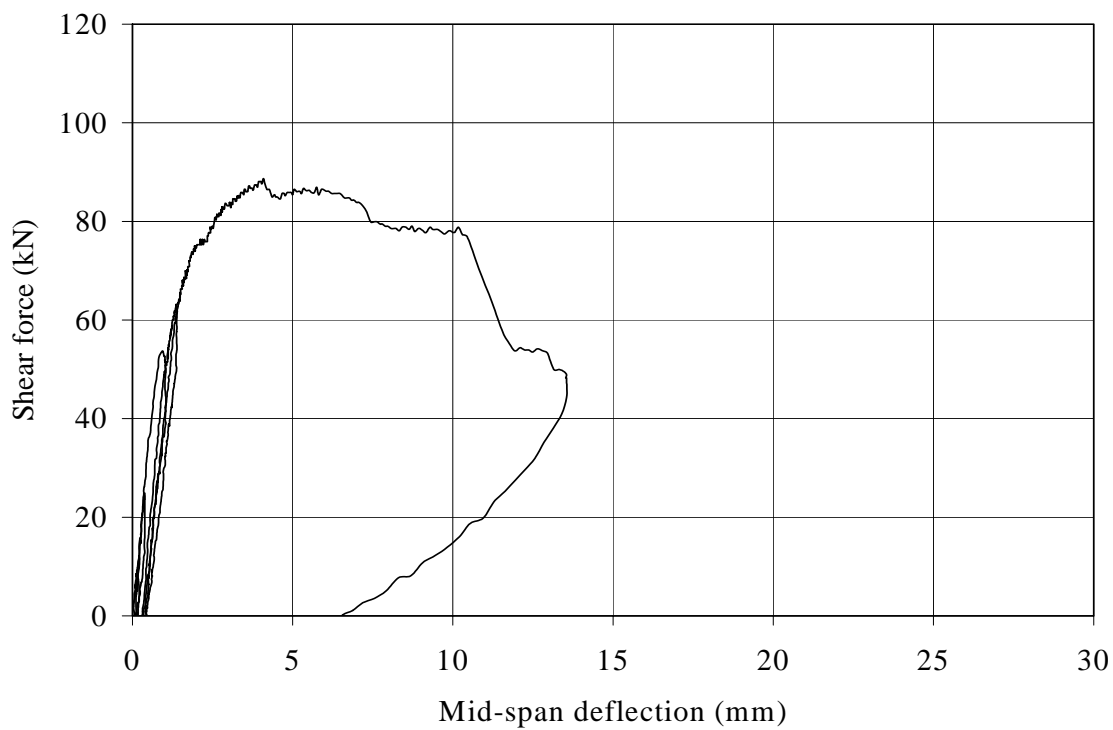


**Figure B-16.** Applied shear force versus mid-span deflection for Specimen B-CO2

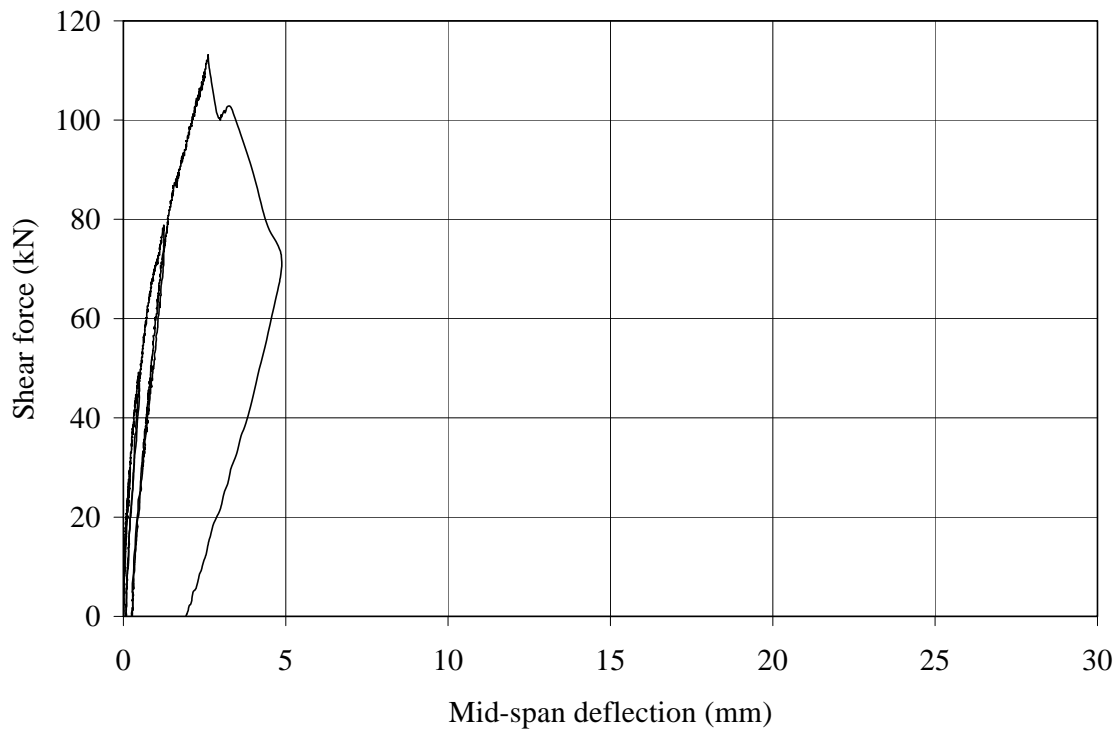


**Figure B-17.** Applied shear force versus mid-span deflection for Specimen B-CO3

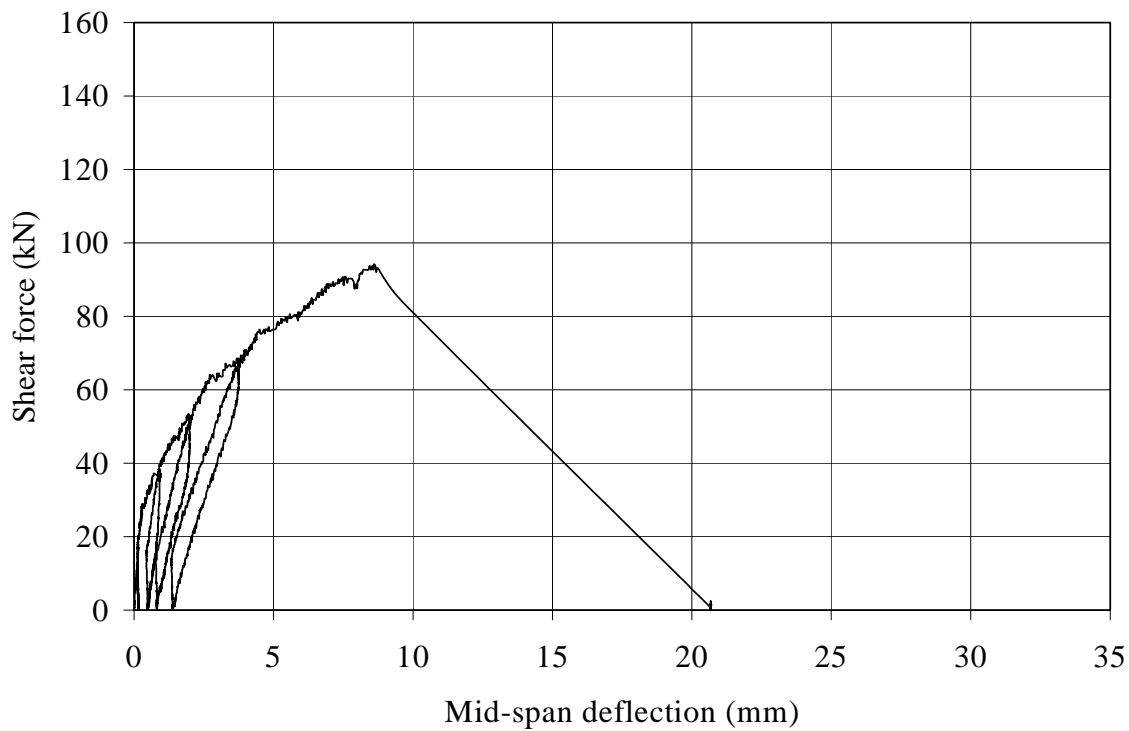


**Figure B-18.** Applied shear force versus mid-span deflection for Specimen B-CF1

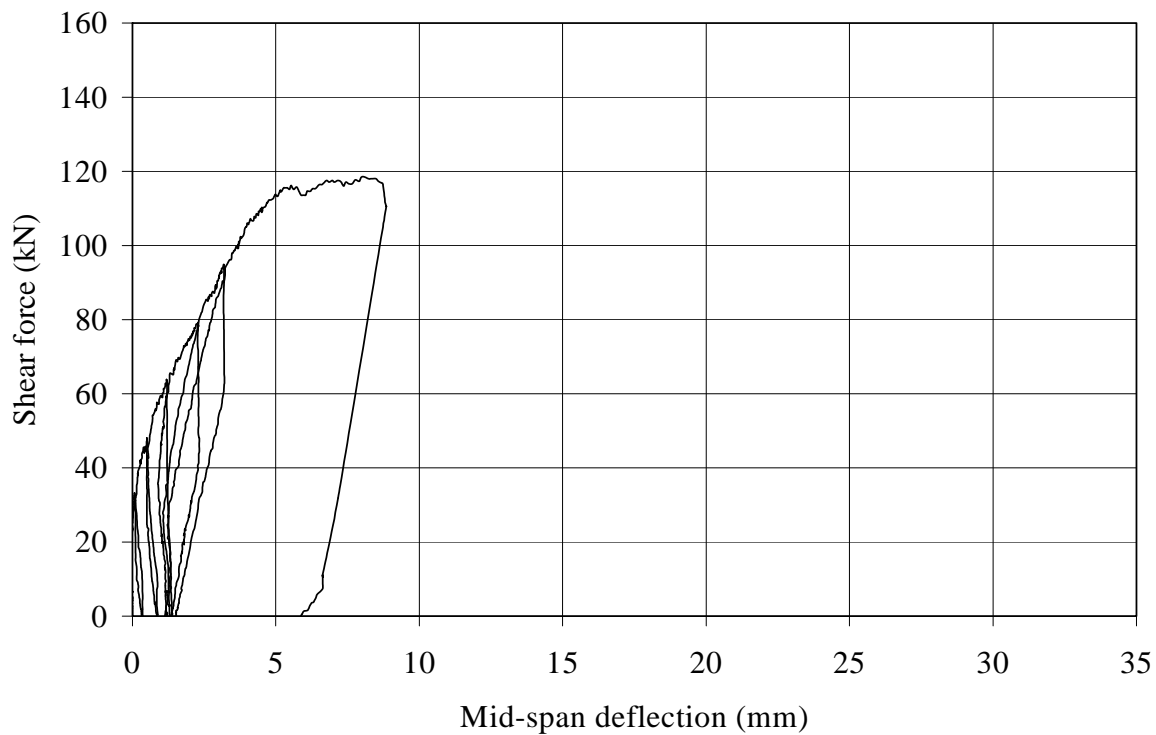


**Figure B-19.** Applied shear force versus mid-span deflection for Specimen B-CF2

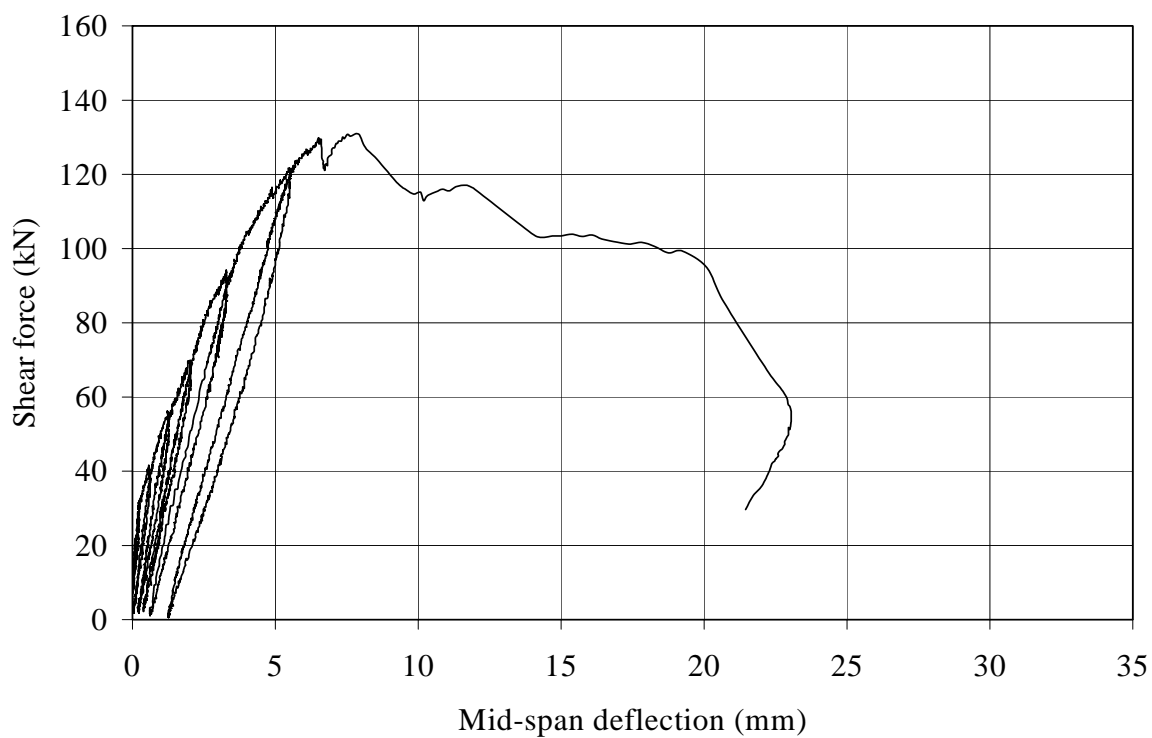


**Figure B-20.** Applied shear force versus mid-span deflection for Specimen B-CF3

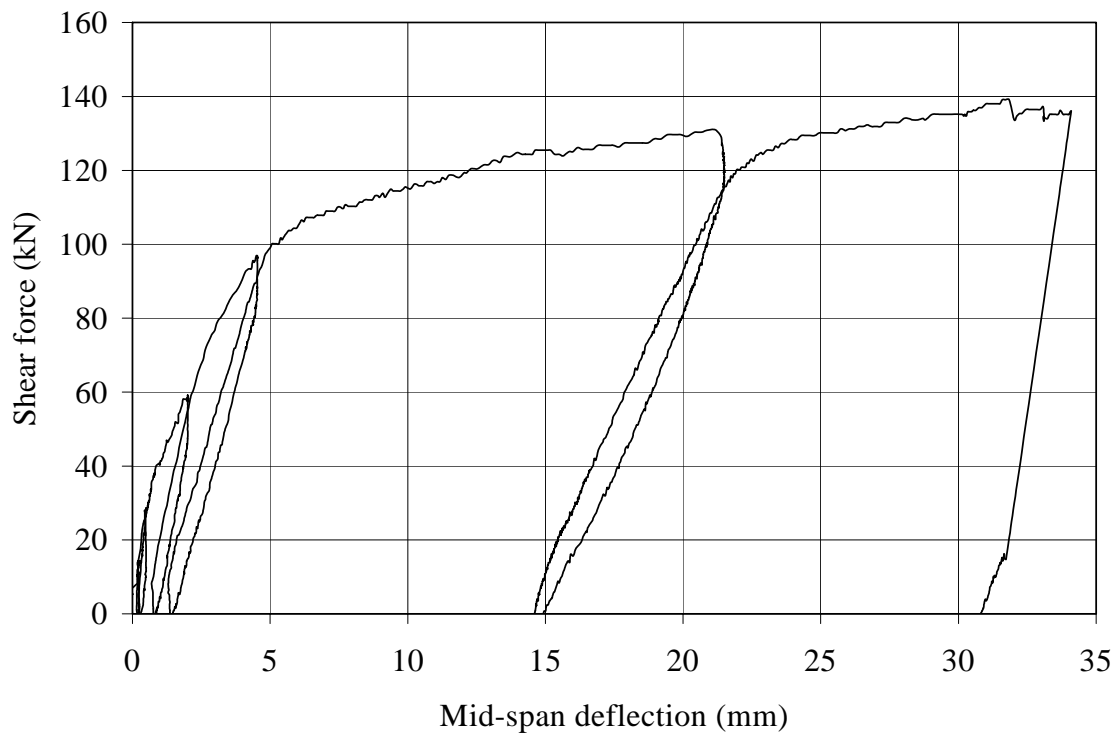


**Figure B-21.** Applied shear force versus mid-span deflection for Specimen B-CF4

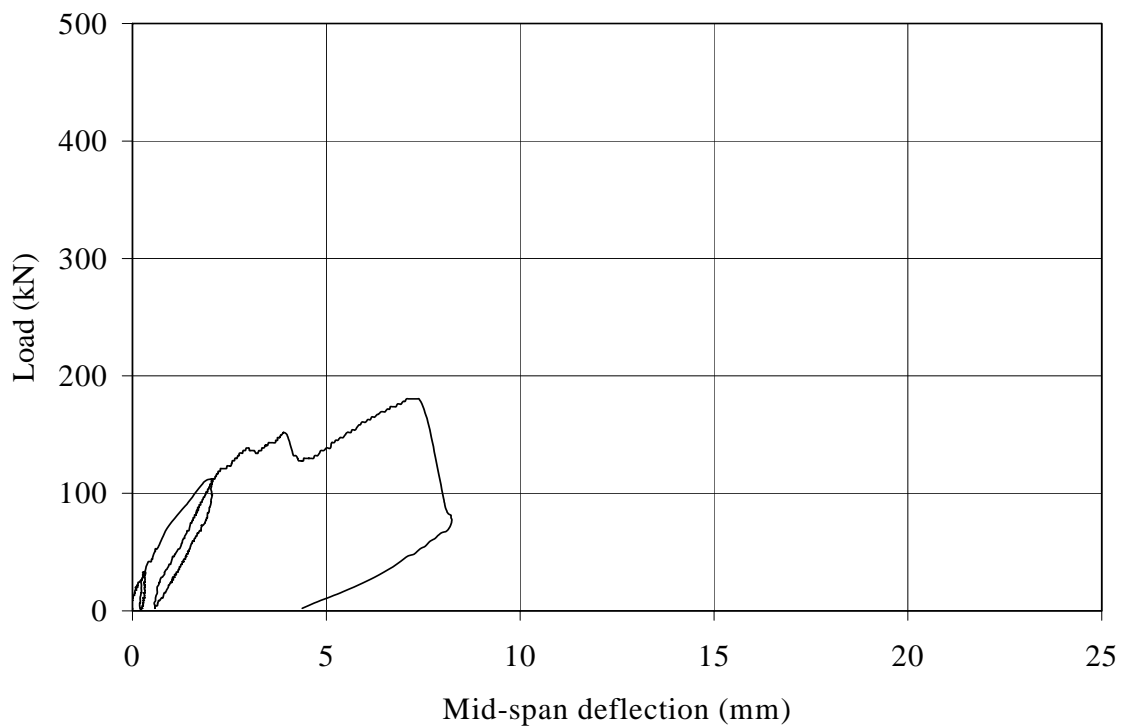


**Figure B-22.** Applied Load versus mid-span deflection for Specimen C-BT1

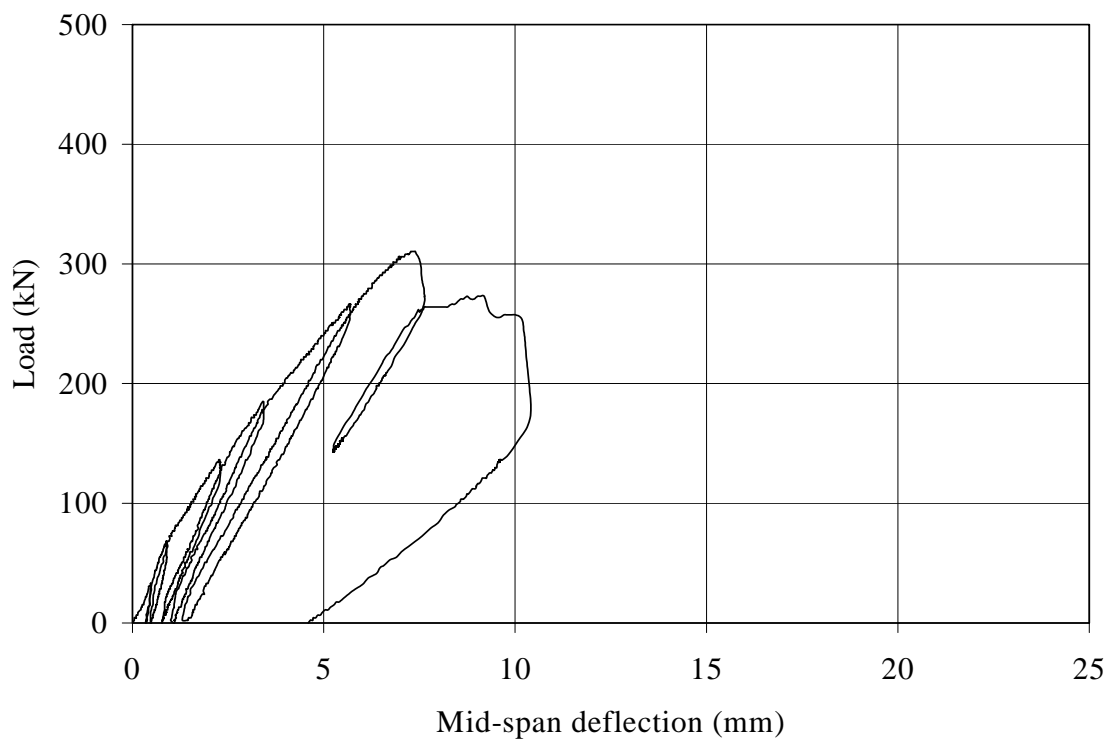


**Figure B-23.** Applied Load versus mid-span deflection for Specimen C-BT2

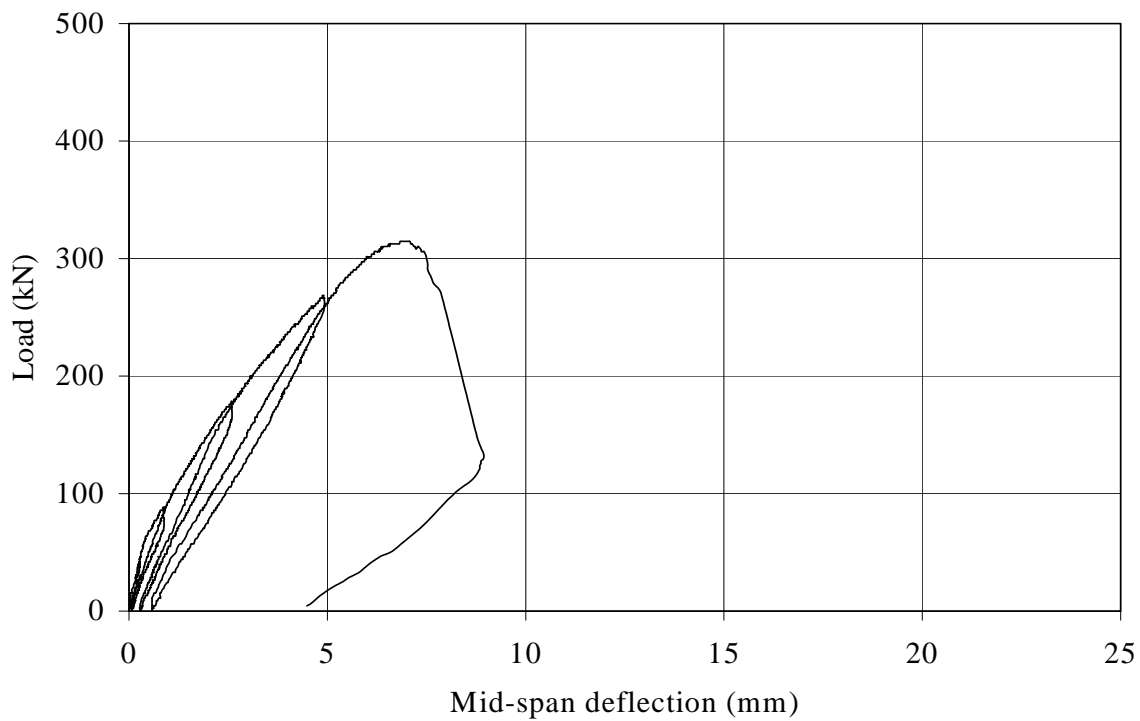


**Figure B-24.** Applied Load versus mid-span deflection for Specimen C-BT3

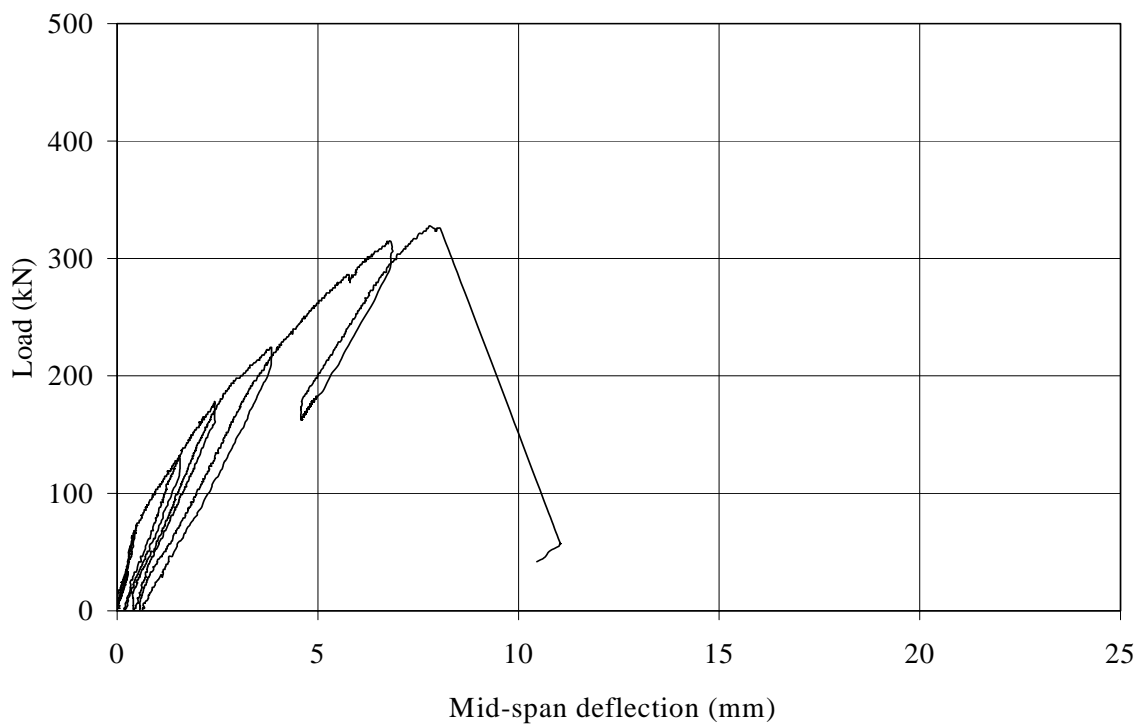


**Figure B-25.** Applied Load versus mid-span deflection for Specimen C-BT4

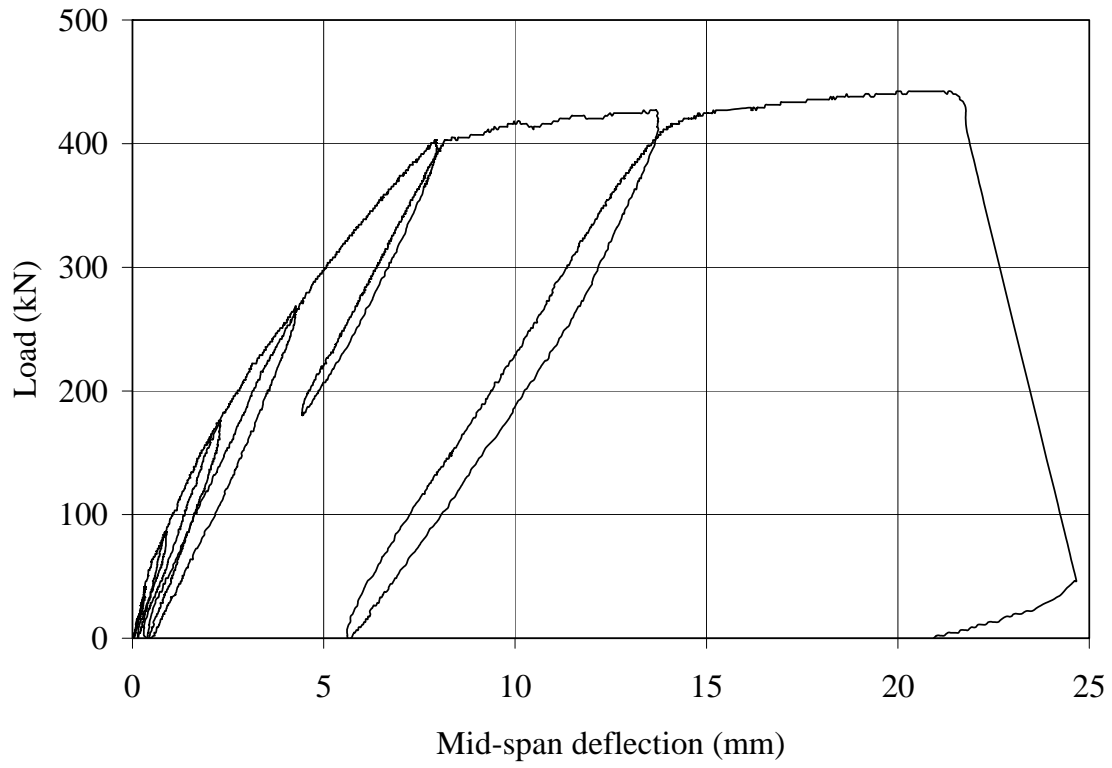


**Figure B-26.** Applied Load versus mid-span deflection for Specimen C-BT6

## **APPENDIX C**

### **LOAD VERSUS STRAIN CURVES**

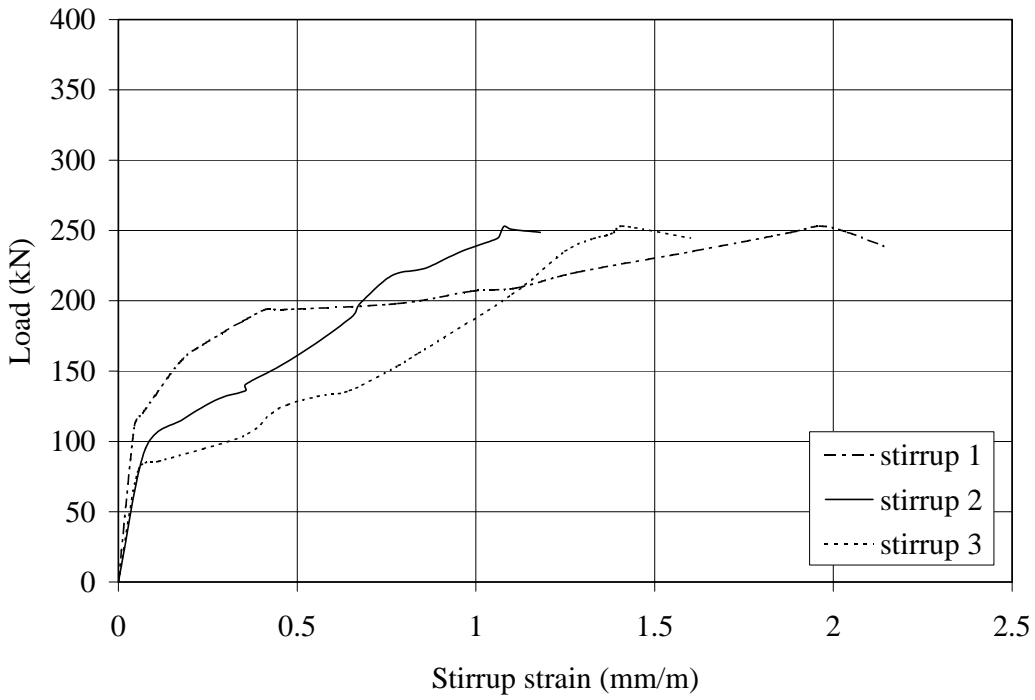


**Figure C-1.** Applied load versus strain in stirrups for Specimen A-SW3-1

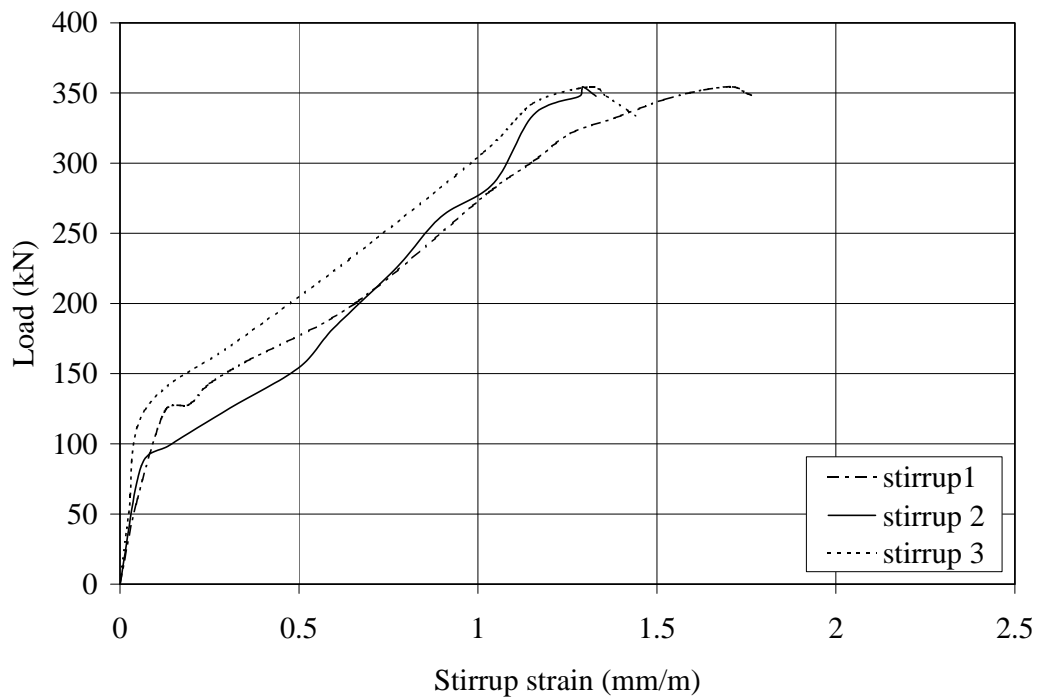


**Figure C-2.** Applied load versus strain in stirrups for Specimen A-SW3-2

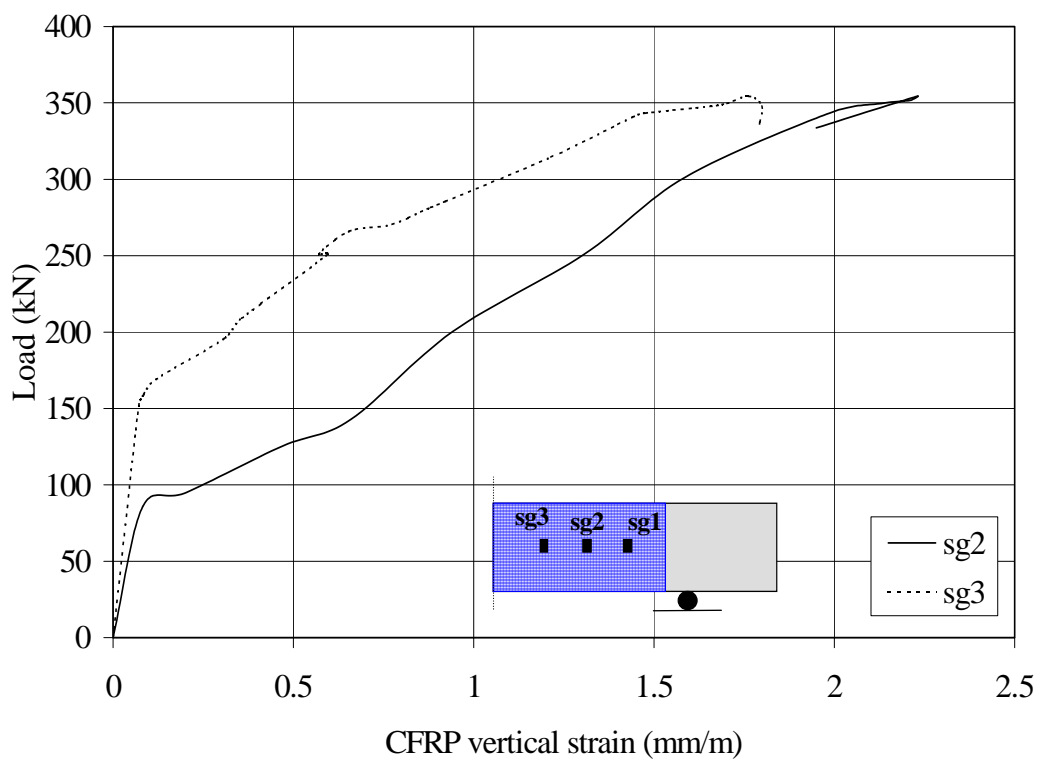


**Figure C-3.** Applied load versus CFRP vertical strain for Specimen A-SW3-2

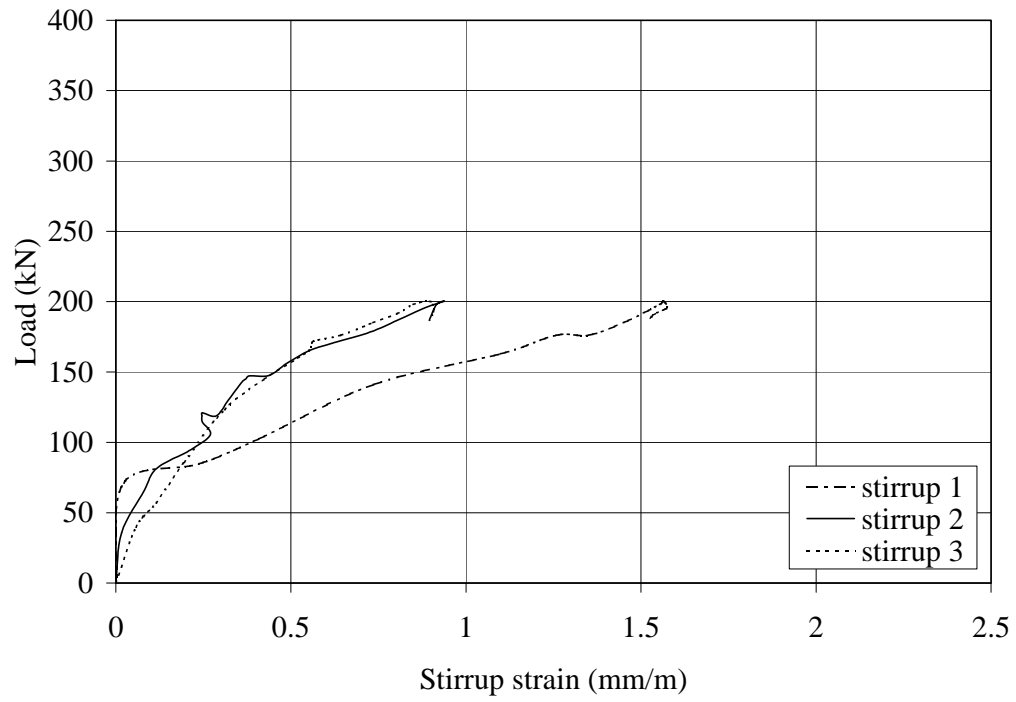


**Figure C-4.** Applied load versus strain in stirrups for Specimen A-SW4-1

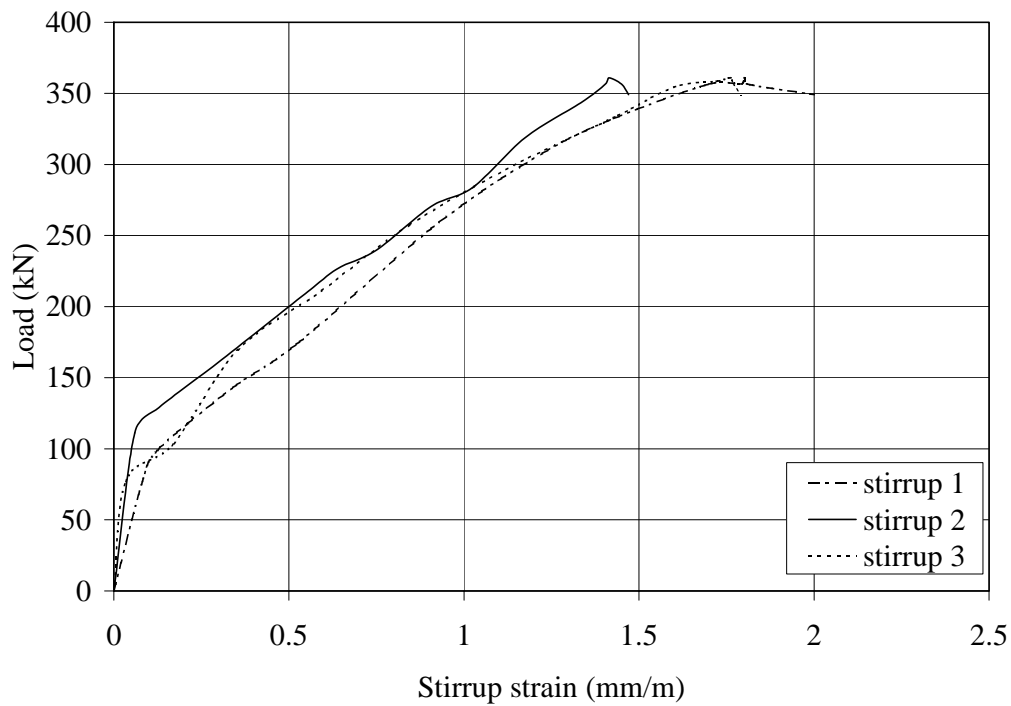


**Figure C-5.** Applied load versus strain in stirrups for Specimen A-SW4-2

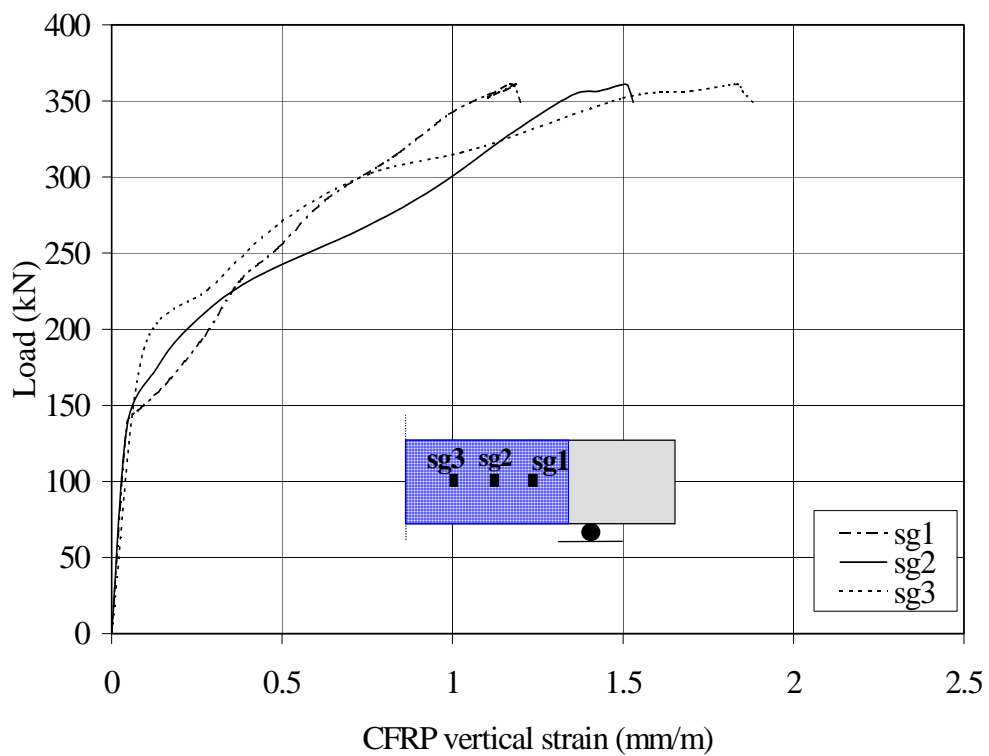


**Figure C-6.** Applied load versus CFRP vertical strain for Specimen A-SW4-2

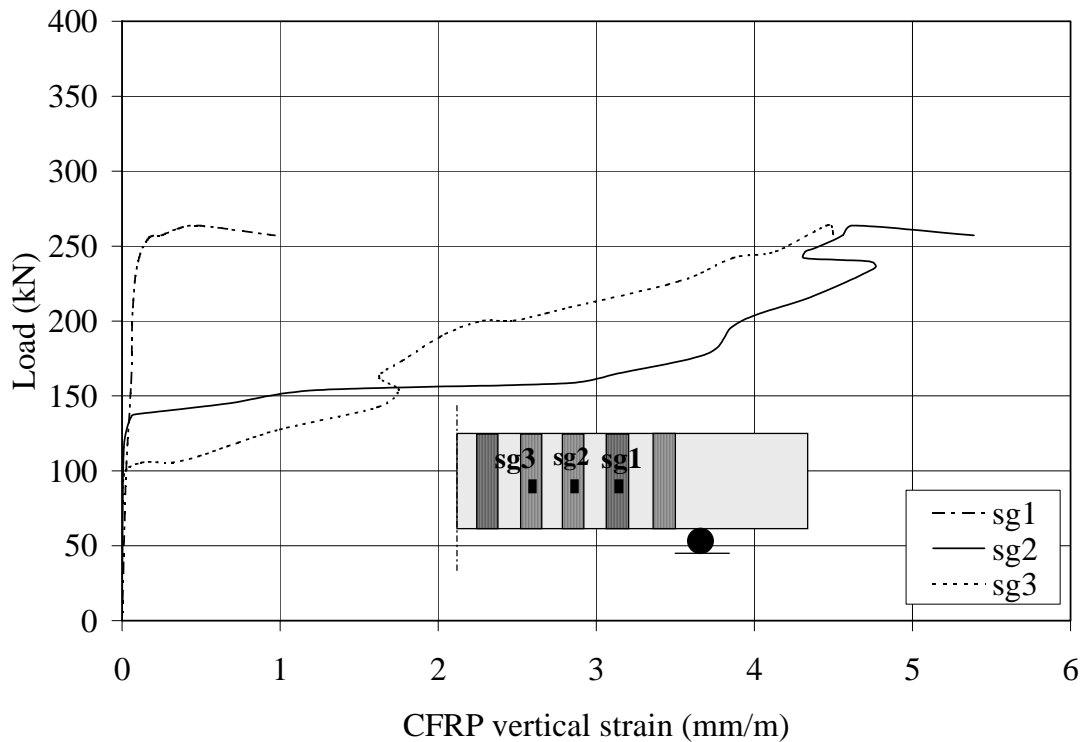


**Figure C-7.** Applied load versus CFRP vertical strain for Specimen A-SO3-2

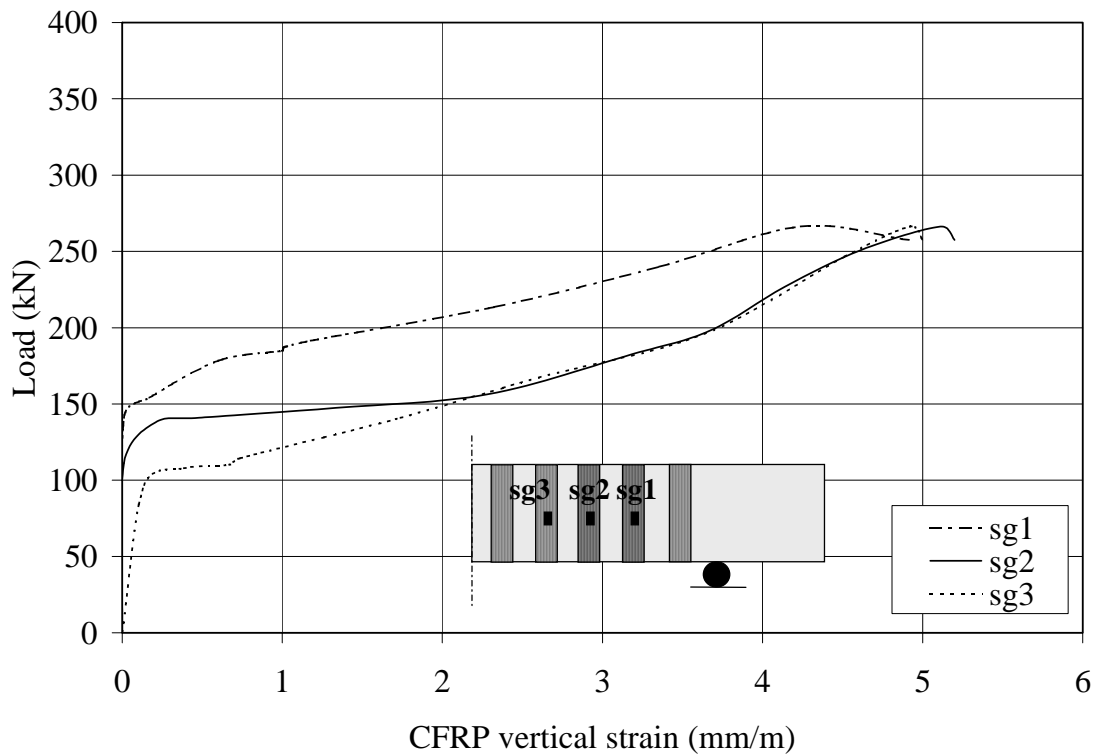


**Figure C-8.** Applied load versus CFRP vertical strain for Specimen A-SO3-3

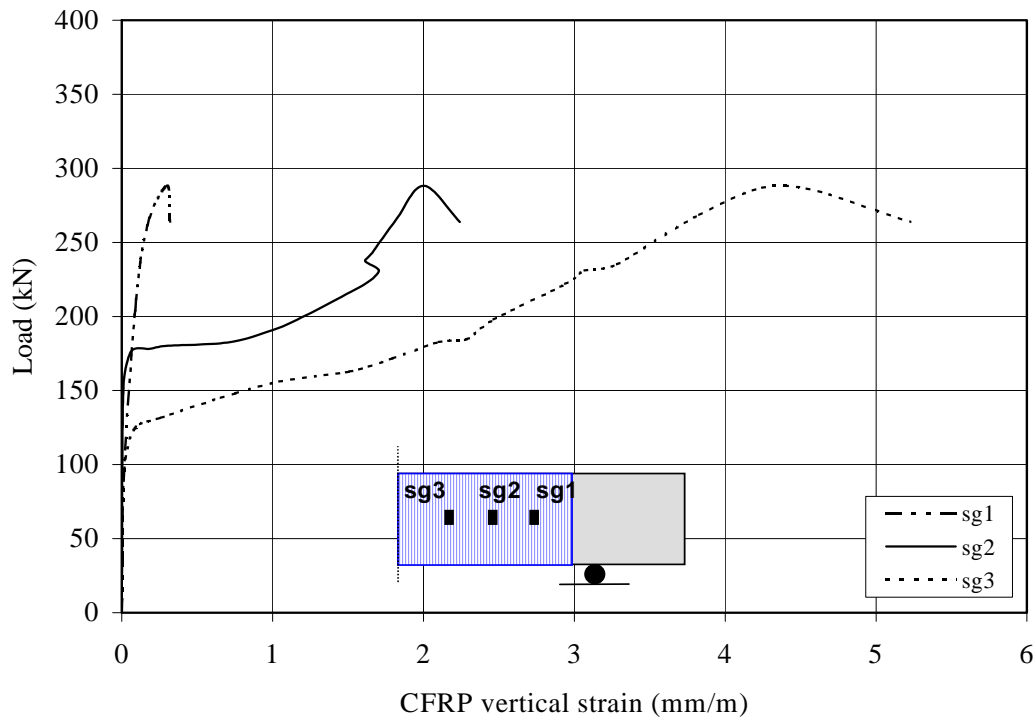


**Figure C-9.** Applied load versus CFRP vertical strain for Specimen A-SO3-4

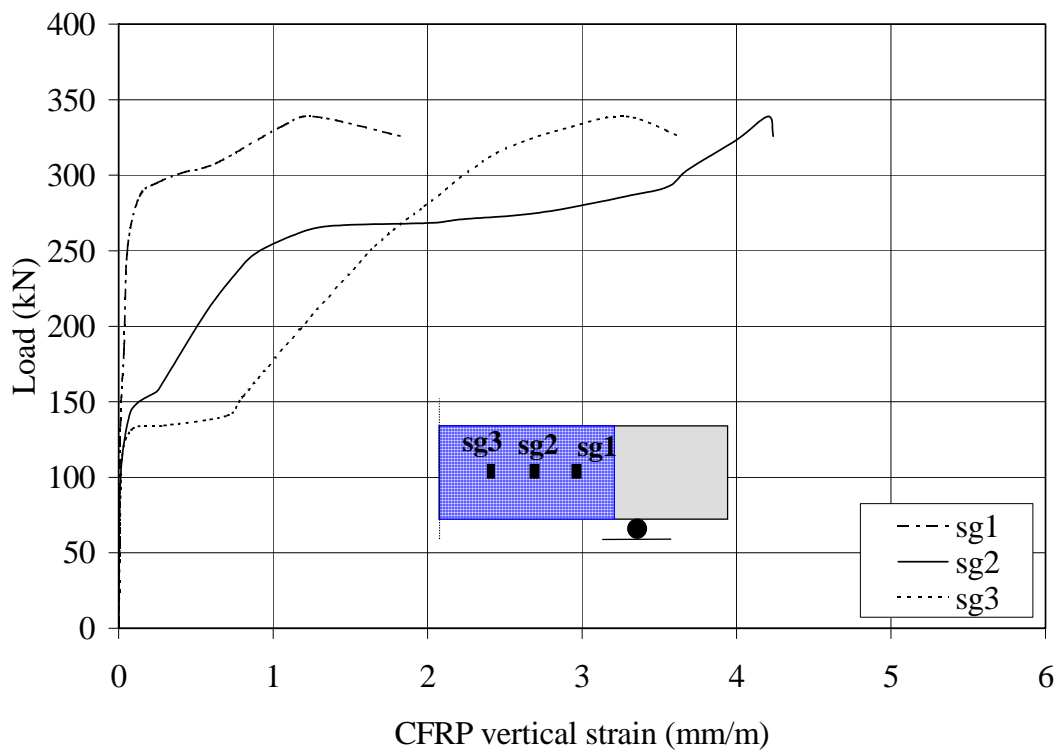


**Figure C-10.** Applied load versus CFRP vertical strain for Specimen A-SO3-5

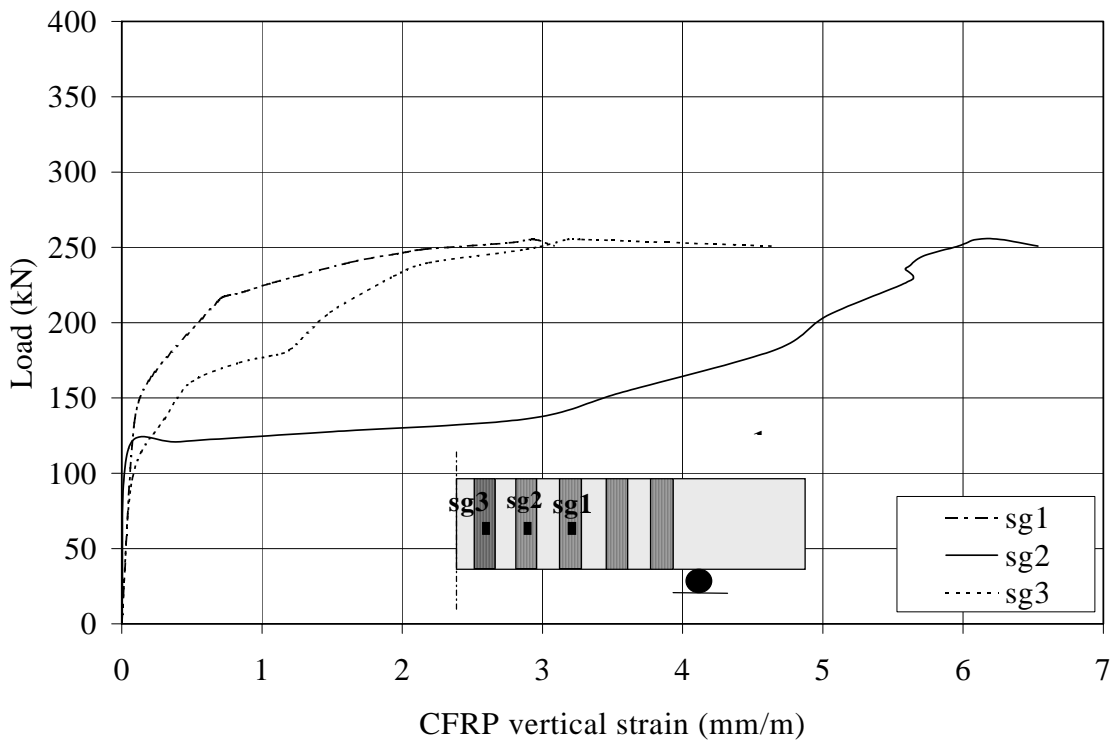


**Figure C-11.** Applied load versus CFRP vertical strain for Specimen A-SO4-2

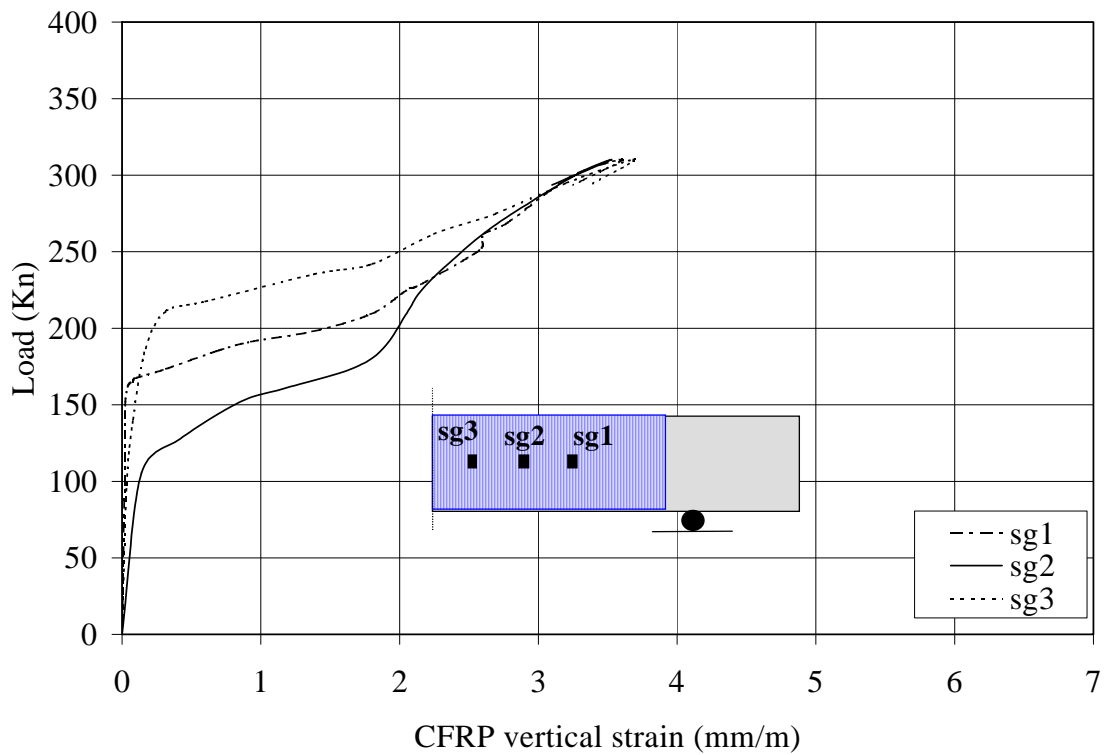


**Figure C-12.** Applied load versus CFRP vertical strain for Specimen A-SO4-3

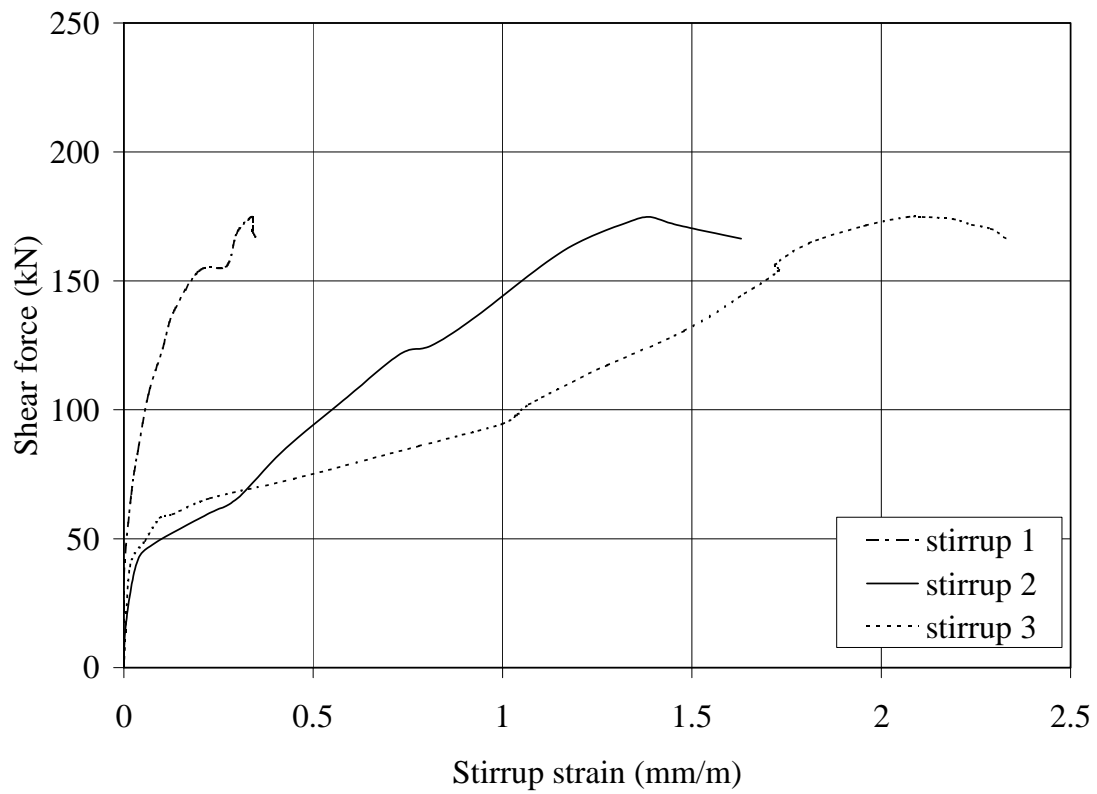


**Figure C-13.** Applied shear force versus strain in stirrups for Specimen B-CW1

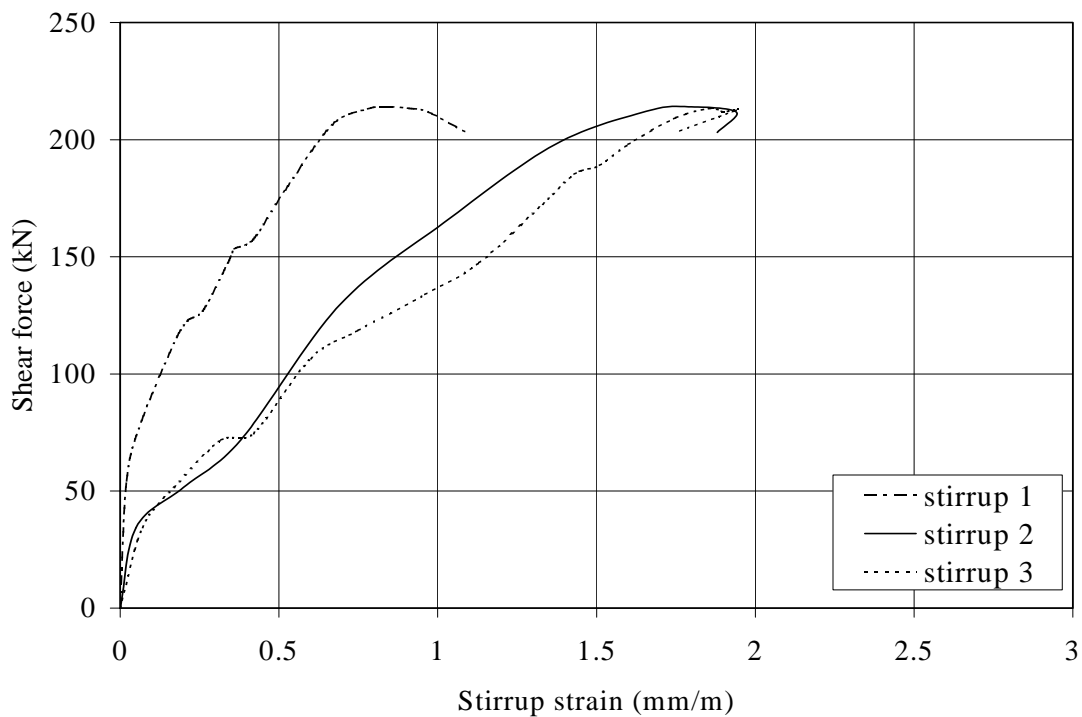


**Figure C-14.** Applied shear force versus strain in stirrups for Specimen B-CW2

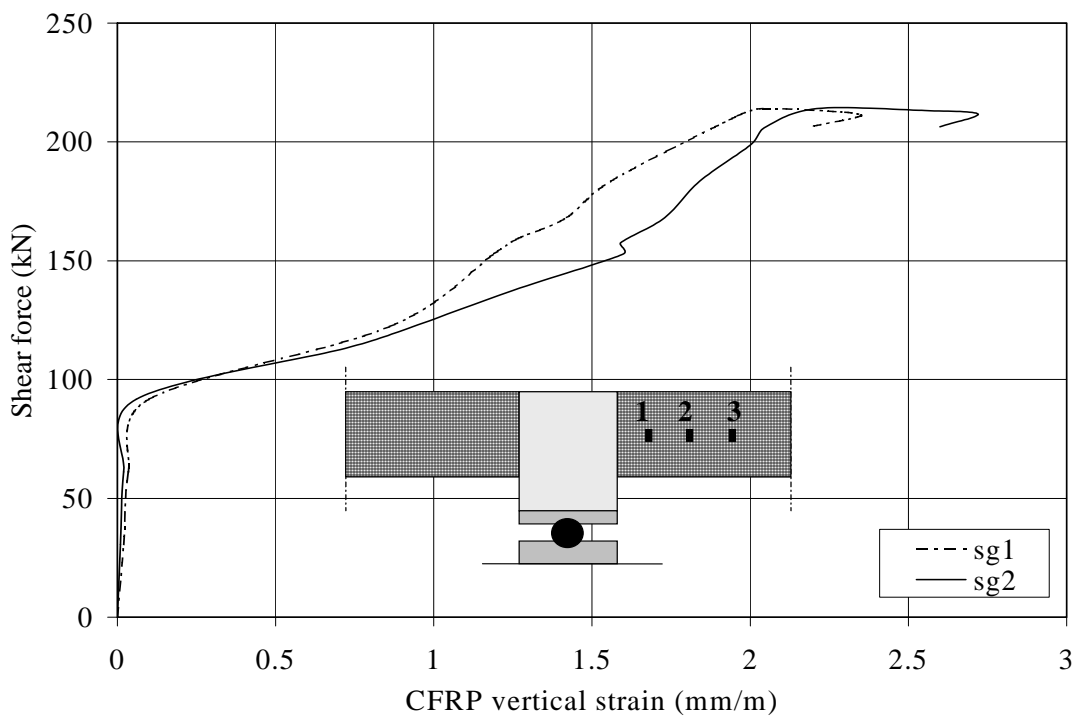


**Figure C-15.** Applied shear force versus CFRP vertical strain for Specimen B-CW2

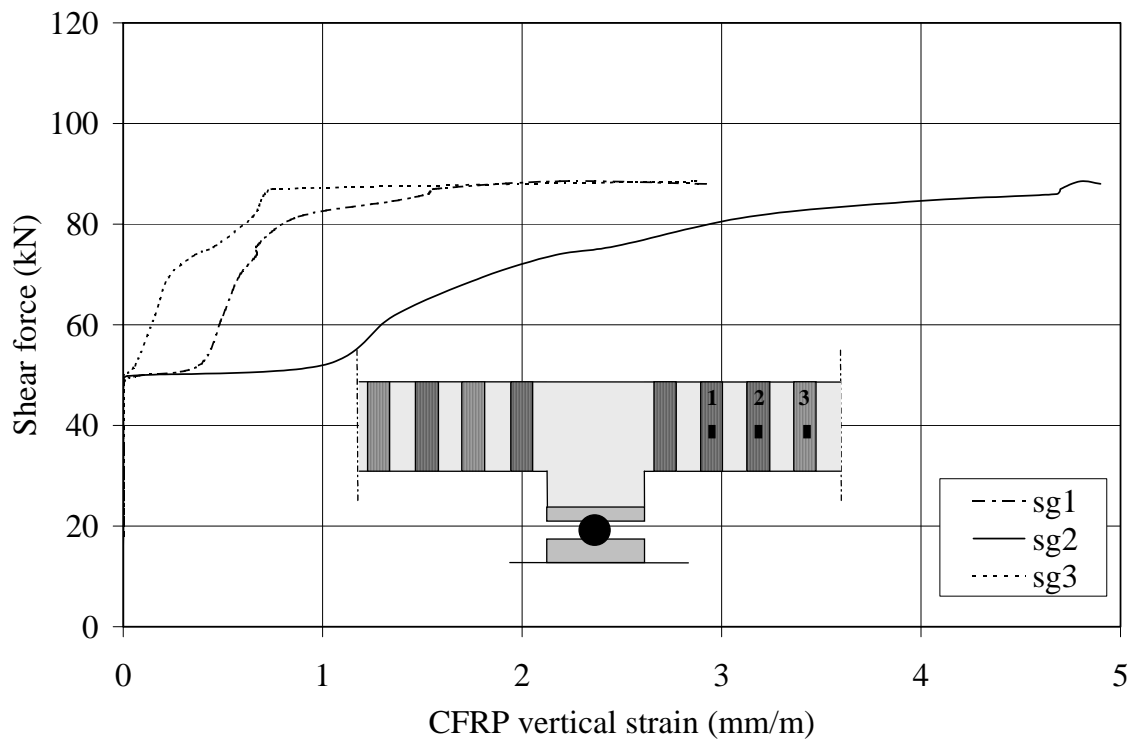


**Figure C-16.** Applied shear force versus CFRP vertical strain for Specimen B-CO2

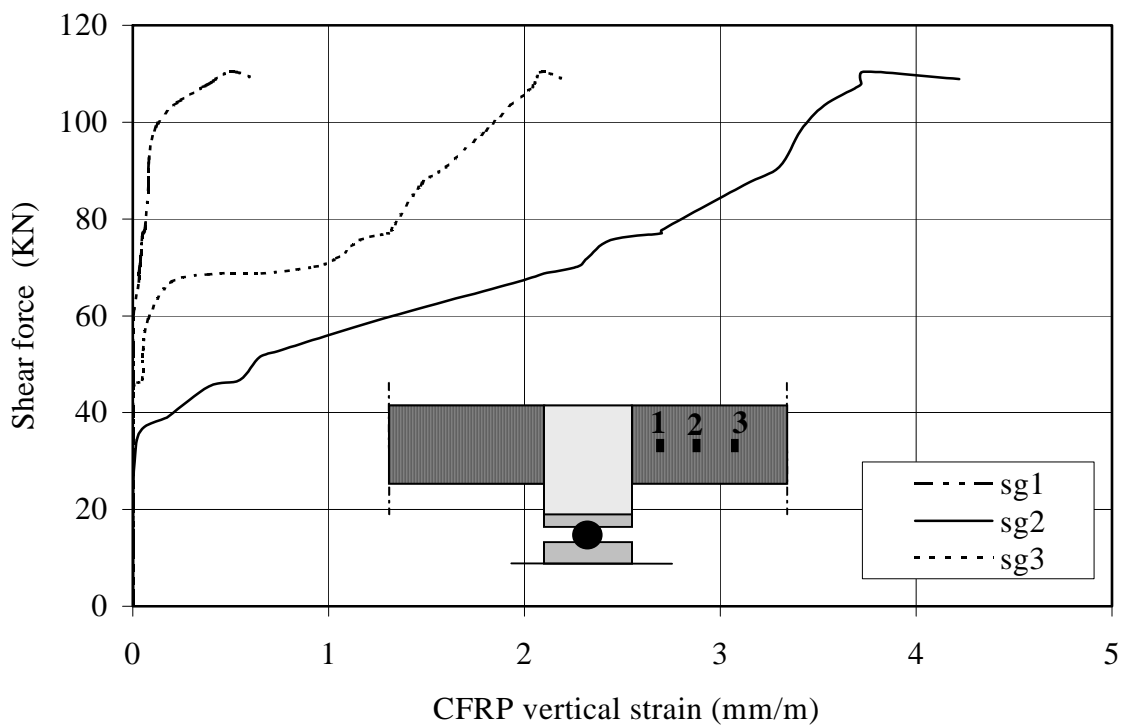


**Figure C-17.** Applied shear force versus CFRP vertical strain for Specimen B-CO3

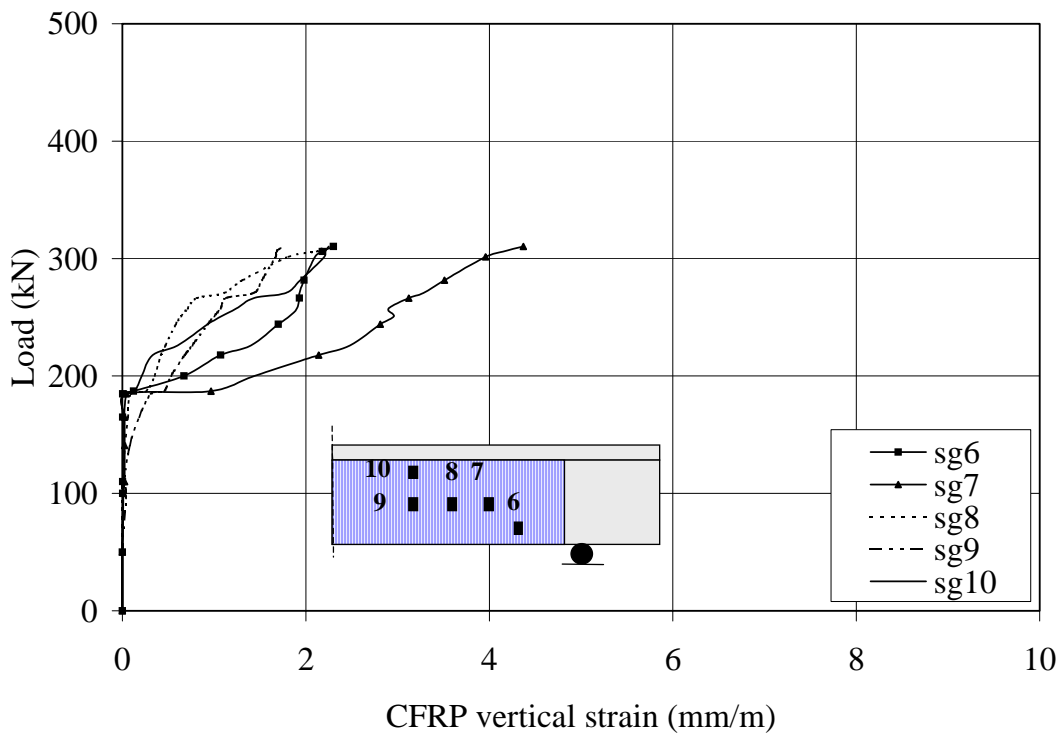


**Figure C-18.** Applied force versus CFRP vertical strain for Specimen C-BT2

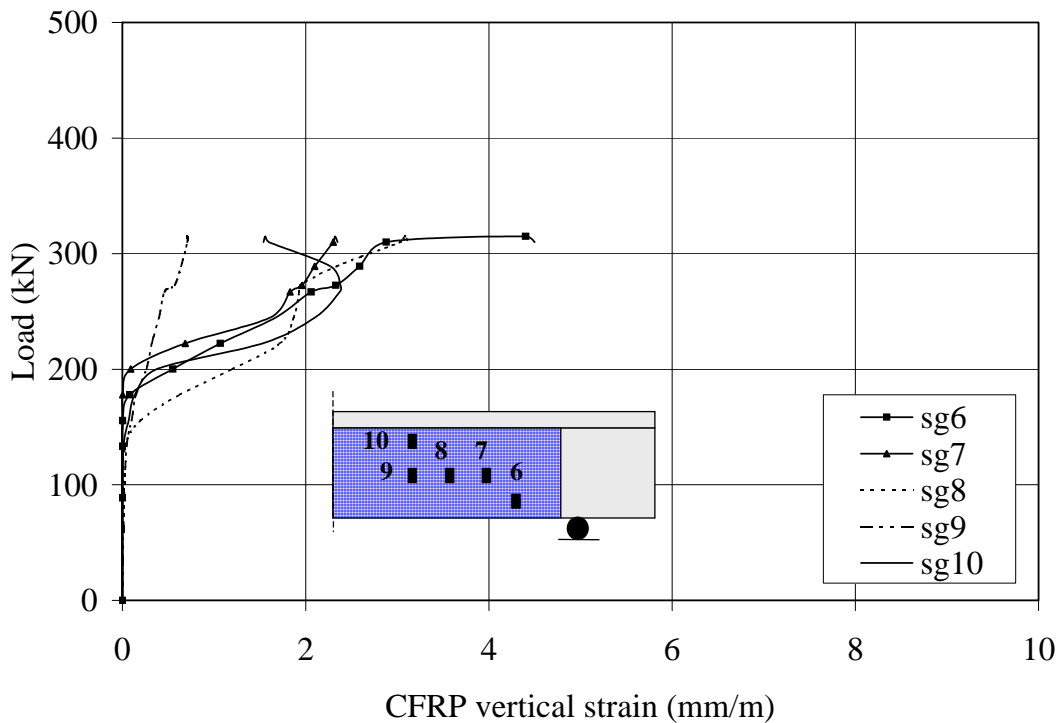


**Figure C-19.** Applied force versus CFRP vertical strain for Specimen C-BT3

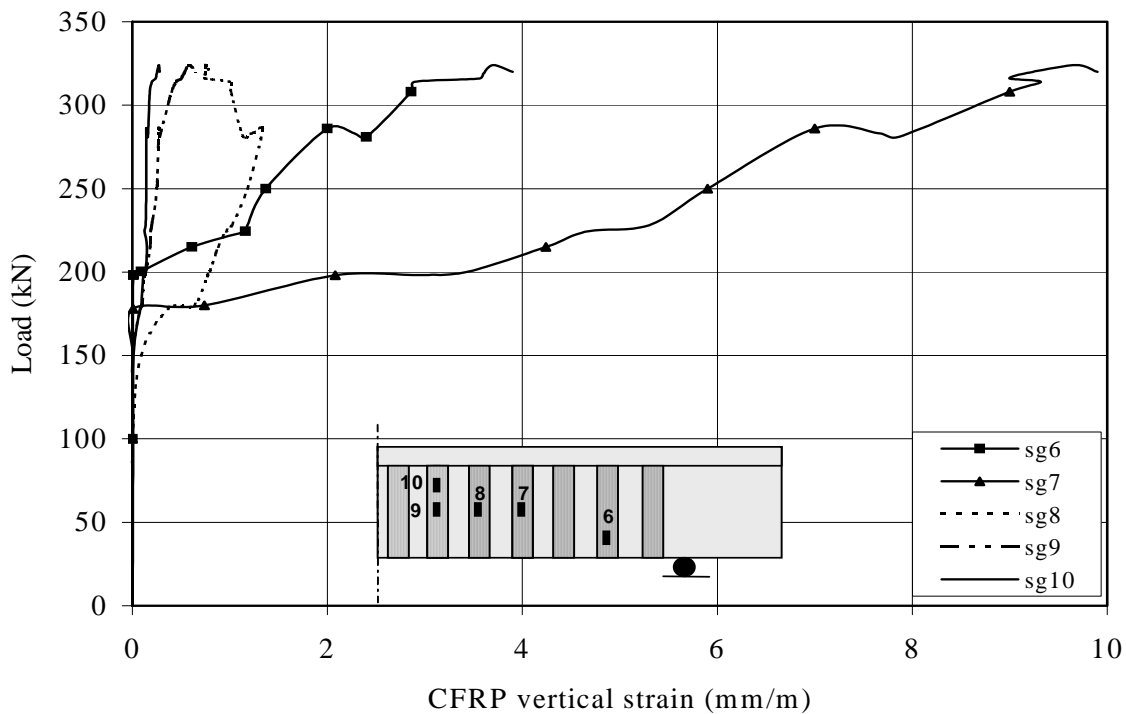


**Figure C-20.** Applied force versus CFRP vertical strain for Specimen C-BT4

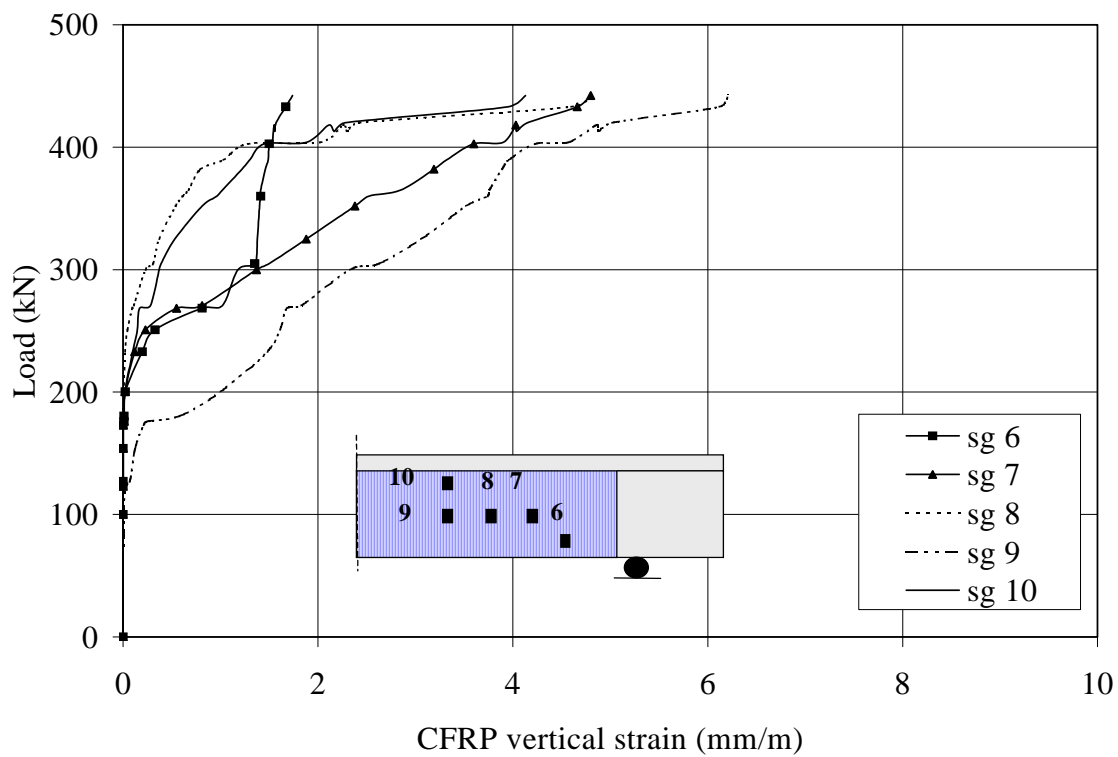


**Figure C-21.** Applied force versus CFRP vertical strain for Specimen C-BT6

## **APPENDIX D**

### **DESIGN EXAMPLE**

## DESIGN EXAMPLE

Figure (D-1) shows the cross section of a simply supported T beam having a clear span of 10 m. The beam supports a uniformly distributed service (unfactored) dead load of 20 kN/m, including its own weight, and a uniformly distributed service live load of 24 kN/m. The beam was originally designed with 10-mm diameter ( $A=100 \text{ mm}^2$ ) steel stirrups spaced at 250 mm over mid-span and 125 mm near the support. However, some of the stirrups near the support were omitted during construction leaving stirrups spaced at 250 mm throughout the entire length of the beam. It is desired to correct the design by using externally bonded CFRP. The concrete strength is 25 MPa, the yield stress of the stirrups is 300 MPa, the sheet thickness of CFRP is 0.165 mm, the modulus of elasticity of CFRP is 228 GPa, the tensile strength of CFRP is 3790 MPa.

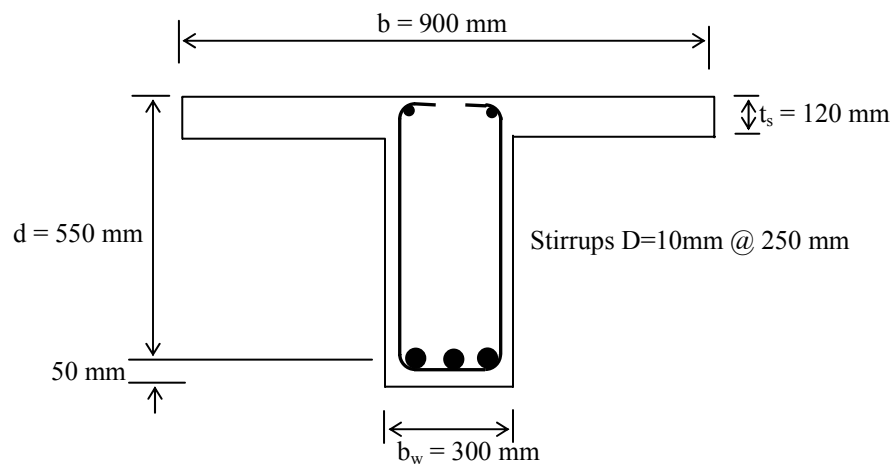


Figure D-1. T-beam cross-section

### Solution

- Compute the design factored shear force

The total factored load  $w_u = 1.4 \times 20 \text{ kN/m} + 1.7 \times 24 \text{ kN/m} = 68.8 \text{ kN/m}$

Factored dead load  $w_{Du} = 1.4 \times 20 \text{ kN/m} = 28.0 \text{ kN/m}$

Instead of three loading cases, we shall approximate the shear force envelope with straight lines (Fig. D-2).

$V_u = \frac{w_u l}{2} = 344 \text{ kN}$  at the ends and  $V_u = \frac{w_{lu} l}{8} = 51 \text{ kN}$  at mid span, where  $w_u$  is the factored live and dead load and  $w_{lu}$  is the factored live load.

Since the beam is loaded on the top flange and supported on the bottom flange, the critical section is located at  $d = 0.55 \text{ m}$  from support.

$$V_u = 51 + \frac{(5 - 0.55)}{5} (344 - 51) = 312 \text{ kN}$$

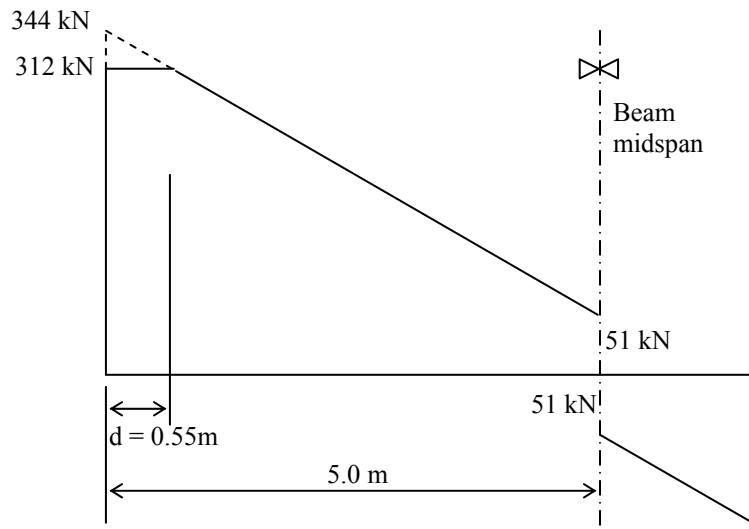


**Figure D-2.** Factored shear envelope

- **Compute the nominal shear capacity of the beam before strengthening**

Compute the shear contribution of the concrete and steel in the traditional (ACI) manner.

$$V_c = \frac{\sqrt{f'_c} b_w d}{6} = \frac{\sqrt{25} \text{ MPa} \times 300 \text{ mm} \times 550 \text{ mm}}{6 \times 1000} = 137.5 \text{ kN}$$

$$V_s = \frac{A_s f_y d}{s} = \frac{2(100)(300)(550)}{250 \times 1000} = 132 \text{ kN}$$

$$V_{n,\text{existing}} = V_c + V_s = 137.5 + 132 = 269.5 \text{ kN}$$

$$\phi V_{n,\text{existing}} = 0.85 (269.5) = 229 \text{ kN}$$

Since  $V_u = 312 \text{ kN}$  exceeds  $\phi V_{n,\text{existing}}$ , shear strengthening is required. Figure (D-3) shows the shear diagram with the locations where shear strengthening is required along the length of the beam.

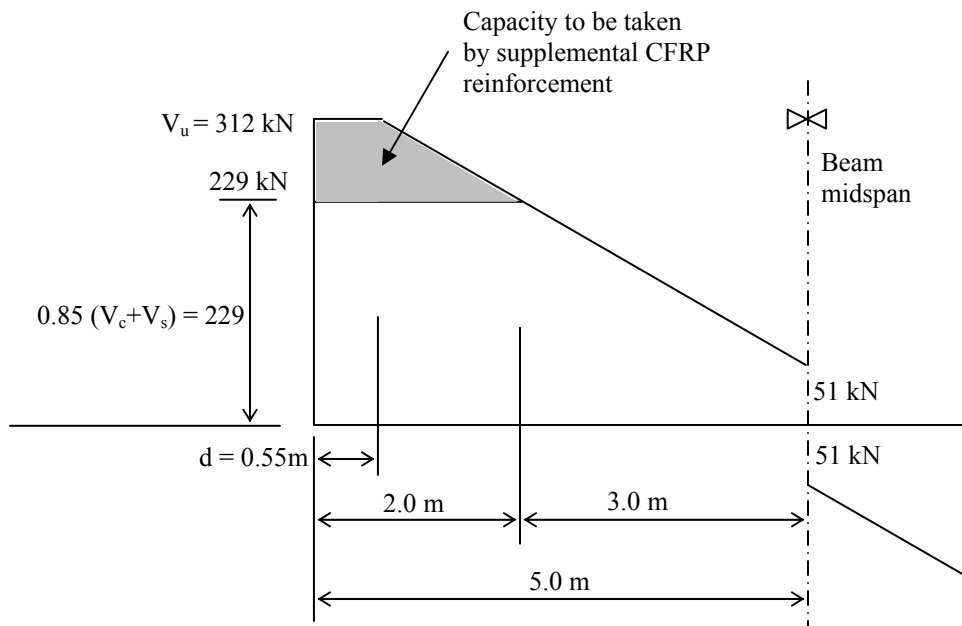


**Figure D-3.** Shear diagram-showing demand versus existing capacity.

- Find the required shear contribution that must be provided by CFRP,  $V_{f,\text{req}}$ .

$$V_u \leq \phi V_n$$

Use Equation (5-26) to calculate  $V_{f,\text{req}}$ .

$$V_u = 0.85 (V_c + V_s) + 0.7 V_f$$

$$312 = 229 + 0.7 V_f$$

$$\therefore V_{f,req} = 118.6 \text{ kN}$$

- **Determine the reduction Coefficient for failure controlled by CFRP fracture**

Assume one ply continuous U-wrap, without end anchor, will be used.

Compute  $\rho_f$ :

$$\rho_f = \frac{2 t_f}{b_w} \left( \frac{w_f}{s_f} \right)$$

For continuous vertical oriented ( $\beta = 90^0$ ) CFRP,  $w_f / s_f = 1$

$$\rho_f = \frac{2 (0.165)}{300} = 0.0011$$

$$\rho_f E_f = 0.0011 \times 228 = 0.25 \text{ G Pa} < 0.7 \text{ GPa} \therefore \text{Equation (5-13) is applicable.}$$

Using Equation (5-13).

$$R = 0.56 (\rho_f E_f)^2 - 1.22 (\rho_f E_f) + 0.78$$

$$\therefore R_1 = 0.56 (0.25)^2 - 1.22 (0.25) + 0.78 = 0.518$$

- **Determine the reduction Coefficient for failure controlled by CFRP debonding**

$$d_f = d - t_s = 550 - 120 = 430 \text{ mm}$$

Consider the effective bond length  $L_e = 75 \text{ mm}$

The effective width of CFRP reinforcement can then be found from Equation (5-17a).

$$w_{fe} = d_f - L_e = 430 - 75 = 355 \text{ mm}$$

$$t_f E_f = 0.165 \times 228 = 37.62 \text{ mm. GPa} \quad 90 \geq t_f E_f \geq 20 \text{ mm. GPa} \therefore \text{Equation (5-21) is applicable.}$$

$$R = \frac{(f'_c)^{2/3} w_{fe}}{\epsilon_{fu} d_f} [738.93 - 4.06 (t_f E_f)] \times 10^{-6}$$

$$\therefore R_2 = \frac{(25)^{2/3} (355)}{(0.0167)(430)} [738.93 - 4.06 (37.62)] \times 10^{-6} = 0.248$$

- **Determine the reduction Coefficient to control the shear crack width and loss of aggregate interlock**

Using Equation (5-22):

$$R = \frac{0.006}{\epsilon_{fu}}$$

$$\therefore R_3 = \frac{0.006}{0.0167} = 0.36$$

- **Determine the controlling reduction coefficient for the governing failure mode**

$$R = \min. (R_1 \ R_2 \ R_3)$$

$$\therefore R = 0.248$$

- **Compute the average effective stress of CFRP at ultimate**

$$f_{fe} = R f_{fu}$$

$$f_{fe} = 0.248 \times 3790 = 940 \text{ MPa}$$

- **Find the shear contribution of the CFRP and compare to the required value**

Using Equation (5-25):

$$V_f = \frac{A_f f_{fe} (\sin\beta + \cos\beta) d_f}{s_f} \leq \left[ \frac{2 \sqrt{f'_c} b_w d}{3} - V_s \right]$$

$$= \frac{2(0.165)(1)(940)(1+0)(430)}{(1)(1000)} \leq \left( \frac{2\sqrt{25}(300)(550)}{3(1000)} - 132 \right)$$

$$= 133.38 \text{ kN} < 368 \text{ kN}$$

$V_f = 133.38 \text{ kN} > V_{f,\text{req}} = 118.6 \text{ kN} \therefore$  one ply continuous U-wrap without end anchor is sufficient.

### Final design

The final design is summarized in Figure (D-4). Note that, In this case, CFRP sheet assumed to extend beyond the critical point with distance equal to the stirrups spacing (0.25 m).

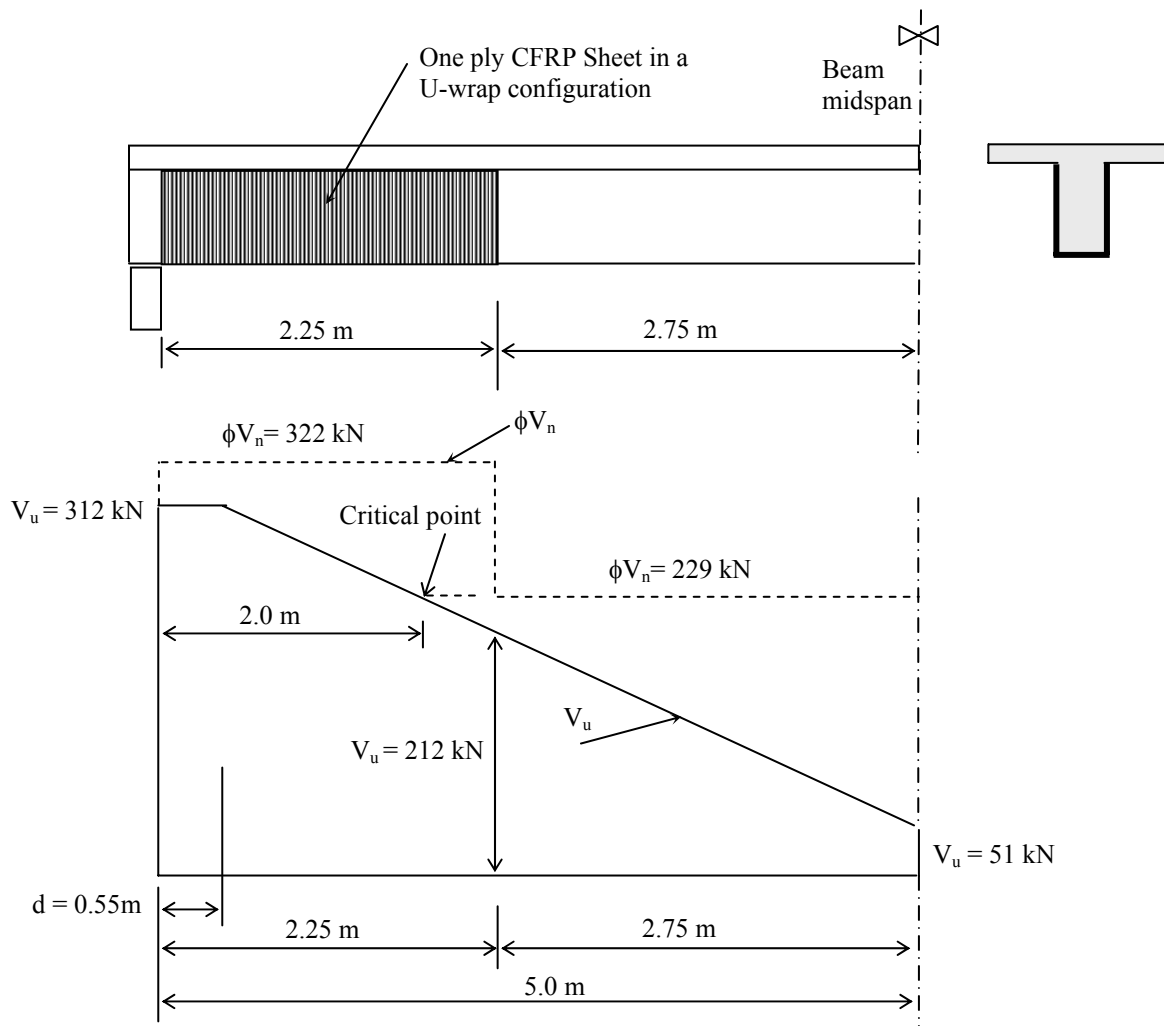


**Figure D-4.** Final design and shear diagram

## Alternative Solution

FRP strengthening system offers the designer several options for shear strengthening. As discussed earlier in this dissertation, U-wrap CFRP with end anchor is the most effective strengthening method especially if CFRP debonding controls the design. In this section, the same design example is solved using the end anchor.

- **Determine the controlling reduction coefficient for the governing failure mode**

$$R = \min. (R1 \quad R3)$$

Note that, for the case of using U-wrap with end anchor, the failure mode of CFRP debonding is not to be considered.

$$R = 0.36$$

- **Compute the average effective stress of CFRP at ultimate**

$$f_{fe} = R f_{fu}$$

$$f_{fe} = 0.36 \times 3790 = 1364.4 \text{ MPa}$$

- **Find the required amount of CFRP**

$$V_f = \frac{2 t_f w_f f_{fe} (\sin \beta + \cos \beta) d_f}{s_f}$$

$w_f/s_f$  may consider equal 1.0 as assumed earlier. Thereafter, compute  $V_f$  and compare between its value and  $V_{f,req}$ . On the other hand one can consider that the spacing and the width of the strips are the two design variables. For convenience it will be helpful to compute the ratio  $w_f/s_f$ . Based on the  $w_f/s_f$  ratio, the following conclusions can be drawn:

If  $w_f/s_f < 1.0$ , it is acceptable to use one-ply strips with a width to spacing ratio greater than or equal to  $w_f/s_f$ .

If  $w_f/s_f = 1.0$ , it is acceptable to use continuous one-ply sheet.

If  $w_f/s_f > 1.0$ , one ply will not be sufficient; more plies will be required.

$$V_f = 118.6 \text{ (kN)} = \frac{2 (0.165) w_f (1364.4)(1+0)(430)}{s_f (1000)} \Rightarrow w_f/s_f = 0.612$$

Thus, it will be permissible to use evenly spaced, one-ply strips with end anchor. It should be better to place the FRP strips between the existing steel reinforcement. Then, assuming  $s_f = 250$  mm.

$$\therefore w_{f,\text{req}} = 153 \text{ mm.}$$

For practical application, consider  $w_f = 160$  mm. Thus, the  $w_f/s_f$  ratio becomes 0.64, which is greater than the required ratio.

- **Check the capacity and spacing requirements**

To get R1, we assumed that  $w_f/s_f = 1$ . In this case, R1 has to recalculate according to the actual ratio of  $w_f/s_f$ .

$$\rho_f = 0.000704$$

Using Equation (5-13)

$$R1 = 0.6$$

Compared with R3 ( $R3 = 0.36$ ), R3 controls the design as we considered.

$$V_f = \frac{2 (0.165)(160)(1364.4)(1+0)(430)}{(250)(1000)} = 123.9 \text{ kN} > V_{f,\text{req}} \quad \text{O.K.}$$

$$\frac{2 \sqrt{f'_c} b_w d}{3} - V_s = 368 \text{ kN}$$

$$V_f = 123.9 < 368 \text{ kN} \quad \text{O.K.}$$

Check the 250-mm spacing is less than the maximum of:

$$s_{f,\text{max.}} = w_f + d/4 = 160 + 550/4 = 297.5 \text{ mm}$$

$$s_f = 250 \text{ mm} < s_{f,\text{max.}} \quad \text{O.K.}$$

### Final Design

The final design of the alternative solution is summarized in Figure (D-5). The strip width is 160 mm with center-to-center spacing of 250 mm. Compared with the first solution (continuous U-wrap without end anchor), using of the end anchor result in saving of 36% of CFRP materials.

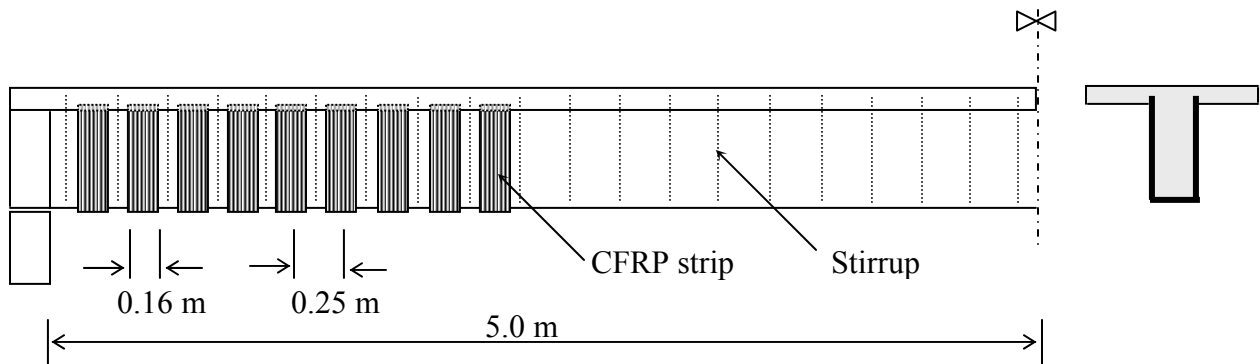


**Figure D-5.** Final design of the alternative solution

## REFERENCES

- 1- Arduini, M. and A. Nanni, "Behavior of Pre-Cracked RC Beams Strengthened with Carbon FRP Sheets," *Journal of Composites for Construction - ASCE*, Vol. 1, No. 2, 1996, pp. 63-70.
- 2- Berset, J., "Strengthening of Reinforced Concrete Beams for Shear Using FRP Composites," MSC thesis, Department of Civil and Environmental Engineering, Massachusetts Institute of Technology, Jan. 1992.
- 3- Uji, K., "Improving Shear Capacity of Existing Reinforced Concrete Members by Applying Carbon Fiber Sheets," *Transactions of the Japan Concrete Institute*, Vol. 14, 1992, pp. 253-266.
- 4- Ohuchi, H., Ohno, S., Katsumata, H., Kobatake, Y., Meta, T., Yamagata, K., Inokuma, Y., and Ogata, N., "Seismic strengthening Design Technique for Existing Bridge Columns with CFRP," *Seismic Design and Retrofitting of Reinforced Concrete Bridges*, edited by Park, R., 1994, pp. 495-514.
- 5- Chajes, M. J., Januska, T.F., Mertz, D.R., Thomson, T.A., and Finch, W.W., "Shear Strengthening of Reinforced Concrete Beams Using Externally Applied Composite Fabrics," *ACI Structural Journal*, Vol. 92, No. 3, May - June 1995, pp. 295-303.
- 6- Sato, Y., Ueda, T., Kakuta, Y., and Tanaka, T., "Shear Reinforcing Effect of Carbon Fiber Sheet Attached to Side of Reinforced Concrete Beams," *Advanced Composite Materials in Bridges and Structures*, edited by El-Badry, M.M., 1996, pp. 621-627.
- 7- Sato, Y., Ueda, T., Kakuta, Y., and Ono, S., "Ultimate Shear Capacity of Reinforced Concrete Beams with Carbon Fiber Sheets," *Non-Metallic (FRP) Reinforcement for*

- Concrete Structures, Proceedings of the Third Symposium*, Vol. 1, Japan, Oct 1997, pp. 499-506.
- 8- Umezu, K., Fujita, M., Nakai, H., and Tamaki, K., "Shear Behavior of RC Beams with Aramid Fiber Sheet," *Non-Metallic (FRP) Reinforcement for Concrete Structures, Proceedings of the Third Symposium*, Vol. 1, Japan, Oct. 1997, pp. 491-498.
  - 9- Araki, N., Matsuzaki, Y., Nakano, K., Kataoka, T., and Fukuyama, H., "Shear Capacity of Retrofitted RC Members with Continuous Fiber Sheets," *Non-Metallic(FRP) Reinforcement for Concrete Structures, Proceedings of the Third Symposium*, Vol. 1, Japan, Oct. 1997, pp. 515-522.
  - 10- Taerwe, L., Khalil, H., and Matthys, S., "Behavior of RC Beams Strengthened in Shear by External CFRP Sheets," *Non-Metallic(FRP) Reinforcement for Concrete Structures, Proceedings of the Third Symposium*, Vol. 1, Japan, Oct. 1997, pp. 483-490.
  - 11- Funakawa, I., Shimono, K., Watanabe, T., Asada, S., and Ushijima, S., "Experimental Study on Shear Strengthening with Continuous Fiber Reinforcement Sheet and Methyl Methacrylate Resin," *Non-Metallic (FRP) Reinforcement for Concrete Structures, Proceedings of the Third Symposium*, Vol. 1, Japan, Oct. 1997, pp. 475-482.
  - 12- Miyauchi, K., Inoue, S., Nishibayashi, S., and Tanaka, Y., "Shear Behavior of Reinforced Concrete Beam Strengthened with CFRP sheet," *Transactions of the Japan Concrete Institute*, 1997, pp. 97-104.
  - 13- Ono, K., Matsumura, M., Sakanishi, S., and Miyata, K., "Strength Improvement of RC Bridge Piers by Carbon Fiber Sheet," *Non-Metallic (FRP) Reinforcement for Concrete Structures, Proceedings of the Third Symposium*, Vol. 1, Japan, Oct. 1997, pp. 563-570.

- 14- Talijsten, B., "Strengthening of Concrete Structures for Shear with Bonded CFRP Fabrics," *Recent Advances in Bridge Engineering*, U. Meier and R. Betti, 1997, pp. 67-74.
- 15- Malek, A., and Saadatmanesh, H., " Ultimate Shear Capacity of Reinforced Concrete Beams Strengthened with Web-Bonded Fiber-Reinforced Plastic," *ACI Structural Journal*, July-Aug. 1998, pp. 391-399.
- 16- Triantafillou, T.C., "Shear Strengthening of Reinforced Concrete Beams Using Epoxy-Bonded FRP Composites," *ACI Structural Journal*, Mar.-Apr. 1998, pp. 107-115.
- 17- Sato, Y., Katsumata, H., and Kobatake, Y., "Shear Strengthening of Existing Reinforced Concrete Beams by CFRP Sheet," *Non-Metallic (FRP) Reinforcement for Concrete Structures, Proceedings of the Third Symposium*, Vol. 1, Japan, Oct. 1997, pp. 507-514.
- 18- Darwish, N., "Shear Strengthening of High Strength Concrete Beams with Carbon Fibers Reinforced Polymers (CFRP) Strips," *The Second middle East Symposium on Structural Composites for Infrastructure Applications*, Egypt, Apr. 1999.
- 19- Nanni, A., M. Norris, and N. Bradford , "Lateral Confinement of Concrete Using FRP Reinforcement," *Proceedings of the International Symposium on FRP Reinforcement*, Vancouver, Canada, Mar. 29-31, 1993, SP-138, American Concrete Institute, Detroit, MI, pp. 193-209.
- 20- Hartley, A., Mullins, G., and Sen, R. , "Repair of Concrete Masonry Block Walls Using Carbon Fiber," *Proceedings of the Second International Conference on Advanced Composite Materials in Bridges and Structures (ACMBS-II)*, Montreal, Canada, 1996, pp. 853-860.
- 21- Triantafillou, T.C., "Innovative Strengthening of Masonry Monuments with Composites," *Proceedings of the Second International Conference on Advanced Composite Materials in Bridges and Structures (ACMBS-II)*, Montreal, Canada, 1996, pp. 473-480.

- 22- Arizona Public Service Corporation, "Carbon Fiber Locks Out Pipeline Corrosion," *Civil Engineering Magazine-ASCE*, Vol. 67, No. 12, 1997, pp. 10 and 12
- 23- High-performance Composites "Composite Reinforcement of Civil Structures Gains Global Acceptance," Sep.-Oct. 1998, pp. 53-56.
- 24- Mallick, P., "Fiber-Reinforced Composites-Materials, Manufacturing, and Design" *Marcel Dekker, Inc.*, New York and Basel, 1988, 469 pp.
- 25- Nanni, A., "Fiber-Reinforced-Plastic (FRP) Reinforcement for Concrete Structures - Properties and applications" *Elsevier Science Publishers*, 1993, 450 pp.
- 26- Meier, U., "Bridge Repair with High Performance Composite Materials," *Material und Technik*, Vol. 4, 1987, pp. 125-128.
- 27- Fukuyama, H., Nakai, H., Tanigaki, M., and Uomoto, T., "JCI State-of-the-Art on retrofitting by CFRM part1- Materials, Construction and Application," *Non-Metallic (FRP) Reinforcement for Concrete Structures, Proceedings of the Third Symposium, Japan*, Vol. 1, Oct. 1997, pp. 605-612.
- 28- ACI Committee 440, "State-of-the-Art Report on Fiber Reinforced Plastic (FRP) Reinforcement for Concrete Structures," American Concrete Institute, Detroit, Michigan, 1996, 68 pp.
- 29- Master Builders Technologies, "MBrace Composite Strengthening System-Engineering Design Guidelines," Second Ed., Cleveland, OH, 1998, 140 pp.
- 30- Khalifa, A., Alkhrdaji, T., Nanni, A., and Lansburg, A., "Anchorage of Surface Mounted FRP Reinforcement," *Concrete International, ACI*, 1999, to Appear.
- 31- Hutchinson, R., Abdelrahman, A., Rizkalla, S., and Smith, G., " Shear Strengthening Using FRP Sheets for a Highway Bridge in Manitoba, Canada," *Non-Metallic (FRP)*

- Reinforcement for Concrete Structures, Proceedings of the Third Symposium, Vol. 1, Japan, Oct. 1997, pp. 531-538.*
- 32- Khalifa, A., and Nanni, A., “ Rehabilitation of Rectangular Simply Supported RC Beams with Shear Deficiencies Using CFRP Composites,” *Journal of Construction and Building Materials*, 2000, Submitted for Publication.
- 33- Khalifa, A., Belarbi, A., and Nanni, A., “Shear Performance of RC Members Strengthened with Externally Bonded FRP Wraps,” *12<sup>th</sup> World Conference on Earthquake Engineering (12WCEE)*, New Zealand, January 2000, to Appear.
- 34- Khalifa, A., Tumialan, G., Nanni, A., and Belarbi, A., “Shear Strengthening of Continuous RC Beams Using Externally Bonded CFRP Sheets,” *Fourth International Symposium on Fiber Reinforced Polymer for Reinforced Concrete Structures, (FRPRCS-4)*, Oct. 1999, to Appear.
- 35- Khalifa, A., and Nanni, A., “ Improving Shear Capacity of Existing RC T-Section Beams Using CFRP Composites,” *Journal of Cement & Concrete Composites*, Submitted for Publication.
- 36- Khalifa, A., Gold, W., Nanni, A., and Abdel -Aziz M. I., “Contribution of Externally Bonded FRP to the Shear Capacity of RC Flexural Members,” *Journal of Composites for Construction*, ASCE, Vol. 2, No. 4, Nov. 1998, pp. 195-202.
- 37- ACI Committee 318, Building Code Requirements for Structural Concrete (ACI 318-95) and commentary (ACI 318R-95), *American Concrete Institute*, Detroit, 1995, 369 pp.
- 38- Maeda, T.; Asano, Y.; Sato, Y.; Ueda, T.; and Kakuta, Y., “A Study on Bond Mechanism of Carbon Fiber Sheet,” *Non-Metallic (FRP) Reinforcement for Concrete Structures, Proceedings of the Third Symposium, Vol. 1, Japan, Oct. 1997, pp. 279-286.*

- 39- Miller, Brian D., "Bond Between Carbon Fiber Reinforced Polymer Sheets and Concrete," MS Thesis, Department of Civil Engineering, *University of Missouri, Rolla, MO*, 1999.
- 40- Horiguchi, T., and Saeki, N., "Effect of Test Methods and Quality of Concrete on Bond Strength of CFRP Sheet," *Non-Metallic (FRP) Reinforcement for Concrete Structures, Proceedings of the Third Symposium*, Vol. 1, Japan, Oct 1997, pp. 265-270.
- 41- Egyptian Code of Practice for Reinforced Concrete Structures, *permanent committee for the Code of practice for Reinforced Concrete Structures*, 1995, 243 pp.
- 42- Eurocode No. 2, Design of Concrete Structures, *European Committee for Standardization*, Lausanne, 1992.

## VITA

Ahmed Mahmoud Khalifa was born on 12 September 1964 in Desouq, Egypt. He spent five years as an undergraduate student in the Faculty of Engineering, Alexandria University, Egypt. After the preparatory year, he enrolled in the Civil Engineering Department for four years. Mr. Khalifa received his Bachelor of Science Degree from Alexandria University in June 1987 with a final grade of Distinction with Degree of Honor and ranked first among of total number of 800 students. He received the same grade and rank in all of his undergraduate study years.

After receiving his undergraduate degree, he joined the Egyptian Army for fifteen months. In April 1989, he went back to Alexandria University to pursue his graduate studies in the Structural Engineering Department. He was selected for a teaching assistant position through which he served in undergraduate teaching duties for structural analysis, steel structures, and steel bridges. Mr. Khalifa received his Master of Science Degree in Civil Engineering in October 1993. During the period of June 1987 through June 1997, he worked as a part-time structural engineer, designer, and then supervisor in several consultant firms in Alexandria.

Mr. Khalifa has been registered as a Ph.D. student in Alexandria University since March 1996. He received an Egyptian Government Internal Grant through which he pursued his Ph.D research work in the University of Missouri-Rolla in the United States of America during the period of September 1997 through September 1999.

Mr. Khalifa is a member of the American Concrete Institute and the American Society of Civil Engineers. He has authored or co-authored several papers about strengthening of reinforced concrete structures using fiber reinforced polymer (FRP) composites. These papers appear in scientific journals such as Journal of Composites for Construction, Concrete International, and Construction and Building Materials.